OPAL-CR118
May 1993

HEAVY FLAVOUR PHYSICS

JANIS A. McKENNA
University of Victoria and IPP Canada
Department of Physics, University of Victoria, P.O. Box 3055
Victoria, B.C., V8W 3P6, Canada

Abstract

The physics of the heavy beauty and charm quarks is reviewed. The heaviest quarks present a great laboratory for studying and testing the Standard Model. The underlying theory and models of heavy quark physics are reviewed, and highlights of recent experimental results from e^+e^-colliders and fixed target experiments are presented and discussed.

Contents

[1]Invited lectures presented at the Lake Louise Winter Institute on Collider Physics, February 21-27, 1993.

1 Introduction

The physics of heavy quarks, beauty and charm (they are 'heavy' relative to the QCD mass scale, Λ_{QCD}) presents a great environment for testing and studying the Standard Model. The study of heavy quarks involves examining the weak interaction under the influence of the strong interaction, as the heavy quarks are not free, but are bound in hadrons. The presence of a heavy quark makes the system theoretically simpler to understand than those systems involving only light quarks, because in the heavy systems, often the electroweak and the strong QCD interactions are factorizable, enabling us to study and disentangle the strong and electroweak properties of the heavy quarks. It is hoped that the study of heavy flavours will eventually lead us to uncover new physics beyond the Standard Model.

In the past few years, a great deal of progress has been made, both theoretically and experimentally, in understanding the physics of heavy quarks. In this set of lectures an attempt is made to focus on the experimental highlights of the study of beauty and charm, and their impact on theory, including the phenomenology and modeling of weak decays.

In view of the large number of graduate students attending the institute, and in order to define terms and nomenclature used, a brief introduction to the Standard Model and motivation for studying weak decays of heavy quarks is included.

A caveat – as the lectures presented by J.Martin & D.Gingrich, P.Jenni and K.Ragan [1] at this Institute beautifully covered the progress and tantalizing prospects for heavy quark physics at ep, pp, and $p\overline{p}$ colliders, this set of lectures is confined to heavy quark physics at e^+e^-colliders and fixed target experiments only.

1.1 A Brief Introduction to the Standard Model

The Standard Model ties together the successes of the Glashow-Weinberg-Salam [2] electroweak theory and Quantum ChromoDynamics (QCD), the theory of the strong interaction. It is a gauge theory based on the group SU(3)$\otimes$SU(2)$\otimes$U(1). (For a detailed review of the gauge structure of the Standard Model, see for example [3].)

Three of the four known forces, namely the strong, electromagnetic and weak, are described in a common framework. We have yet to pull them together into a grand unified theory incorporating the gravitational force. The matter fields are the quarks and leptons. The quarks feel all four forces, the charged leptons feel all except the strong force, while the neutrinos are only sensitive to the weak force.

QED

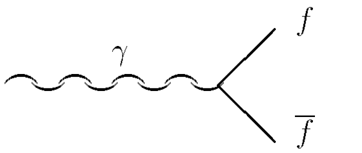

$-ie\,Q_f\,\gamma^\mu$ V

EW - CC

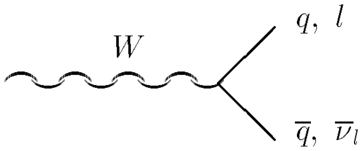

$\frac{-ig}{\sqrt{2}}\,\gamma^\mu\,\frac{1}{2}(1-\gamma^5)$ V−A

EW - NC

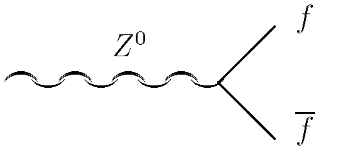

$\frac{-ig}{\cos\theta_W}\,\gamma^\mu\,\frac{1}{2}\left(c_V^f - c_A^f\gamma^5\right)$ part V part A

with $g = \frac{e}{\sin\theta_W}$

c_V and c_A are the vector and axial-vector couplings

$$\begin{aligned} c_V^f &= T_3^f - 2Q_f\sin^2\theta_W \\ c_A^f &= T_3^f \end{aligned} \qquad T_3 = \text{weak isospin, } \tfrac{1}{2} \text{ or } -\tfrac{1}{2}$$

Figure 1: Feynman rules for tree level vertices in electroweak interactions

Forces:

Photon	γ
Weak Gauge Bosons	$Z^0\ W^\pm$
Gluon	g
Graviton	G

Matter:

Quarks	$\binom{u}{d}$	$\binom{c}{s}$	$\binom{t}{b}$
Leptons	$\binom{e}{\nu_e}$	$\binom{\mu}{\nu_\mu}$	$\binom{\tau}{\nu_\tau}$

The Feynman rules for tree-level vertices of the SU(2)⊗U(1) gauge structure are depicted in Figure 1. The electromagnetic force has a pure vector gauge structure; the weak charged current interaction has a pure $V-A$ gauge structure. The weak neutral current is part vector, part axial-vector, where the couplings c_V^f and c_A^f are analogous to a 'weak-charge' and are predicted within the context of the Standard Model in terms of the charge of the fermion Q_f, and the third component of weak iso-spin, T_3^f, as specified in Figure 1.

The charged current couples the W boson to both hadrons and leptons:

$$J_\mu^{CC} = (\overline{\nu}_e, \overline{\nu}_\mu, \overline{\nu}_\tau)\,\gamma_\mu(1-\gamma_5)\begin{pmatrix} e \\ \mu \\ \tau \end{pmatrix} \;+\; (\overline{u}, \overline{c}, \overline{t})\,\gamma_\mu(1-\gamma_5)V_{KM}\begin{pmatrix} d \\ s \\ b \end{pmatrix} \tag{1}$$

where V_{KM} is the Kobayashi-Maskawa quark-mixing matrix. The neutral current is:

$$J_\mu^{NC} = \sum_j \overline{f}_j \left(\frac{-ig}{\cos\theta_W}\,\gamma_\mu\,\frac{1}{2}\left(c_V^f - c_A^f\gamma^5\right)\right) f_j \tag{2}$$

where thef_j's are all fermions: all the quarks and leptons. The lowest order weak Hamiltonian is therefore:

$$\mathcal{H}^0 = \frac{G_F}{\sqrt{2}}\left\{\left(J_\mu{}^{CC}J^{\mu\dagger CC} + h.c.\right) + 2\left(J_\mu{}^{NC}J^{\mu NC}\right)\right\} \tag{3}$$

The amplitude for the transition $i \to f$ is obtained by sandwiching the Hamiltonian between the initial and final states:

$$\text{Amplitude}\,(i \to f) \equiv \langle\ f \mid \mathcal{H} \mid i\ \rangle \tag{4}$$

1.2 Fundamental Parameters in the Standard Model and the Kobayashi-Maskawa Matrix

The fundamental parameters of the Standard Model are the electromagnetic coupling constant or the fine structure constant, α, which has been measured very precisely in the $g-2$ muon magnetic moment experiments, and the Josephson effect; G_F, the Fermi coupling constant, which is known to high precision through measurements of the μ lifetime; and α_S, the strong coupling constant of QCD, which is at present well measured in e^+e^-experiments, deep inelastic scattering fixed target experiments, and will be measured to much higher precision over a wide scale by the HERA ep experiments.

α	Fine Structure Constant	g-2, Josephson effect
G_F	Fermi Constant	μ lifetime
m_Z	Z Boson Mass	Mark-II & LEP
α_S	Strong Coupling Constant	e^+e^-, DIS, HERA

Two parameters are necessary to describe the weak coupling constant, and now that m_Z has been measured to better precision than $\sin^2\theta_W$, we choose to list m_Z and G_F as the weak coupling fundamental parameters of the Standard Model.

Unfortunately, there are at least 16 more parameters of the Standard Model, which hopefully are not all 'fundamental'. These include the masses of 6 quarks and 3 leptons, the Higgs mass, the quark mixings (specified by 3 angles plus 1 phase), the strong interaction phase angle, and a classical gravitational constant.

In the study of heavy quarks, many of these parameters are experimentally accessible, in particular: α_S, V_{cd}, V_{cs}, V_{cb}, V_{ub}, V_{td}, V_{ts}, m_c, m_b, m_t, δ, (CKM matrix elements, quark masses, and CP-phase angle).

Leptons and quarks interact weakly via the $V-A$ weak charged current, as specified in Equation 1, but the details of weak decays differ drastically, due to the fact that quarks mix and therefore couple between generations, while the leptons apparently interact only within their own generation. (In an extension beyond the Standard Model, in which the neutrinos have mass, a similar mixing could be introduced in the lepton sector, but in the Standard Model the neutrinos are massless, by construction.)

The hadronic charged current involves a mixing matrix, since the weak and flavour eigenstates are not the same. The quark weak eigenstates are related to the mass eigenstates by a generalized rotation, specified by the Cabibbo-Kobayashi-Maskawa mixing matrix[4]. By convention, the $Q=+\frac{2}{3}$ quarks are unmixed, *i.e.* the weak and flavour eigenstates are the same, while the mixing in the $Q=-\frac{1}{3}$ sector is specified by the matrix V_{KM}:

$$\begin{pmatrix} d' \\ s' \\ b' \end{pmatrix} = \begin{pmatrix} V_{ud} & V_{us} & V_{ub} \\ V_{cd} & V_{cs} & V_{cb} \\ V_{td} & V_{ts} & V_{tb} \end{pmatrix} \begin{pmatrix} d \\ s \\ b \end{pmatrix} \tag{5}$$

where (d', s', b') are the weak eigenstates, and (d, s, b) are the flavour eigenstates. This unitary matrix V_{KM} may be parameterized in terms of 3 real angles and 1 complex phase. Unfortunately no theory exists to predict the values of the KM matrix elements. They may however be measured and constrained experimentally.

It is interesting to note that Kobayashi and Maskawa postulated a third quark generation doublet and this mixing ansatz at a time when only 3 quarks had been discovered; a third generation of quarks with mixing, which introduces a phase along with 3 rotation angles, can accommodate CP-violation.

Many parameterizations of the KM matrix exist. It is convenient to think of the matrix as 3 rotations, one between each pair of generations, plus the phase δ.

$$V_{KM} = \begin{pmatrix} 1 & 0 & 0 \\ 0 & c_{23} & s_{23} \\ 0 & -s_{23} & c_{23} \end{pmatrix} \begin{pmatrix} c_{13} & 0 & s_{13}e^{i\delta} \\ 0 & 1 & 0 \\ -s_{13}e^{i\delta} & 0 & c_{13} \end{pmatrix} \begin{pmatrix} c_{12} & s_{12} & 0 \\ -s_{12} & c_{12} & 0 \\ 0 & 0 & 1 \end{pmatrix} \tag{6}$$

where $c_{ij} = \cos\theta_{ij}$ and $s_{ij} = \sin\theta_{ij}$. Multiplying out these matrices results in the parametrization advocated by the Particle Data Group [5]:

$$\begin{pmatrix} V_{ud} & V_{us} & V_{ub} \\ V_{cd} & V_{cs} & V_{cb} \\ V_{td} & V_{ts} & V_{tb} \end{pmatrix} = \begin{pmatrix} c_{12}c_{13} & s_{12}c_{13} & s_{13}e^{-i\delta} \\ -s_{12}c_{23} - c_{12}s_{23}s_{13}e^{i\delta} & c_{12}c_{23} - s_{12}s_{23}s_{13}e^{i\delta} & s_{23}c_{13} \\ s_{12}s_{23} - c_{12}c_{23}s_{13}e^{i\delta} & c_{12}s_{23} - s_{12}c_{23}s_{13}e^{i\delta} & c_{23}c_{13} \end{pmatrix} \tag{7}$$

At present, the KM matrix elements are as fundamental as quark masses in the Standard Model. A better understanding of the matrix elements is essential and could give us a sneak preview to new physics (composite quarks or leptons, or superstrings!) beyond the Standard Model. At 90% CL, the magnitudes of the KM matrix elements are [5]:

$$\begin{pmatrix} V_{ud} & V_{us} & V_{ub} \\ V_{cd} & V_{cs} & V_{cb} \\ V_{td} & V_{ts} & V_{tb} \end{pmatrix} = \begin{pmatrix} .9747 \text{ to } .9759 & .218 \text{ to } .224 & .002 \text{ to } .007 \\ .218 \text{ to } .224 & .9735 \text{ to } .9751 & .032 \text{ to } .054 \\ .003 \text{ to } .018 & .030 \text{ to } .054 & .9985 \text{ to } .9995 \end{pmatrix} \tag{8}$$

Our knowledge of KM-matrix is from experiment:

V_{ud} Nuclear β decay compared with muon decay.
V_{us} Semileptonic kaon and hyperon decay.
V_{cd} ν and $\overline{\nu}$ production of charm from nucleons (containing valence d quarks); semileptonic branching ratios of charm to non-strange particles; charmed hadron lifetimes.
V_{cs} ν and $\overline{\nu}$ production of charm from strange quarks in the parton sea; semileptonic branching ratios of charm to strange particles.
V_{ub} semileptonic decays $b \to u$ from endpoint of lepton spectrum; reconstructed exclusive semileptonic charmless B decays
V_{cb} semileptonic decays $b \to c$; B hadron lifetime.
V_{td} ${B_d}^0 - \overline{B_d}^0$ mixing.
V_{ts} ${B_s}^0 - \overline{B_s}^0$ mixing (in the future, penguin b decays as well).
V_{tb} Not even any indirect measurements yet.

Note that the matrix elements involving the heavier quarks are the least well known: experimental measurements of heavy quark decays have recently greatly improved our understanding of these elements, and more detailed heavy quark studies will help zero in on these matrix elements.

These measurements suggest a pattern, as noted by Wolfenstein [6]:

$$\begin{pmatrix} 1 & \lambda & \lambda^3 \\ -\lambda & 1 & \lambda^2 \\ -\lambda^3 & -\lambda^2 & 1 \end{pmatrix} \tag{9}$$

(ignoring CP violation) with $\lambda \sim \sin\theta_C \sim .22$, This striking pattern hints at perhaps a hierarchy of the couplings between quark generations, perhaps a new sign of symmetries beyond the Standard Model.

1.3 Why Study Heavy Flavours?

- Through weak decays the V-A structure of the charged current ${J_\mu}^{CC}$ may be tested.

- c_V^f and c_A^f in the weak neutral current ${J_\mu}^{NC}$ may be measured and tested. To date, such studies have shown that the b quark is indeed a member of an isopin doublet, with as yet undiscovered partner, the top quark.

- Verify absence of flavour changing neutral currents (FCNC) in weak decays in the Standard Model.
- Heavy quarks are separable from light u, d, s quarks, enabling us to test the Standard Model for each quark flavour separately.
- Heavy quarks have large mass – therefore a perturbative expansion in Λ_{QCD}/m_Q makes possible some QCD calculations.
- c's and b's have a 'long' lifetime ($\sim$ 1 ps); at LEP, they typically travel 1-3mm before decaying.
- $B^0 - \overline{B^0}$ mixings are observed to be large, suggesting that CP violation and CP asymmetries in the B system may likewise be relatively large.

Measurements of heavy quark decay will help improve errors on many of the KM matrix elements:

$\tau_c,\ \tau_D$	$V_{cd},\ V_{cs}$
$\tau_b,\ \tau_B$	$V_{ub},\ V_{cb}$
$\mathrm{Br}(B \to X_c\ (X_u)\ l\ \nu)$	$V_{cb},\ V_{ub}$
$\mathrm{Br}(D \to X_s\ (X_d)\ l\ \nu)$	$V_{cs},\ V_{cd}$
$B\ \overline{B}$ Mixing	$V_{td},\ V_{ts}$
Penguin B decays	$V_{td},\ V_{ts}$

Our aim in studying heavy quarks is to test the electroweak sector of the Standard Model, and to examine the consistency of the Standard Model, mixings and masses for clues to new physics.

1.4 A Little Historical Perspective

No attempt will be made to review the history of the weak interaction and discovery of the heavy b and c quarks, as the literature is already extensive.[7] However, a little historical perspective might help set the stage for the theories and experiments which we will examine in these lectures.

1963 Cabibbo postulated mixing between the d and s quarks to explain the observation of strangeness-changing currents.[8]

1970 Glashow, Iliopoulos and Maiani introduced an extra quark, charm, as the iso-spin partner of the strange quark, in order to explain the absence of flavour-changing neutral currents in K decay.[9]

1973 Kobayashi and Maskawa proposed a 3^{rd} generation of quarks in order to accommodate CP-violation in the Standard Model. At least one phase is present in the mixing matrix for 3 or more quark generations (1 phase in the case of 3 generations, 3 phases in the case of 4 generations).[4] The presence of such a phase was shown to be able to accommodate the CP-violating effects observed in the neutral kaon system.

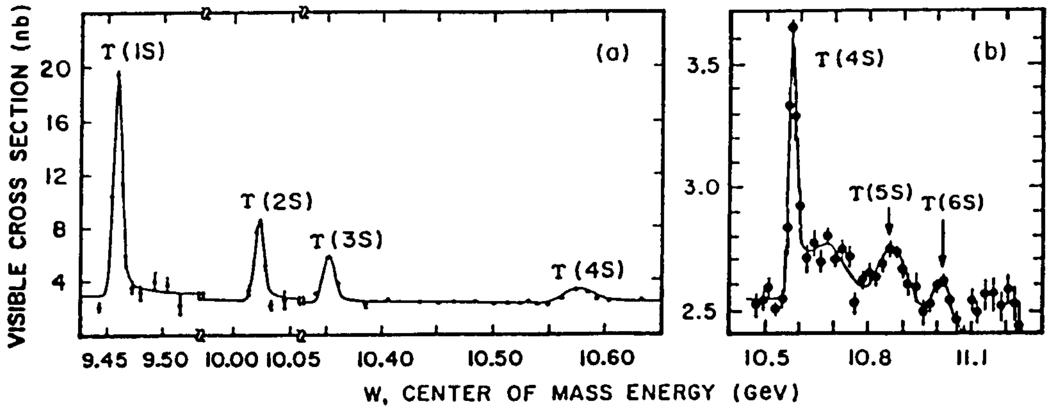

Figure 2: The hadronic cross-section in the Υ region.[15]

1974 Gaillard, Lee and Rosner [10] outlined the phenomenology, spectroscopy, production, decays, and mixing of charmed particles, just months before their discovery!

The charm quark was discovered simultaneously at SLAC at the SPEAR e^+e^-collider and at BNL in a fixed target experiment $p+N \to \psi X$, in 1974.[11] The b quark was first seen in 1977 at Fermilab [12] in a fixed target experiment $p + N \to \Upsilon(1S)\, X$, followed by the decay $\Upsilon(1S) \to \mu^+\mu^-$. The rich structure of the hadronic cross section in the 10 GeV region is shown in Figure 2.[13, 14, 15] The $\Upsilon(4S)$ $b\bar{b}$ state lies just above the threshold for $B\overline{B}$ production, and most of the B meson data collected with the ARGUS, CLEO, Crystal Ball and CUSB detectors was from the $\Upsilon(4S)$ resonance.

2 The Spectator Model

Heavy quark decay is in many ways analogous to nuclear-β decay or μ decay. In the naïve spectator model, the heavy quark decays freely: the light quarks to which it is bound, and any gluons present, have no role in the decay. The Feynman diagrams for the two processes are identical, and are shown in Figure 3. The partial decay width for free quark decay in the naïve spectator model is therefore calculable, by analogy to muon decay, which is well-understood:

$$\Gamma_l \;\equiv\; \Gamma(Q \;\to q\; l\; \nu_l) \;=\; \frac{{G_F}^2 {m_Q}^5}{192\pi^3}\; |V_{qQ}|^2\; \mathcal{P} \qquad (10)$$

Mixing in the quark sector is specified by the KM matrix element V_{qQ}. The $\mathcal{P}$ is a phase space factor due to the finite mass of the final state quark relative to the initial quark. $\mathcal{P} \sim .5$ for $b \to ce(\mu)$ and $c \to se(\mu)$ decays.

This naïve model enabled prediction of charm and beauty lifetimes: since the weak interaction is short range, it is expected that we may decouple the heavy quark from the light degrees of freedom – factorization of the free heavy quark from its accompanying light spectator quark partner, as shown in Figure 4.

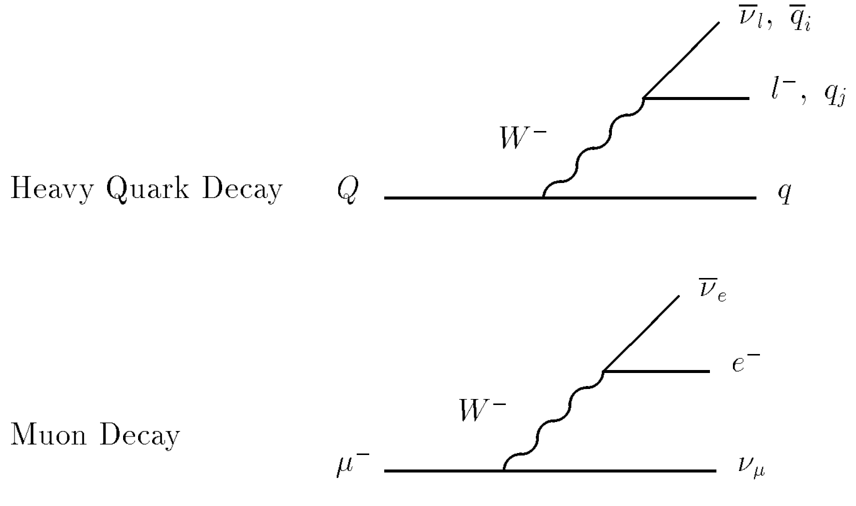

Figure 3: Feynman diagrams for μ decay and for free quark decay

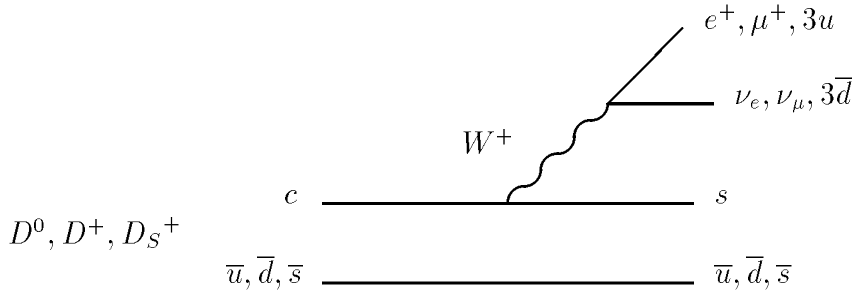

Figure 4: Spectator decay of charmed mesons

The spectator model therefore predicts $\tau(D^0) = \tau(D^+) = \tau(D_s{}^+) = \tau(\Lambda_c{}^+)$. It also predicts the semileptonic branching ratios of all charmed particles to be 20%: if the masses of the leptons and quarks to which the W decays are ignored, there are five equally likely sets of W decay products, each set occurring 20% of the time (two leptons and three quark colours).

The total decay width can be used to crudely estimate charmed lifetimes, within the context of the naïve spectator model. For $m_c \simeq$1.5 GeV and $|V_{cs}| \simeq 1$, with Γ_l as specified in Equation 10:

$$\tau_c = \frac{1}{\Gamma_{tot}} \simeq \frac{1}{5\Gamma_l} \simeq 1.5 \times 10^{-12} s \tag{11}$$

The B hadron lifetime may be estimated similarly; spectator model predictions for B lifetime are: $\tau(B^+) = \tau(B_d{}^0) = \tau(B_s{}^0) = \tau(\Lambda_b{}^+)$.

In B decay, shown in Figure 5, the masses of the leptons and quarks to which the W couples are not negligible in the cases of $(\tau, \overline{\nu}_\tau)$, and $(c\overline{s})$. While there are 9 channels available to which W may decay, the phase space reduction

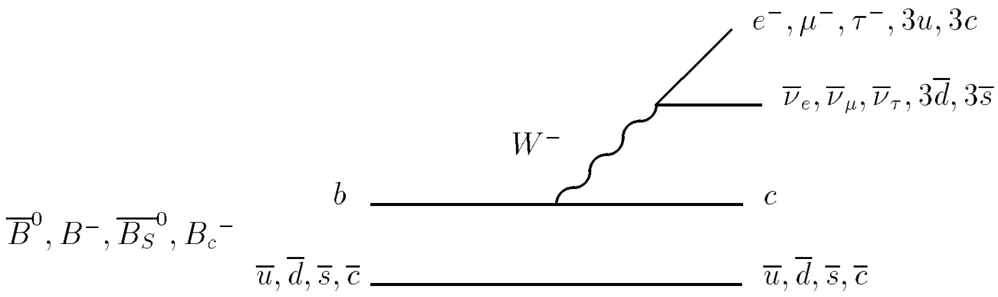

Figure 5: Spectator decay of B mesons

makes it effectively around 7 channels, so that B semileptonic branching ratios to e and μ are predicted to be equal, and about 14% each, in the spectator model.

Historically, after the discovery of the b quark, before its lifetime was measured, it had been predicted that the lifetime would be immeasurably small, a few tens of femtoseconds. ARGUS and CLEO had determined that b quarks couple predominantly to c quarks, and it was at first assumed that $|V_{cb}| \simeq .22$, the Cabibbo angle, the same inter-generational coupling between the second and third generations as between the first two generations.(!!)[16] Under this (false!) assumption of $b \to c$ Cabibbo-mixing, with $m_b \simeq$5 GeV, the first crude predictions for the B lifetime were very small:

$$\tau_b = \frac{1}{\Gamma_{tot}} \simeq \frac{1}{7\Gamma_l} \simeq 6 \times 10^{-14} s \tag{12}$$

Immeasurably small!

It was therefore a big surprise when the MAC [17] and Mark-II [18] collaborations measured the average B hadron lifetime to be in the picosecond range! This apparent 'problem' disappears if $|V_{cb}| \simeq .045$, so that $\tau_b \simeq 1.5$ps, by the pure spectator model.

2.1 Measurements of Charm Lifetimes

Enormous effort has been spent measuring charmed particle lifetimes, particularly at e^+e^-colliders and fixed target experiments. The standard method has typically been to reconstruct the charmed particle and its decay vertex. If decay products are not all fully detected, one can often impose some constraints, so as to effectively fit a fully reconstructed particle and its decay vertex.

In fixed target experiments, full 3-D reconstruction of vertex is performed using either an emulsion target, bubble chamber, or silicon microstrip detectors. In e^+e^-colliders, typically only a 2-D projection of the vertex is reconstructed, as until very recently, vertex drift-chambers and silicon detectors have had excellent resolution only in the plane perpendicular to the beam axis. For the

1993 run, all four LEP detectors will have silicon micro-vertex detectors, with three of the four having high precision in three dimensions. The e^+e^-detectors typically have vertex drift chamber hit resolutions in the 50μm region, and the new silicon micro-vertex detectors achieve resolutions of 15μm. Unfortunately, these precise detectors are placed outside the beampipe, usually at least 3-5 cm from the primary interaction vertex, introducing a long lever-arm which dilutes the high precision measurement when extrapolated back to the beam position.

The recent articles by Lüth [19] and Atwood and Jaros [20] review the present experimental situation, and detail many of the detectors and analysis techniques used to measure heavy quark lifetimes.

2.1.1 Charmed Lifetimes at Fixed Target Experiments

The most precise and highest statistics measurements of charmed lifetimes to date come from fixed target experiments, most notably two spectrometers at Fermilab: E-691 and E-687.

We choose to illustrate techniques and resolutions in charmed lifetime measurement with the E-687 Spectrometer, primarily because it has run more recently. In the E-687 experiment, photons are produced in a wideband 600 GeV electron beam at Fermilab, which impinges on a target, producing a bremstrahlung photon beam. The photon beam is tagged by detecting the recoil electron, and charm is produced via photoproduction. The spectrometer features a silicon microstrip detector, several dipole magnets, proportional chambers, Čerenkov counters, electromagnetic and hadronic calorimeters, and muon detectors. The particle identification capabilities are excellent; the vertexing capabilities are also excellent, with resolution (at the target plane):

$$\sigma_x = 11\mu\mathrm{m}\sqrt{1+\left(\frac{17.5GeV}{p}\right)^2} \qquad \sigma_y = 7.7\mu\mathrm{m}\sqrt{1+\left(\frac{25.GeV}{p}\right)^2} \tag{13}$$

The E-687 trigger requires a tagged photon, and at least two charged tracks in the spectrometer. Over 60 million triggers were logged on tape, yielding a fully reconstructed sample of over 9,000 charmed mesons. Two complementary techniques were used to analyze the charm sample: a 'candidate driven' vertex method, and a 'stand-alone' vertex method.[21, 22]

In the candidate driven method, a vertex is built up starting with a seed track, with other tracks in the event added into either the secondary or primary vertex. The charmed particle invariant mass distributions for five charmed meson decay chains used in the candidate driven lifetime analysis are shown in Figure 6.[1] The lifetime evolution for the same five D samples is shown in Figure 7. The lifetimes are measured by fitting a background subtracted modified proper time distribution to an exponential function.

[1] Throughout this article, whenever a particular particle or decay chain is mentioned, the conjugate particle or decay chain is implied.

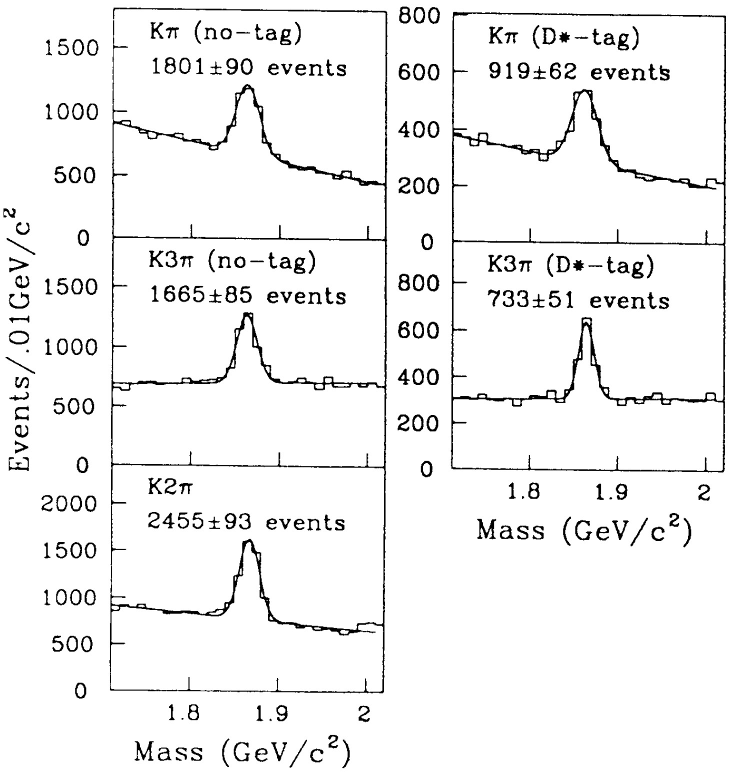

Figure 6: E-687 D lifetime analysis: D^0 and D^+ signals in the 'candidate-driven' lifetime analysis.[21]

In E-687's alternate 'stand-alone' vertex-method, events with a clean, isolated secondary vertex are selected. A charm candidate consists of a single isolated vertex which includes no additional tracks. While the charm samples obtained are very clean, the algorithm is clearly biased to be less efficient at shorter decay lengths. The charmed particle invariant masses in the clean samples obtained using this technique are shown in Figure 8.

The results from these E-687 analyses, with over 8000 D candidates reconstructed, along with the results of the other competitive D^0 and D^+ lifetime experiments, are tabulated in Table 1. It is apparent that the D^0 and D^+ lifetimes are appreciably different: they differ by a factor of approximately 2.5! While the naïve spectator model does indeed predict an excellent estimate of the average of the charmed D lifetimes, specific D^0 and D^+ lifetimes certainly are not identical.

The sample used in the E-687 $\phi\pi^+$ analysis is shown in Figure 9. It is interesting to note how the relative amplitude of the $D_S \to \phi\pi$ channel to the Cabibbo-suppressed $D^+ \to \phi\pi$ channel decreases as the L/σ_L cut increases, qualitatively indicating that the D^+ lifetime is longer than that of the ${D_S}^+$. The proper time distribution, after background subtraction, is fit and the lifetime extracted. The results, along with the results of several other D_S^+ and Λ_C^+ lifetime measurements, are summarized in Table 2.

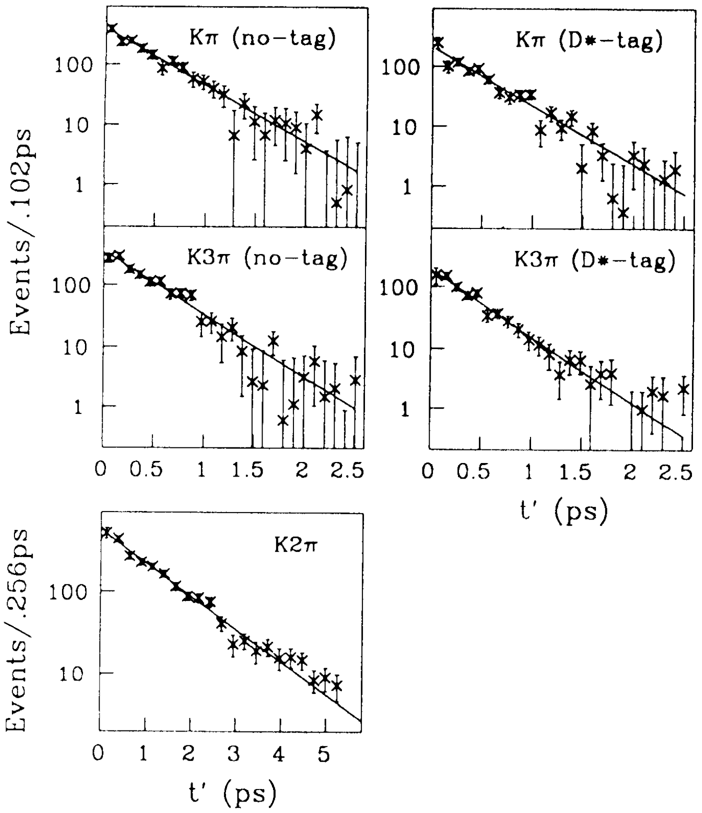

Figure 7: E-687 D lifetime analysis: Background subtracted and Monte Carlo corrected lifetime evolution for the five charm samples.[21]

Once again, we may make a crude remark: The naïve spectator model predicts the correct magnitude of charmed lifetimes, but clearly we must go beyond this simple model in order to explain the observed lifetime hierarchy:

$$\tau(D^+) \; > \; \tau(D_S{}^+) \; \geq \; \tau(D^0) \; > \tau(\Lambda_c{}^+) \tag{14}$$

Before going beyond the spectator model, it is useful to examine several other heavy quark spectator model predictions in order to have a feeling of just where the shortcomings of the spectator model lie.

2.2 Semileptonic D Branching Ratios

As previously mentioned, another prediction of the of spectator model is that in the charm system, all the semileptonic branching ratios are equal, $\mathrm{Br}(D^+ \to Xe^-\overline{\nu}_e) \; = \; \mathrm{Br}(D^0 \to Xe^-\overline{\nu}_e) = 20\%$, if we ignore the small e^-, μ^-, u, and d masses; see Figure 4. The Mark-III experiment at the SPEAR e^+e^-storage ring at center-of-mass energy 3.8 GeV, measured the semileptonic branching ratios of the D^0 and D^+ mesons.[37]

Isospin symmetry dictates:

$$\Gamma(D^- \to Xe^-\overline{\nu}_e) = \Gamma(\overline{D}^0 \to Xe^-\overline{\nu}_e) \tag{15}$$

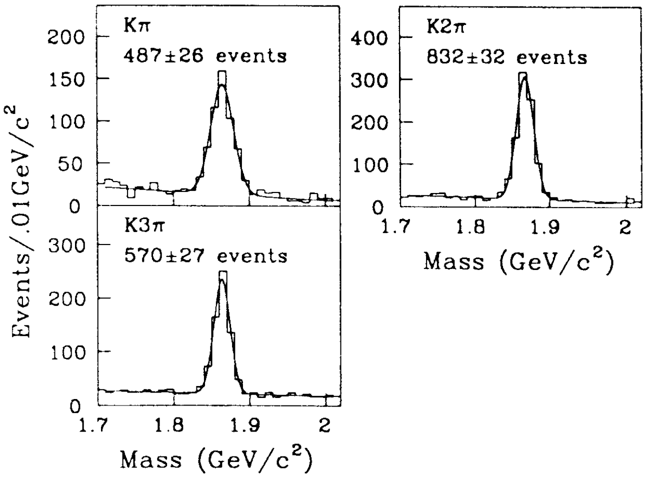

Figure 8: D meson mass peaks in the E-687 D lifetime analysis: Stand-alone secondary vertex finding analysis.[21]

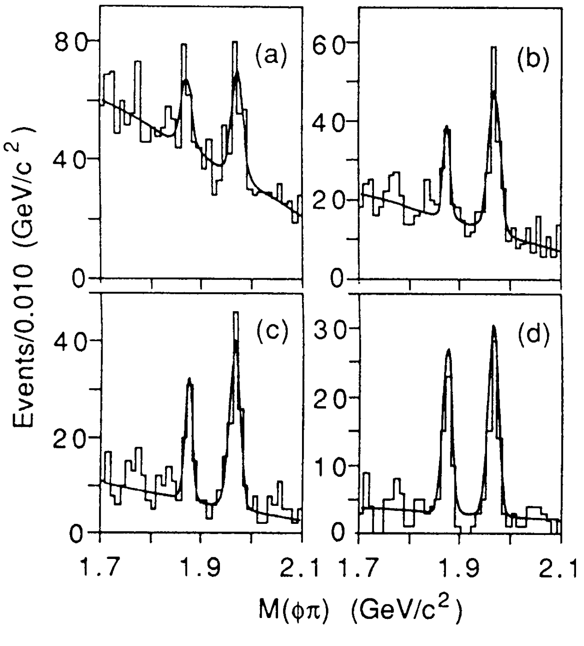

Figure 9: E-687 effective mass distribution for $\phi\pi$ combinations with increasingly stricter cuts on the decay length significance: a) $\frac{L}{\sigma_L} > 2.0$ b) $\frac{L}{\sigma_L} > 3.0$ c) $\frac{L}{\sigma_L} > 4.0$ d) $\frac{L}{\sigma_L} > 5.0$ [22]

A simple prediction from the spectator model relates the semileptonic D branching ratios and D lifetimes, under the assumption of isospin symmetry:

$$\frac{\mathrm{Br}(D^- \to Xe^-\overline{\nu}_e)}{\mathrm{Br}(\overline{D}^0 \to Xe^-\overline{\nu}_e)} = \frac{\frac{\Gamma(D^- \to Xe^-\overline{\nu}_e)}{\Gamma(D^- \to \text{ anything})}}{\frac{\Gamma(\overline{D}^0 \to Xe^-\overline{\nu}_e)}{\Gamma(\overline{D}^0 \to \text{ anything})}} \simeq \frac{\Gamma(\overline{D}^0 \to \text{ anything})}{\Gamma(D^- \to \text{ anything})} \equiv \frac{\tau(D^-)}{\tau(\overline{D}^0)} \quad (16)$$

Experiment	D^0 $\tau(10^{-13}s)$	D^+ $\tau(10^{-13}s)$	Reference
E-531	$4.3 \pm ^{.7}_{.5} \pm ^{.1}_{.2}$	$11.1 \pm ^{4.4}_{2.9}$	[23]
Photon Emulsion		$5.0 \pm ^{1.5}_{1.0} \pm 1.9$	[24]
LEBC		$11.2 \pm ^{1.4}_{1.1}$	[25]
SHF		$8.6 \pm 1.3 \pm ^{.7}_{.3}$	[26]
ACCMOR	$3.88 \pm ^{.23}_{.21}$	$10.5 \pm ^{.77}_{.72}$	[27]
NA14	$4.17 \pm .18 \pm .15$	$10.3 \pm .8 \pm .6$	[28]
E-687	$4.24 \pm .11 \pm .07$	$10.75 \pm .40 \pm .18$	[21]
TPS (E-691)	$4.22 \pm .08 \pm .10$	$10.90 \pm .30 \pm .25$	[29]
CLEO		$11.4 \pm 1.6 \pm .7$	[30]
ARGUS	$4.8 \pm 0.4 \pm 0.3$	$10.5 \pm .8 \pm .7$	[31]
HRS		$9.2 \pm ^{1.7}_{1.3} \pm 1.6$	[32]
World Average	4.20 ± 0.08	10.66 ± 0.23	[5]

Table 1: Measurements of lifetimes of charmed mesons, D^0, D^+.

Due to the presence of an undetected neutrino, it is difficult to reconstruct semileptonic decays with low backgrounds. At Mark-III, the analysis took advantage of the decays of the $\psi(3770)$ to either D^+D^- or $D^0\overline{D}^0$ pairs by fully reconstructing a D^0 or D^+ in a hadronic decay mode ($D^0 \to K^-\pi^+$, $K^-\pi^+\pi^0$, $K^-\pi^+\pi^+\pi^-$ and $D^+ \to K^-\pi^+\pi^+$, $\overline{K}^0\pi^+$). The rest of the event therefore consisted only of the decay products of the partner D meson. By simply looking at the fraction of events in which there is an electron recoiling against the hadronic D tag, the semileptonic branching ratio is measured. The hadronic D-tag signals are shown in Figure 10.

The extremely small background contamination under the signals ensures that the uncertainty in the branching ratio measurement will be very small. The D sample is clean, with excellent resolution. The total energy of the D^0 or D$^+$ is constrained to beam energy, since the $\psi(3770)$ is just above the $D\overline{D}$ production threshold. Time-of-Flight is used for particle identification, and electrons are identified using the Time-of-Flight system and the electromagnetic calorimeter. A correction for a small, known electron misidentification is applied.

The recoil electron spectra in the D^0 and D^+ tagged events are shown in Figure 11; the superimposed curves are the expected spectra for $D \to Ke\overline{\nu}_e$ and $D \to K^*e\overline{\nu}_e$.

The resulting semileptonic branching ratios are [37]:

$$\mathrm{Br}(D^+ \to Xe^-\overline{\nu}_e) = (17.0 \pm 1.9 \pm 0.7)\% \tag{17}$$

Experiment	$D_s{}^+$ $\tau(10^{-13}s)$	$\Lambda_c{}^+$ $\tau(10^{-13}s)$	Reference
E-531	$2.6 \pm {}^{1.6}_{0.9}$	$2.0 \pm {}^{.7}_{.6}$	[23]
Photon-Emulsion		$2.3 \pm {}^{.9}_{.6} \pm .4$	[24]
LEBC		$1.2 \pm {}^{.5}_{.3}$	[33]
ACCMOR	$4.69 \pm {}^{1.02}_{.86}$	$1.96 \pm {}^{.23}_{.20}$	[27]
NA14	$3.3 \pm {}^{1.2}_{0.8} \pm .3$	$1.8 \pm .3 \pm .3$	[28]
NA1		$1.1 \pm {}^{.8}_{.4}$	[34]
NA11/NA32	$3.3 \pm {}^{1.0}_{0.6}$		[35]
E-687	$5.0 \pm .6 \pm .3$	$2.0 \pm .3 \pm .3$	[22]
TPS (E-691)	$4.7 \pm .4 \pm .2$	$2.2 \pm .3 \pm .2$	[29]
CLEO	$4.7 \pm 2.2 \pm .5$		[30]
ARGUS	$5.6 \pm {}^{1.3}_{1.2} \pm .8$		[31]
HRS	$3.1 \pm {}^{2.4}_{2.0} \pm .5$		[32]
TASSO	$5.7 \pm {}^{3.6}_{2.6} \pm .9$		[36]
World Average	$4.50 \pm {}^{.30}_{.26}$	$1.91 \pm {}^{.15}_{.12}$	[5]

Table 2: Measurements of the lifetimes of the charmed hadrons, $D_s{}^+$ and $\Lambda_c{}^+$.

$$\mathrm{Br}(D^0 \to Xe^-\overline{\nu}_e) = \quad (7.5 \pm 1.1 \pm 0.4)\% \tag{18}$$

This is not the 20% predicted by the spectator model, but

$$\frac{\tau_{D^+}}{\tau_{D^0}} = \frac{\mathrm{Br}(D^+ \to Xe^-\overline{\nu}_e)}{\mathrm{Br}(D^0 \to Xe^-\overline{\nu}_e)} \simeq 2.4 \tag{19}$$

The measured semileptonic branching ratios are not only smaller than predicted, by the naïve spectator model, but they are (very) unequal! It is becoming apparent that something is a little deficient in the spectator model. However, since the ratio of lifetimes is equal to the ratio of branching ratios, this gives us a clue that the leptonic sector itself looks consistent, and it's likely to be the hadronic sector which is responsible for either an enhancement in D^0 decays, or a suppression in D$^+$ decays which does not fit into the simple spectator model.

2.3 Measurements of Beautiful Lifetimes

Very few fast-flying beautiful particles have been completely reconstructed. The ARGUS and CLEO experiments have reconstructed hundreds of B's, but they produce B's from the decay of the $\Upsilon(4S)$ at rest. The B's are almost at

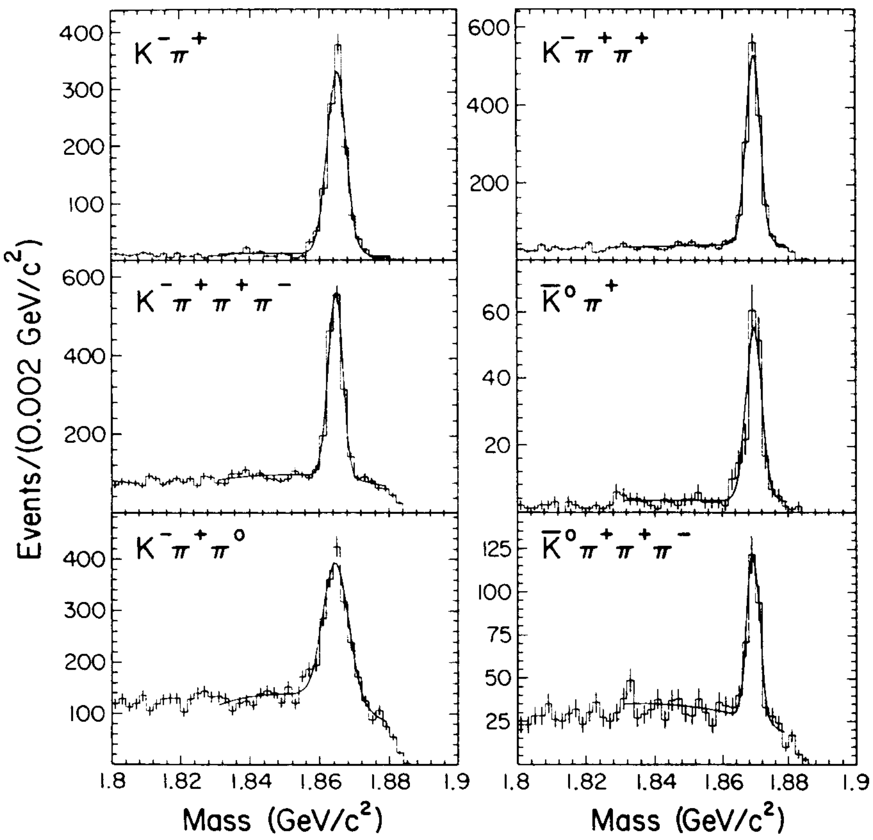

Figure 10: Mark-III hadronic D^0 and D^+ tag signals used to measure semileptonic D branching ratios.[37]

rest and do not move a measurable distance before decaying, so in the foreseeable future, it will not be possible to measure B lifetimes directly at the $\Upsilon(4S)$ experiments. The most successful techniques used in the fixed target experiments for determining charmed lifetimes, with emulsion targets and silicon microvertex detectors at the target plane, are not yet fully developed for b lifetime measurements, but are expected to be practical in the near future.

Ideally, the B-hadron lifetime may be measured by determining the B decay length and the B momentum. When relying on partially reconstructed B hadrons to measure the b lifetime, neither the decay length nor the momentum are well measured. The most widely used method of measuring the B hadron lifetime is to tag a lepton from b decay and measure the miss distance of the lepton track to the primary event vertex.

2.3.1 Using Leptons to Tag B's

At e^+e^-colliders, leptons are relatively easy to identify. B's are heavy (relative to the QCD scale $\Lambda_{QCD} \simeq .1\,\mathrm{GeV}$), so that light quark QCD fragmentation doesn't slow them down much when they hadronize, as illustrated in Figure 12.

Leptons from semileptonic B decay tend to have high energy relative to the

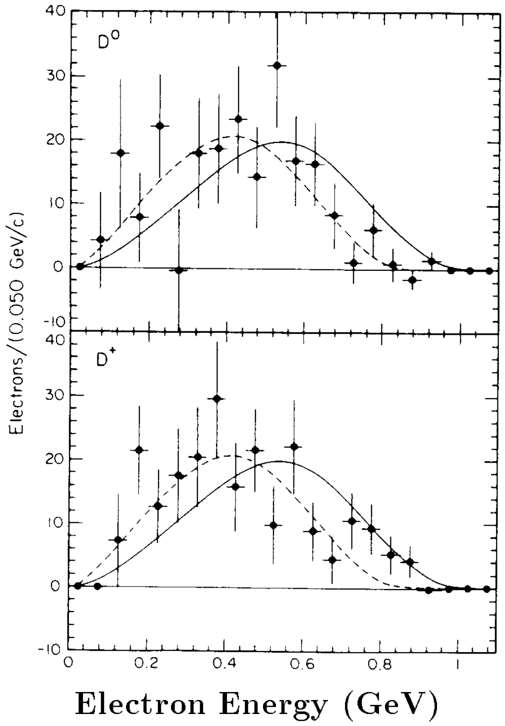

Figure 11: Mark-III electron spectra in D^0 and D^+ tagged events. Curves are the expected spectra for $D \to Ke\overline{\nu}_e$ (solid) and $D \to K^*e\overline{\nu}_e$ (dashed). [37]

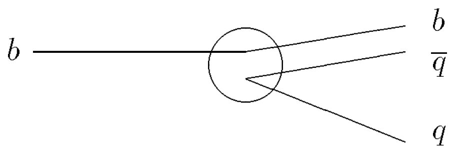

Figure 12: Due to hard heavy quark fragmentation, the b quark direction is approximately the B hadron direction, and the b quark energy goes almost entirely into the B hadron's energy.

beam energy. Furthermore, since leptons from B decay have a high momentum in the B rest frame, they often have very high p_{T} with respect to the B direction. Particularly at LEP, jets are narrow and approximate the B direction quite well. The b-quark direction is typically approximated by the 'jet direction' or 'thrust axis'.

A physics process of interest in measuring semileptonic branching ratios or B-hadron lifetimes is direct $b \to l$ decay. Backgrounds, due to both 'fake' leptons, and leptons from non-b sources complicate the measurement. The signal, as well as the background processes from primary charm, and cascade decays of $b \to c \to l$ or $b \to \tau \to l$ are depicted in Figure 13.

a) $b \to l^-$

b) $c \to l^+$

c) $b \to c \to l^+$

d) $b \to \overline{c} \to l^-$

d) $b \to \tau^- \to l^-$

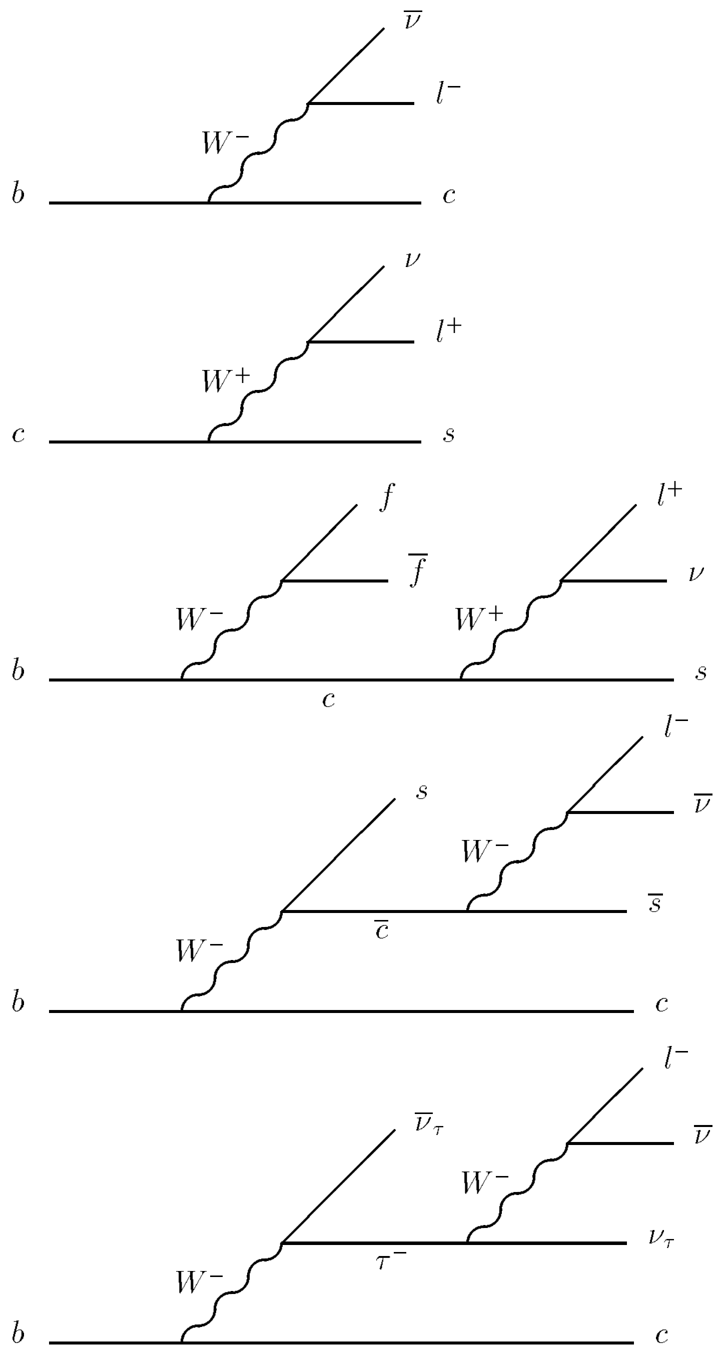

Figure 13: Lepton sources: a) signal b) primary charm background c) & d) cascade $b \to c \to l$ decays to lepton of either sign e) $b \to \tau \to l$ decays.

2.3.2 Lepton Selection

Leptons are typically selected by making use of particle identification capabilities of the detector. In an e^+e^-detector, this involves for:

Electrons: dE/dx in the drift chamber, energy deposition in the electromagnetic calorimeter compared to momentum in drift chamber and

	longitudinal and lateral shower energy deposition in the electromagnetic calorimeter.
Muons:	minimum ionizing deposition in electromagnetic and hadron calorimeters, and track segments in μ-chambers behind the hadron calorimeter.

Backgrounds are typically due to:

- K, π which decay in flight, producing μ's
- Hadronic 'punchthrough' to μ chambers
- $\pi^{\pm}$ π^0 overlap in calorimeter which can fake electrons
- Dalitz decays, $\pi^0 \rightarrow \gamma\ e^+\ e^-$ provide a copious source of electrons, but fortunately most are at very low energies.
- Photons may converted in the beampipe or in interfaces between chambers where there is lots of material: $\gamma_c \rightarrow e^+\ e^-$.

The lepton parent composition as a function of momentum and transverse momentum is shown in Figure 14. The higher p and p_{T} regions have a much larger b-quark enrichment.

2.3.3 The Impact Parameter Method

The 'signed 2D-impact parameter' technique is the 'classic' method [20, 38] to measure average B hadron lifetime. The B decay length is given by $l = \beta\gamma c\tau_B$. The impact parameter is the distance of closest approach from a track to the primary production vertex. The signed 2-dimensional impact parameter, δ, illustrated in Figure 15, is the projection of this distance of closest approach onto the plane perpendicular to the beam direction (the xy plane). Until recently, the extrapolated track resolution in the z direction has been typically much worse than the resolution in the xy plane, and the luminous region in an e^+e^-machine has much smaller dimensions in the xy plane than in the z direction.

$$\delta = l \sin\psi |\sin\theta| \tag{20}$$

$$= \gamma\beta c\tau \sin\psi |\sin\theta| \qquad \text{(See Figure 15)} \tag{21}$$

The impact parameter of a lepton track from semileptonic B decay, averaged over all types of B hadrons, averaged over decay lengths, fragmentation kinematics and production fractions, is proportional to the average lifetimes of all species of B hadrons, τ_i, weighted by their semi-leptonic branching fractions, f_i:

$$\overline{\tau_b} = \sum_i f_i \tau_i \tag{22}$$

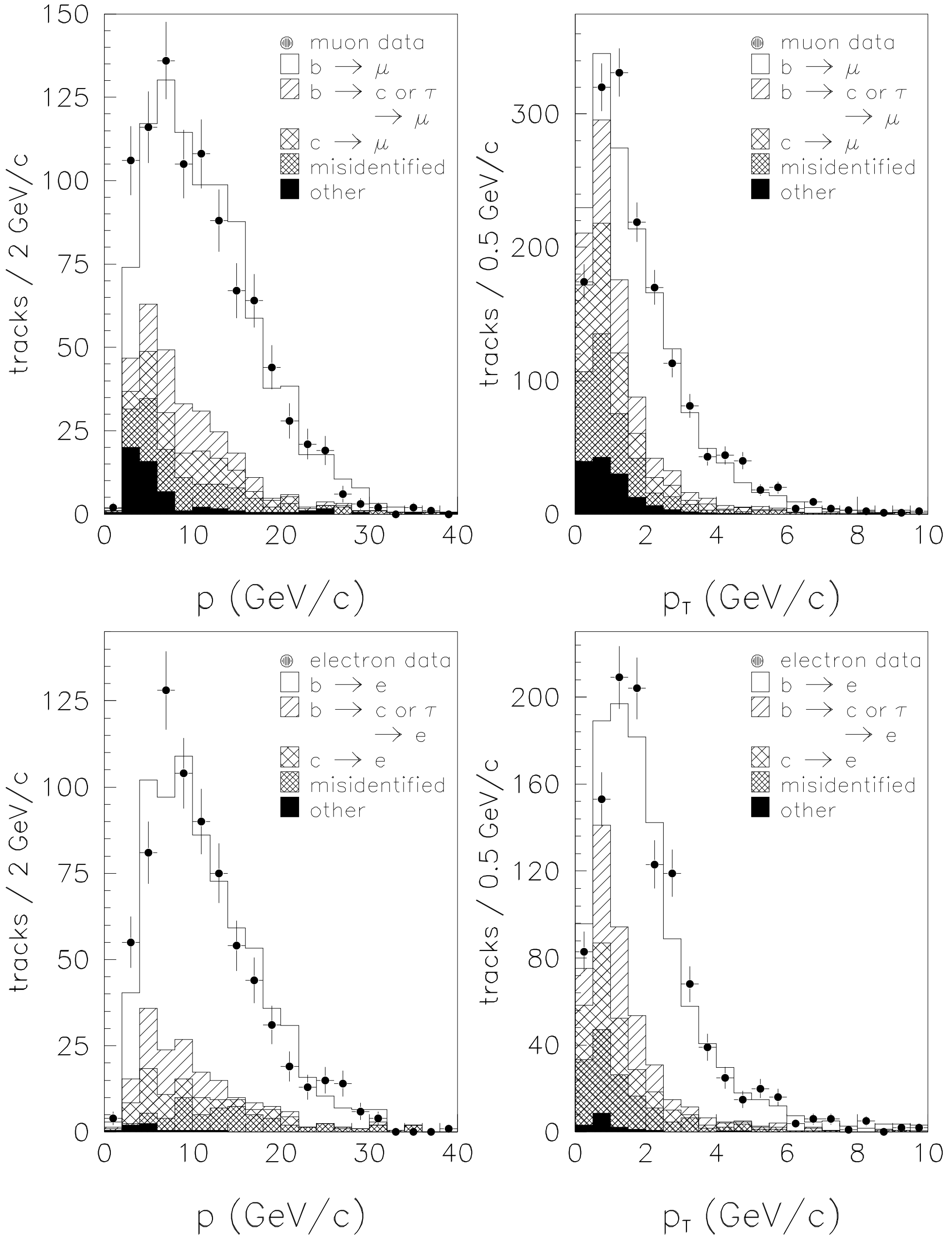

Figure 14: Momentum and transverse momentum distributions of lepton candidates, for the electron and muon samples at OPAL. The data are points with errors, the solid shaded areas are lepton signal and background contributions.

The impact parameter is signed, using the convention that if the lepton trajectory crosses the thrust axis in the same (opposite) hemisphere, the sign is positive (negative). Although the impact parameter is ideally a positive quantity, negative impact parameters are possible due to tracking resolution, imperfect jet axis determination, mistracking, and other systematic errors.

For example, at OPAL the average B hadron lifetime measurement has been performed using high p, high p_{T} leptons. The impact parameter distributions

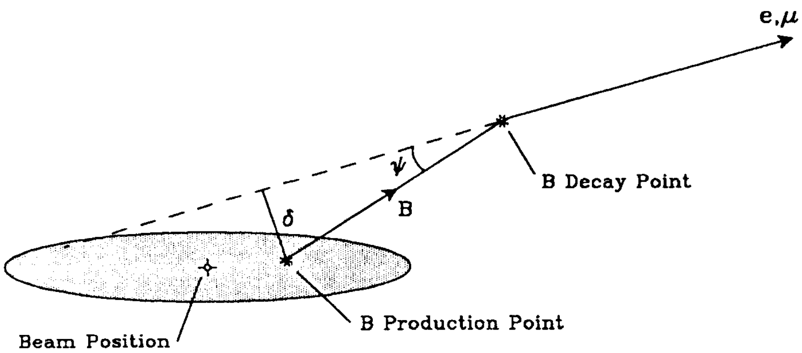

Figure 15: The 2-D signed impact parameter method. The 2-D projection of the B trajectory is labeled B, δ is the impact parameter.[38]

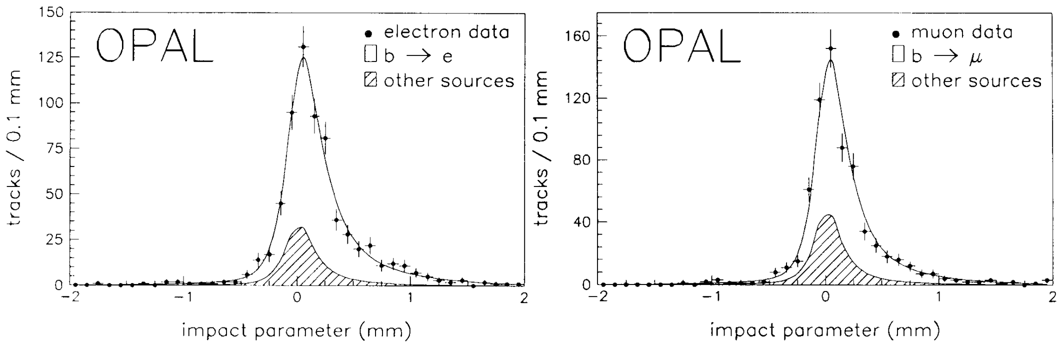

Figure 16: Impact parameter distributions for muon and electron candidates. The shaded areas shows background contributions.[39]

for muon and electron candidates are shown in Figure 16.

The impact parameter distribution is fit to a sum of impact parameter distributions from semileptonic B decays and background components. The resulting τ_b from OPAL is [39]:

$$\tau_b \;=\; 1.37 \;\pm\; .07 \;\pm .06 \text{ ps} \tag{23}$$

Experimental results for average B hadron lifetimes are summarized in Table 3.

No one had expected the b quark to live this long! If however $|V_{cb}| \simeq \cos^2\theta_C \simeq .045$, then the spectator model describes the average b lifetime very well. A new type of hierarchy problem has been introduced here though: why are the $2^{nd} - 3^{rd}$ generation quark couplings so much smaller than the $1^{st} - 2^{nd}$ generation quark couplings?

The KM matrix element $|V_{cb}|$ may be extracted from this lifetime measurement:

$$\frac{Br\,(B \to Xl\overline{\nu})}{\tau_b} = \Gamma\,(B \to Xl\overline{\nu}) = K_c \mid V_{cb} \mid^2 \;+\; K_u \mid V_{ub} \mid^2 \tag{24}$$

where K_c and K_u are derived from theoretical models and fundamental constants. Using the world average B lifetime, and an average of two semileptonic

PEP & PETRA, e^+e^- 20 − 44 GeV:

Experiment	B $\tau(10^{-13}s)$
Mark-II	$9.8 \pm 1.2 \pm 1.3$
JADE	$13.6 \pm {}^{2.5}_{2.3}$
TASSO	$13.5 \pm 1.0 \pm 2.4$
DELCO	$11.7 \pm {}^{2.7}_{2.2} \pm {}^{1.7}_{1.6}$
MAC	$12.9 \pm 2.0 \pm 2.1$
HRS	$10.2 \pm {}^{4.2}_{3.9}$

LEP, e^+e^- 90 GeV:

Experiment	B $\tau(10^{-13}s)$
ALEPH	$14.9 \pm 0.3 \pm 0.6$
DELPHI	12.8 ± 1.0
OPAL	$13.7 \pm 0.7 \pm 0.6$
L3	$13.2 \pm 0.8 \pm 0.9$
LEP Average	14.0 ± 0.40

Table 3: Experimental τ_b results, Impact Parameter Method, from References [40, 38, 41, 39].

decay models to deduce K_c and K_u (described and compared with experiment in Sections 4.1 4.3, and 4.4), we obtain: $V_{cb} = .043 \pm .008$. As we shall examine in detail later, uncertainties in theoretical modeling dominate the error, so that interpretation of the average B hadron lifetime is dominated by systematic uncertainties in the theory.

While the spectator model does an acceptable job in describing the average B hadron lifetime, there are clear shortcomings of the spectator model, particularly in the charm sector.

3 Weak Decay Theory

At this point, the simple spectator model does not appear to be the ultimate reality as far as weak decays of heavy quarks are concerned. Non-spectator effects, such as QCD, Pauli interference, final state interactions, and non-spectator diagrams do appear to play a role in weak decays.

A slightly more realistic picture of weak decay is depicted in Figure 17. The weak interaction occurs in the small inner circle, while the confinement region is the large outer circle in Figure 17. Due to QCD confinement, it is evident that both electroweak and strong QCD effects play a role in weak decays. On the short distance scale, the weak interaction and QCD hard gluon radiation may both be exactly calculated. The long distance QCD effects, which include final state interactions, soft gluon radiation, and confinement of quarks to form hadrons, and bound state effects, cannot be calculated perturbatively in QCD:

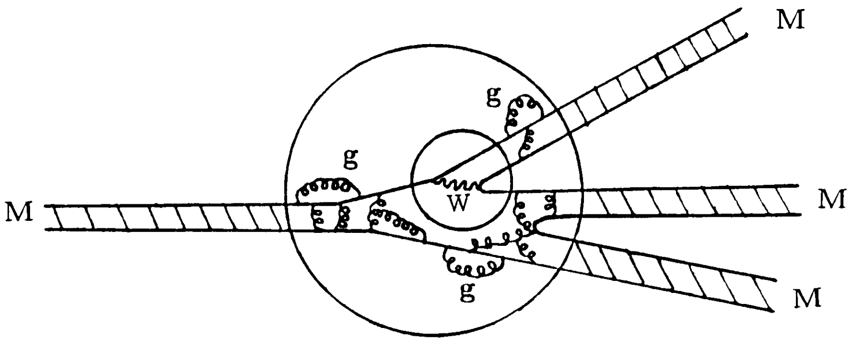

Figure 17: The weak decay involves both electroweak and strong QCD effects. The weak interaction occurs in the small inner circle, with the W intermediate vector boson, while the QCD confinement region is the larger outer circle. Initial and final state mesons are denoted M, and some of the soft gluons are denoted g.

Weak Interaction – Small scale	Exactly Calculable
Hard Gluon Radiation – Small scale	Exactly Calculable
QCD Confinement – Larger scale	Non-Perturbative

Decoupling or factorization [42, 43] simplifies the weak decay problem into two distance scales, and lets us calculate at least some of the QCD corrections, the short range dynamics part, along with the weak interaction. Phenomenological models are still needed to calculate the long-range, non-perturbative QCD effects.

3.1 Hard Gluon Corrections to Spectator Decay

Following the formalism of Rückl [44], the bare spectator Hamiltonian for b decay (with $q \ll M_W$, i.e. point approximation) may be written:

$$\begin{aligned}\mathcal{H}^0_{\Delta b=-1} &= \frac{G_F}{\sqrt{2}}\left[V_{cb}(\overline{c}b)_L + V_{ub}(\overline{u}b)_L\right]\ \Big[V^*_{ud}(\overline{d}u)_L + V^*_{us}(\overline{s}u)_L + V^*_{cd}(\overline{d}c)_L \\ &\qquad + V^*_{cs}(\overline{s}c)_L + (\overline{e}\nu_e)_L + (\overline{\mu}\nu_\mu)_L + (\overline{\tau}\nu_\tau)_L\Big] \qquad (25)\end{aligned}$$

and the analogous expression for charm decay:

$$\mathcal{H}^0_{\Delta c=-1} = \frac{G_F}{\sqrt{2}}\Big[V_{cs}(\overline{s}c)_L + V_{cd}(\overline{d}c)_L\Big]\ \left[V^*_{ud}(\overline{u}d)_L + V^*_{us}(\overline{u}s)_L + (\overline{\nu}_e e)_L + (\overline{\nu}_\mu \mu)_L\right] \qquad (26)$$

where we use the notation $(\overline{c}b)_L \equiv \overline{c}\gamma^\mu(1-\gamma_5)b$.

In most of the following discussion, only the leading term of the Hamiltonian is retained, for simplification purposes only. The leading term of the Hamiltonian for lowest order hard gluon effects in weak b decay at scale μ is:

$$\mathcal{H}^1 = -\frac{G_F}{\sqrt{2}}V_{cb}V^*_{ud}\ \frac{3\alpha_S}{8\pi}\ \ln\frac{M_W^2}{\mu^2}\ (\overline{c}\lambda_a b)_L(\overline{d}\lambda^a u)_L \qquad (27)$$

where the λ_a's obey SU(3) group algebra. Semileptonic decays obviously have no such hard gluon corrections. The hard gluon corrections have introduced an additional operator which has the same chiral structure as the bare spectator Hamiltonian, $\mathcal{H}^0$. The Fierz transformation may be used to simplify this expression:

$$(\bar{c}\lambda_a b)_L(\bar{d}\lambda^a u)_L = -\frac{2}{3}(\bar{c}b)_L(\bar{d}u)_L + 2(\bar{c}u)_L(\bar{d}b)_L \tag{28}$$

The rearrangement clearly illustrates the effect of hard QCD gluon radiation on the Hamiltonian: The first term on the right of Equation 28 has the same effective weak current structure as the original bare Hamiltonian. The second term however, looks like an effective neutral current, which has been induced by hard gluon QCD effects. The Hamiltonian now has a modified leading term:

$$\frac{G_F}{\sqrt{2}}V_{cb}V_{ud}^*\left[\left(1+\frac{\alpha_S}{4\pi}\ln\frac{M_W^2}{\mu^2}\right)(\bar{c}b)_L(\bar{d}u)_L - \frac{3\alpha_S}{4\pi}\ln\frac{M_W^2}{\mu^2}(\bar{c}u)_L(\bar{d}b)_L\right] \tag{29}$$

The strength of the weak current is renormalized, and an effective QCD-induced neutral current is apparent. Hence, both the strength and the structure of the weak interaction is modified by including the effects of short-range hard gluon exchange.

Rückl [44] defines the 4-quark operators:

$$O_\pm \equiv \frac{1}{2}\left[(\bar{c}b)_L(\bar{d}u)_L \pm (\bar{c}u)_L(\bar{d}b)_L\right] \tag{30}$$

so that the bare Hamiltonian with no hard gluon corrections may be written:

$$\mathcal{H}^0 \;=\; \frac{G_F}{\sqrt{2}}V_{cb}V_{ud}^*\left[O_+ + O_-\right] \tag{31}$$

and the Hamiltonian with hard gluon corrections:

$$\mathcal{H} \;=\; \frac{G_F}{\sqrt{2}}V_{cb}V_{ud}^*\left[c_+O_+ + c_-O_-\right] \tag{32}$$

where, to first order, the coefficients are:

$$c_+{}^1 = 1-\frac{\alpha_S}{2\pi}\ln\frac{M_W^2}{\mu^2} \qquad c_-{}^1 = 1+\frac{\alpha_S}{2\pi}\ln\frac{M_W^2}{\mu^2} \tag{33}$$

Rückl [44] used renormalization group methods to extend these scale dependent coefficients to take account of the running of the coupling constant, α_S:

$$c_+ = \left(\frac{\alpha_S(M_W^2)}{\alpha_S(\mu^2)}\right)^{\frac{6}{33-2N_F}} \qquad c_- = \left(\frac{\alpha_S(M_W^2)}{\alpha_S(\mu^2)}\right)^{\frac{-12}{33-2N_F}} \tag{34}$$

where N_F = number of quark degrees of freedom, and α_S, the strong coupling constant, is:

$$\alpha_S(q^2) = \frac{4\pi}{(\frac{33-2N_F}{3})\ln(q^2/\Lambda_{QCD}^2)} \tag{35}$$

To simplify comparison with data, Rückl rewrites the Hamiltonian in terms of the regular charged current term, and the new induced colour mixed term:

$$\mathcal{H} = \frac{G_F}{\sqrt{2}} V_{cb} V_{ud}^* \left[\, c_1 \, (\overline{c}b)_L (\overline{d}u)_L + \, c_2 \, (\overline{c}u)_L (\overline{d}b)_L \right] \tag{36}$$

$$c_1 = \frac{1}{2}(c_+ + c_-), \quad c_2 = \frac{1}{2}(c_+ - c_-) \tag{37}$$

These coefficients are: [45]

$$\begin{array}{l} \text{At } \mu = m_c = 1.5 \text{ GeV}, \; c_1 \approx 1.21, \quad c_2 \approx -.42 \\ \text{At } \mu = m_b = 5.0 \text{ GeV}, \; c_1 \approx 1.1, \quad\; c_2 \approx -.24 \end{array}$$

The case with no QCD corrections is simply $c_1 = 1$ and $c_2 = 0$. These predictions make it simple to measure decay amplitudes and then to compare them with the amplitudes derived from these theoretically predicted coefficients.

The general features of heavy quark decay widths including the hard QCD corrections in terms of the c_+ and c_- coefficients is apparent:

- The b and c hadronic widths increase:

$$\begin{aligned} \Gamma(c \to su\overline{d}) = & \; (2c_+^2 + c_-^2) \tfrac{{G_F}^2 {m_Q}^5}{192\pi^3} \\ \simeq & \; 3.9 \; \tfrac{{G_F}^2 {m_Q}^5}{192\pi^3} \end{aligned} \tag{38}$$

Recall that the simple spectator model predicted:

$$\Gamma(c \to su\overline{d}) \simeq 3.0 \; \frac{{G_F}^2 {m_Q}^5}{192\pi^3} \tag{39}$$

- A larger total width implies that the c and b lifetimes decrease.

- A larger total width implies that the semileptonic branching ratios decrease:

$$Br(c \to se\overline{\nu}_e) \simeq \frac{1}{2 + 2c_+^2 + c_-^2} \simeq 16\% \tag{40}$$

whereas the spectator model predicted Br($c \to se\overline{\nu}_e$) = 20%.

- An effective neutral current is QCD-induced: there is no *real* flavour changing neutral current; this modification is simply due to the exchange of hard gluons between quarks. It is colour rearranged, and sometimes referred to as a "colour suppressed" interaction.

The modified weak Hamiltonian is represented in Figure 18.

Bauer, Wirbel and Stech [45, 46] extended the work of Rückl, starting with the Hamiltonian corrected for hard gluon radiation in Equation 36:

$$\mathcal{H}_{\Delta b=-1} = \frac{G_F}{\sqrt{2}} V_{cb} V_{ud}^* \left[\, c_1(\mu) \, (\overline{c}b)_L (\overline{d}u)_L + \, c_2(\mu) \, (\overline{c}u)_L (\overline{d}b)_L \right] \tag{41}$$

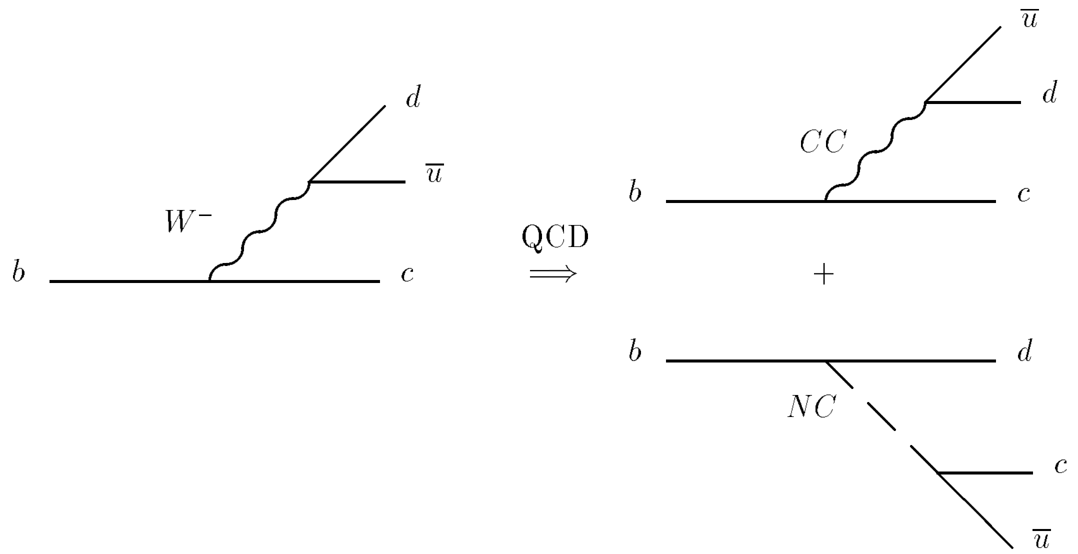

Figure 18: The effect of QCD hard gluon corrections to the weak Hamiltonian.

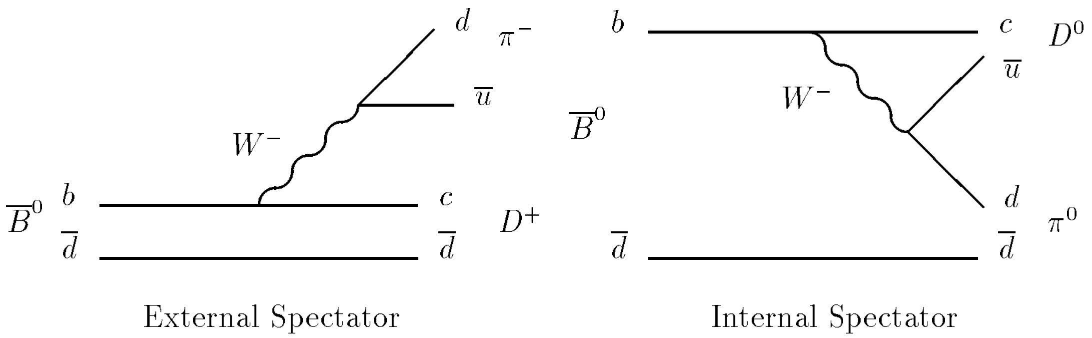

Figure 19: B decay via external spectator diagram, and via internal colour-rearranged spectator diagram.

The first term is the spectator term, renormalized by the factor $c_1(\mu)$, while the second term is the colour rearranged term. These are shown as the external spectator and internal (colour rearranged) spectator diagrams in Figure 19.

Bauer, Wirbel and Stech introduce a_1 and a_2 to quantify 'colour-matching':

$$a_1 = c_1 + \xi c_2, \qquad a_2 = c_2 + \xi c_1 \tag{42}$$

using arbitrary a_1 and a_2, in place of the QCD-determined c_1 and c_2. They proceed to factorize weak decays in terms of a_1 and a_2, and then compare amplitudes with those experimentally determined in order to get some insight into ξ, the colour matching/suppression effects.[47] We naïvely suspect $\xi = \frac{1}{N_c} = \frac{1}{3}$ from colour counting in QCD. Note that $\xi = 1$ corresponds to no colour suppression, while $\xi = \frac{1}{3}$ is expected from crude colour counting.

$\overline{B}^0$ Decay Modes		B^- Decay Modes	
$D^+\pi^-$	$D^+D_s{}^-$	$D^{*0}\pi^-$	$\psi'K^-$
$D^{*+}\pi^-$	$D^{*+}D_s{}^-$	$D^0\pi^-$	$\psi'K^{*-}$
$D^{*+}\rho^-$	$\psi\overline{K}^0$	ψK^-	$D^0D_s{}^-$
$D^{*+}a_1^-$	$\psi\overline{K^*}^0$	ψK^{*-}	ψK^-
$D^0\rho^0$	$\psi'\overline{K}^0$		
$\psi'\overline{K^*}^0$			

D^0, D$^+$, and D* decay modes:

$D^0 \to K^-\pi^+$	$D^+ \to K_S^0\pi^+$	$D^{*+} \to D^0\pi^+$
$D^0 \to K_S^0 - \pi^+\pi^-$	$D^+ \to K^-\pi^+\pi^+$	$D^{*0} \to D^0\pi^0$
$D^0 \to K^-\pi^+\pi^-\pi^+$	$D^+ \to K_S^0\pi^+\pi^-\pi^+$	
$D^0 \to K^-\pi^+\pi^0$		

Table 4: Two body B decays investigated at ARGUS/CLEO

3.1.1 Comparing the Bauer, Stech and Wirbel Model with Data

Prediction for the non-leptonic widths of most conceivable two-body B^0, B$^+$, D^0, D$^+$, and D$_S^+$ decays were calculated by Bauer, Stech and Wirbel [46, 45, 48] in terms of a_1 and a_2, under the factorization approximation. They calculated and tabulated over 150 two-body decays! For example, the decay $D^0 \to K^-\pi^+$ is purely external spectator, hence has a pure a_1 amplitude, with $\Gamma = 9.92a_1^2 \times 10^{10}\mathrm{s}^{-1}$. The decay $D^+ \to \overline{K}^0\pi^+$ has contributions from both internal and external spectator diagrams, and has width $\Gamma = 9.98\ (a_1^2 + 1.23a_2^2\ ) \times 10^{10}\mathrm{s}^{-1}$.

For D decays at Mark-III, Bauer and Stech[46] fit D branching ratios and found consistent results for a fit of 13 two-body D^0 and D$^+$ decay channels.

$$a_1 = 1.2 \simeq c_1(m_c); \quad a_2 = -.7 \simeq c_2(m_c) \tag{43}$$

This implies that ξ is close to 0, the case of maximal colour suppression. They rule out $\xi = 1$, which corresponds to no colour suppression at all.

In the case of B decays, both ARGUS [49] and CLEO [50] have only recently obtained enough statistics to reconstruct enough B decays to investigate the two-body B decays listed in Table 4. As an example of exclusive B reconstruction statistics, some of the B's reconstructed by ARGUS are shown in Figure 20.[49] Note that although the statistics are low in each channel depicted in Figure 20, all the two body channels may be used together to test the hadronic factorization decay model and fit globally for the a_1 and a_2 of BSW.

CLEO's compilation of the branching ratios for many two-body B decays is shown in Figure 21. Both CLEO and ARGUS have performed global fits for the a_1 and a_2 BSW parameters, and they may be compared with the predictions of

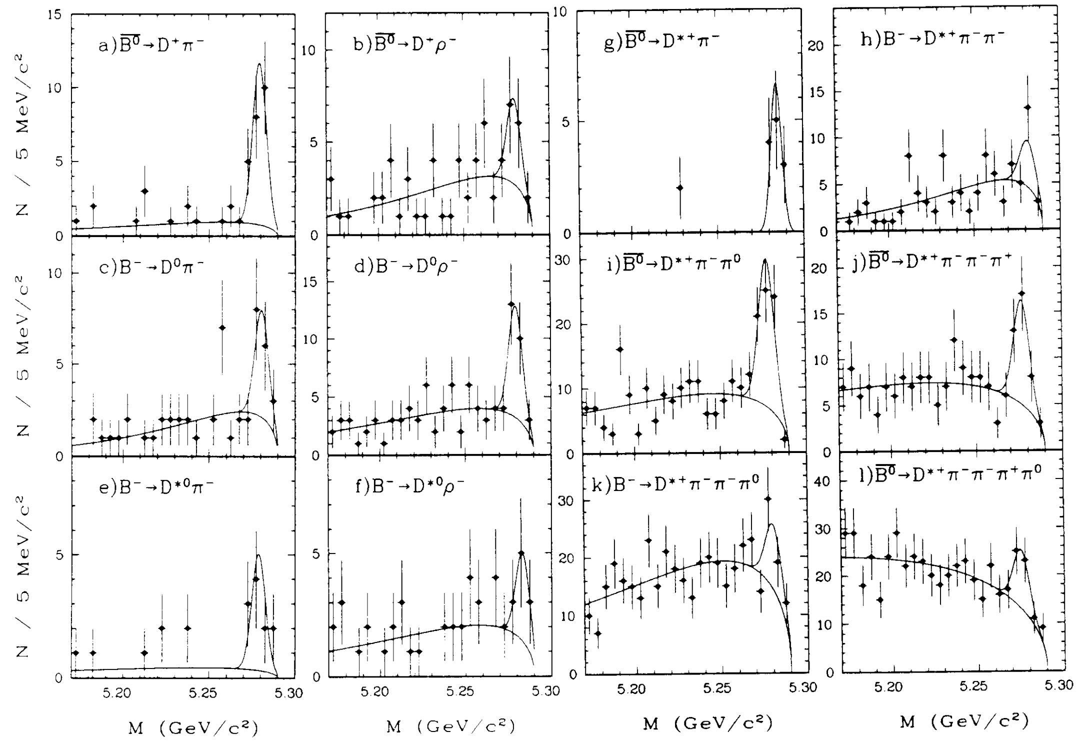

Figure 20: An example of some of mass distributions for exclusive B decays reconstructed with the ARGUS detector. Fits to the B signal and background are shown as solid lines.[49]

Experiment	a_1	a_2	χ^2/N_{DF}
CLEO a	.85±.06	.19±.13	10.1/10
CLEO b	.92±.07	-.17±.03	17.8/10
ARGUS a	.87±.08	.19±.03	9.2/10
ARGUS b	1.03±.09	-.20±.03	6.5/10

Table 5: Results of ARGUS and CLEO fits to the a_1 and a_2 parameters of BSW. Each experiment obtains two possible solutions for a_1 and a_2.[49, 50]

BSW [45] for $\xi = 0$: $a_1 = 1.1$ and $a_2 = -.24$. The ARGUS and CLEO global fit results to a_1 and a_2 parameters are in Table 5. Each experiment obtains two almost equally probable solutions, one of which agrees very well with the theoretical prediction. Additional information, such as input from fits to D decays [46], favour the solution with a relative negative sign, which is close to the theoretically predicted solution.

Therefore two-body hadronic widths are consistent with the BSW factorization model, and ξ is close to 0.

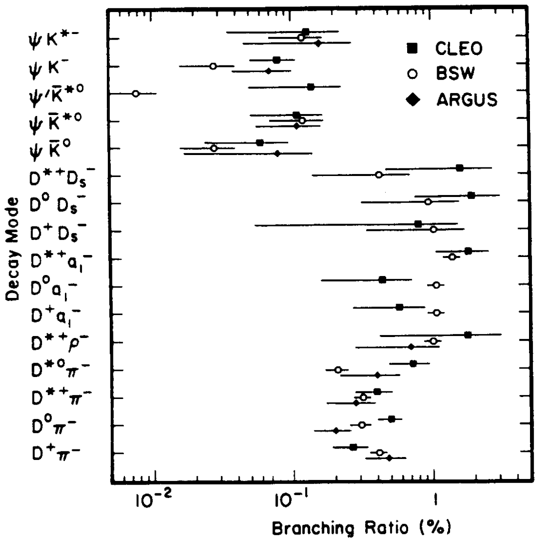

Figure 21: CLEO and ARGUS measurements of two-body B decay modes and the predictions of the Bauer, Stech and Wirbel factorization model.[50]

3.2 Non-Spectator Effects in Weak Decays

The crude spectator model cannot account for the semileptonic and hadronic branching ratios observed, but by considering the effects of hard gluon radiation, the observed D and B hadronic branching ratios can be well-modeled, as was seen in Section 3.1.1. The inclusion of hard gluon radiation, however, does not account for the noticeably different lifetimes of D^0, D^+, and D_S^+ mesons.

It may be concluded that the charm quark alone does not determine charm-hadron decay.

In the D system, at least, the non-leptonic decays must be enhanced, because the ratio of the semileptonic widths is compatible with the lifetime ratio, as we naïvely expected, and was observed by Mark-III, (in Section 2.2).

There are two more effects which we shall consider, which do pose solutions to the problem of differences in lifetimes. They are:

- Interference between final states
- Annihilation and exchange diagram decays

3.2.1 Interference Effects

Consider the analogous external and internal spectator $D^+ \to \overline{K}^0\pi^+$, and $D^0 \to K^-\pi^+$ and $\overline{K}^0\pi^0$ decays, shown in Figure 22.

The Pauli principle tells us that the identical $\overline{d}$ quarks in the D^+ decays can interfere. In fact, in the case of the D^+ decay, not only are the $\overline{d}$ quarks identical, but the final states accessible through two different diagrams are identical, and are expected to interfere as well. It can be shown that the interference is destructive.[44]

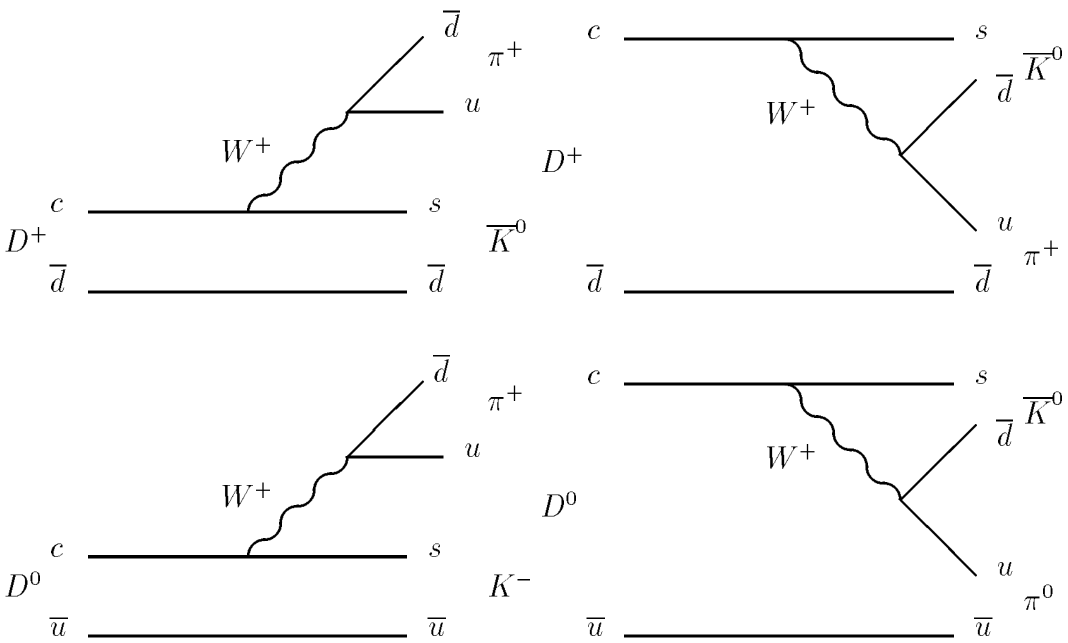

Figure 22: External and internal spectator decays of D mesons. In the D^+ case, the same final state is accessible through both diagrams, and these processes are expected to interfere. In the D^0 case, such identical final states are not accessible through the two different diagrams.

This interference would account for the D$^+$ lifetime being longer than that of the D^0, but only by up to $\simeq$30%, as shown by Rückl.[44] Rückl also calculates that in the B system, the strength of interference is reduced by:

$$\left(\frac{f_D}{f_B}\right)^2 \left(\frac{M_D}{M_B}\right)^2 \tag{44}$$

where f_D and f_B are the pseudoscalar meson form-factors, and M are masses. Interference is therefore expected to be smaller in the B system than in the D system by about an order of magnitude.

This 30% effect is a significant step in the right direction towards explaining the lifetime differences in the D system, but is not by itself enough.

3.2.2 Annihilation and Exchange Diagram Decays

In the light quark limit, annihilation processes are strongly suppressed by the same helicity argument that makes $\pi^- \to e^-\overline{\nu}_e$ suppressed relative to $\pi^- \to \mu^-\overline{\nu}_\mu$. It has been shown [51] that the presence of soft spin 1 gluons can greatly reduce helicity suppression, so that the amplitude of a non-spectator annihilation or exchange diagram could be quite large. (There are soft gluons flinging around everywhere!)

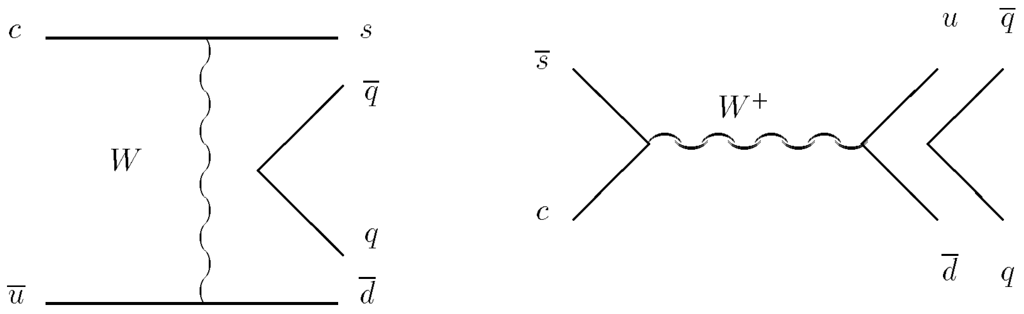

Figure 23: Non-spectator contributions to the weak decay amplitudes in the cases of D^0 and $D_S{}^+$.

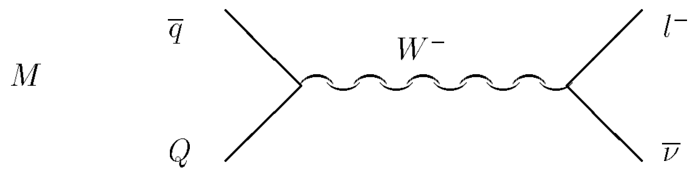

Figure 24: Purely leptonic annihilation of a heavy pseudo-scalar meson.

In the case of the D^0, the exchange diagram has no Cabibbo-like suppression, and the width $D^0 \rightarrow \phi K^0$ is:

$$\Gamma = \left| \frac{G_F}{\sqrt{2}} V_{cb} V_{ud}^* \; a_2 < K\phi | J_\mu | 0 > < 0 | J^\mu | D^0 > \right|^2 \tag{45}$$

where the a_2 is the amplitude factor in the BSW model and the vacuum insertion $|0 > < 0|$ is applied, so that the $< 0|J^\mu|D^0 >$ term is the D form-factor times momentum transfer, $-if_D p^\mu$. The extra non-spectator contributions to the amplitudes for D^0 and $D_S{}^+$ decays are shown in Figure 23. There are no analogous non-spectator, non-Cabibbo-suppressed equivalent diagrams for D^+, so we predict that it will have a smaller decay amplitude and therefore longer lifetime than the other D mesons: $\tau(D^+) > \tau(D^0) \simeq \tau(D_S)$. The proposition that the size of the non-spectator amplitudes are large enough to account for such large lifetime differences is still a hotly debated issue [45, 52], as many of the hadronic decay channels accessible through annihilation diagrams are also possible via final state interactions and rescattering effects.

3.2.3 Purely Leptonic Annihilation Decays

The purely leptonic pseudoscalar meson $\mathrm{M}(Q\overline{q})$ decay $M \rightarrow l\overline{\nu}_l$ is shown in Figure 24. Measurement of such a decay process gives the coupling of the weak hadronic current to the vacuum, or the matrix element:

$$< 0|J_\mu|Q\overline{q} >= -if_M p_\mu \tag{46}$$

The decay width for the leptonic annihilation process is :

$$\Gamma(M \to l\overline{\nu}_l) = \frac{G_F^2}{8\pi}|V_{qQ}|^2 f_M^2 \; m_M \; m_l^2 \left[1 - \frac{m_l^2}{m_M^2}\right]^2 \tag{47}$$

Due to helicity suppression, the rates are very small; vanishing to zero as the mass of the lepton, m_l, decreases.

3.2.4 PseudoScalar Meson Form Factors at WA-75

Until just a few months ago, only the pseudo-scalar meson form-factors $f_\pi = .13$ GeV and $f_K = .16$ GeV had been measured. Recently, f_{D_S} has been measured as well, by the WA75 hybrid emulsion experiment [53] at the CERN SPS. They report observation of the decay $D_S^+ \to \mu^+\nu_\mu$, with branching ratio:

$$\mathrm{Br}(D_S^\pm \to \mu^\pm\nu_\mu) = 4.0 \pm \begin{matrix}1.8\\1.4\end{matrix} \pm \begin{matrix}.8\\.6\end{matrix} \pm 1.7) \times 10^{-3} \tag{48}$$

From this measurement we can deduce the form-factor:

$$f_{D_S} = (232 \pm 45 \pm 20 \pm 48)\mathrm{MeV} \tag{49}$$

which agrees with theoretical expectations.[54] This may be taken as direct evidence for the existence of non-spectator heavy flavour decays, because no final state rescattering or soft effects are present in a purely leptonic final state.

Now that the form factor has been measured, it may be used to predict Br($D_S^+ \to \tau^+\nu_\tau) \simeq (3.7 \pm 2.3)\%$.

In examining the decay $B \to D_S X$, ARGUS [55] has indirectly extracted the weighted average of the $D_S{}^*$ and D_S form-factors, using the BSW model, and HQET(see Section 5):

$$\begin{aligned} f_{D_S}^{(*)} &= (267 \pm 28) \times \sqrt{\tfrac{2.7\%}{\mathrm{Br}(D_s \to \phi\pi)}}\mathrm{MeV} \quad (\mathrm{HQET}) \\ &= (280 \pm 46) \times \sqrt{\tfrac{2.7\%}{\mathrm{Br}(D_s \to \phi\pi)}}\mathrm{MeV} \quad (\mathrm{BSW}) \end{aligned} \tag{50}$$

Additionally, Mark-III has searched for the analogous D annihilation decay, and set a limit on $\mathrm{Br}(D^+ \to \mu^+\nu_\mu) < 7.2 \times 10^{-4}$ at 90% CL, which corresponds to $f_D < 290$ MeV.[56]

We soon hope to measure B decay constant, f_B, via the annihilation decay $B^\pm \to \tau^\pm\nu_\tau$. If $|V_{ub}|/|V_{cb}| \simeq .1$ and $f_B \simeq .3$, we expect $\mathrm{Br}(B^\pm \to \tau^\pm\nu_\tau) \simeq 10^{-4}$.

3.3 Recap on Weak Decays

In Figure 25, the quark level diagrams for heavy quark decay (b quark in this case) are shown. The amplitudes associated with the spectator diagrams are expected to be large. In the case of the charm quark, the non-spectator processes could be competitive with the spectator processes, but in the case

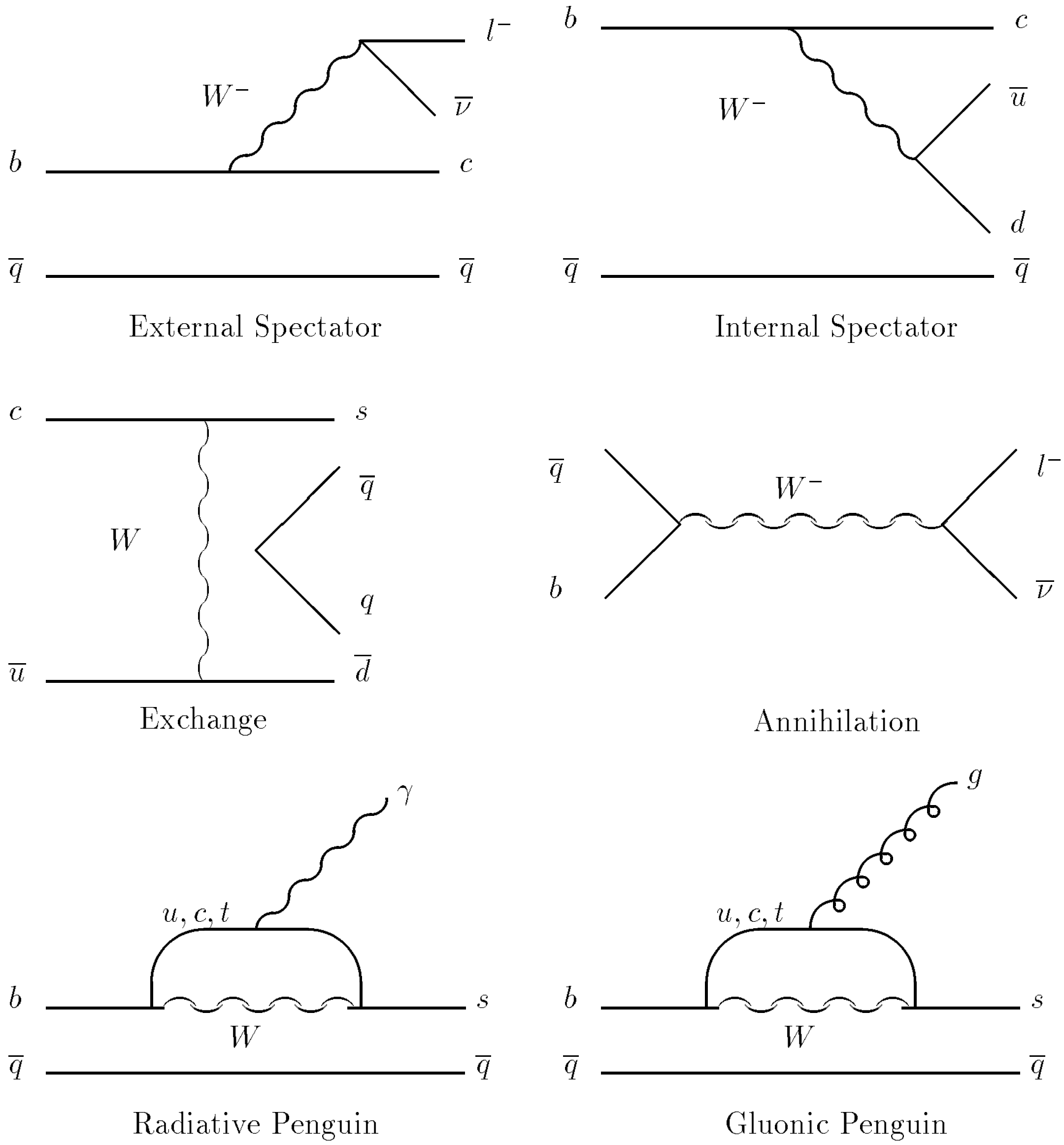

Figure 25: Heavy quark decay diagrams. The first four are tree level spectator and non-spectator decay processes. The penguin decay diagrams are expected to be suppressed due to the small KM matrix elements involved.

of the beauty quark, we expect the non-spectator processes to be small. The one-loop penguin amplitudes in Figure 25 are similarly expected to be highly suppressed, due to the presence of at least one very small KM matrix element.

The theoretical groundwork developed in order to understand weak decays of the charm quark may be applied to help us investigate the beauty system:

What we've learned via extensive studies in the D system:

- The Spectator Model is not so bad.
- It gets even better after including QCD and interference effects.

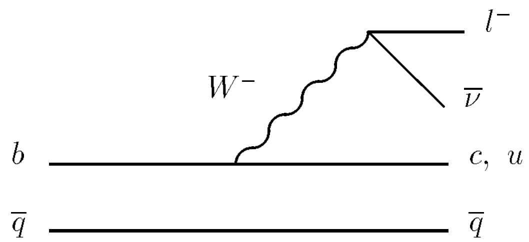

Figure 26: The external spectator diagram relevant for weak semileptonic decay

- The gross features of weak decays, average lifetimes, semileptonic and hadronic decays are predicted well by the spectator model plus QCD corrections.
- In the charm system, non-spectator weak decay effects are non-negligible.
- The present theory explains charm lifetimes, semileptonic branching ratios, and two body hadronic decays reasonably well.

Applications to B System:

- QCD effects are smaller in the B system, the large B mass makes perturbative calculations easier.
- Interference effects are reasonably well understood, and as we saw, they should be smaller in the B system, due to the larger B mass.
- Non-spectator effects in the B system are smaller than in the charm system.
- Annihilation amplitudes in the B system are Cabibbo-suppressed.
- Exchange diagram amplitudes in the B system are smaller due to $m_b \gg m_c$.
- We expect the simple spectator model to be even better in the heavier B system.

4 Semileptonic Heavy Quark Decays

Theoretically, it is much simpler to predict and calculate features of semileptonic heavy quark decay, as only the 'External Spectator' diagram (see Figure 26) is relevant. Since the virtual W decays to leptons, there is no interference between competing amplitudes, and any QCD effects are confined to the hadronic part of the decay. So semileptonic decays are not only easier for experimentalists to reconstruct, but the theory is simpler as well.

Many of the most popular theories assume factorization, so that half the problem, the leptonic part, is exactly calculable. The hadronic part, however, is tough. In general, we write (as in Equation 10):

$$\Gamma_{SL}(B) = \frac{{G_F}^2 {m_b}^5}{192\pi^3} \left(K_1|V_{cb}|^2 + K_2|V_{ub}|^2 \right) \tag{51}$$

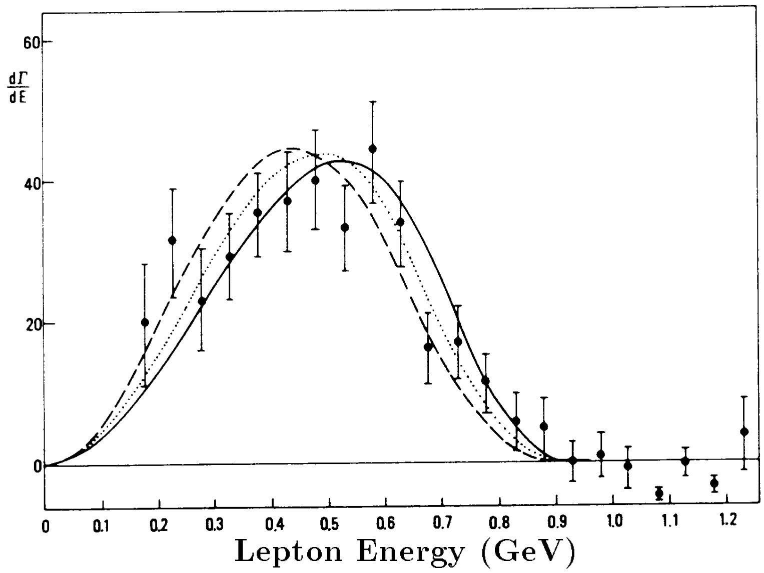

Figure 27: The charged lepton spectrum in D decay from DELCO (in GeV), fit to the ACCMM model, normalized to the number of events, with $p_F = 0$ (solid), .15 (dotted) and .30 (dashed) GeV.[57]

The models use various techniques to calculate K_1 and K_2, to enable extraction of $|V_{cb}|$ and $|V_{ub}|$. (The analogous expression applies for charm, $\Gamma_{SL}(D)$) Unfortunately, the uncertainty in m_b leads to an enormous uncertainty in m_b^5 which makes it difficult to use Equation 51 to extract any precise information on width (or lifetime) and KM matrix elements.

4.1 A Free Quark Model

Historically, one of the earliest successful models of heavy quark semileptonic decay was that of Altarelli *et al.*(ACCMM) [57]. It is an improved spectator model which includes kinematics and the masses of the heavy quark and the light spectator quarks. The lepton spectrum for heavy quark decays includes the Fermi motion of the quarks folded in to the momentum spectrum obtained from free heavy quark decay. A non-relativistic wave function is assumed for the heavy hadron. Soft gluon radiation, which affects lepton spectrum particularly near the high momentum endpoint, is included. The strong m_b dependence in Equation 51 can then be diminished by taking advantage of the kinematics, since the b quark mass is poorly known, while the B meson mass, m_B is well-measured. Then semileptonic branching ratio, p_F (Fermi momentum of the spectator quark), and $\frac{m_c}{m_b}$, (ratio of final and initial state quarks) may be fit to experimental data.

The ACCMM model was fit to D decay lepton spectrum in DELCO data taken at SPEAR ($E_{cm} = 3.77$ GeV)[58], as shown in Figure 27. The agreement between the data and the model is quite good. For charm, if we use the average D lifetime to derive Γ (analogous to Equation 51), in the ACCMM model with a spectator quark mass of .15 GeV and Fermi momentum of .15 GeV, we obtain $|V_{cs}| \simeq 1$, which is consistent with measurements obtained in neutrino charm production experiments. It is interesting to see how well the model fits B data, where the problem is not already over-constrained.

4.2 Exclusive Semi-leptonic Decay Modeling

There are many models for the semileptonic decay of heavy quarks. The standard approach is to factorize the decay into a purely hadronic part and a purely leptonic part. For example the decay $B \to Dl\overline{\nu}$ may be factorized:

$$\text{Amplitude}\,(B \to Dl\overline{\nu}) = \underset{\text{Tough!}}{\underset{\Uparrow}{< D|J_\mu|B >}} \quad \underset{\text{Easy}}{\underset{\Uparrow}{< \nu|J_\mu|l >}} \tag{52}$$

To describe the hadronic part, the procedure is to write down all Lorentz invariant variables; in semileptonic pseudoscalar meson decays we consider $B \to D^* l\overline{\nu}$ and $B \to Dl\overline{\nu}$ for example, which are of the types $P \to Vl\overline{\nu}$ and $P \to Pl\overline{\nu}$, where P represents a pseudoscalar meson, and V a vector meson. There are two Lorentz invariants for $P \to P$ and four for $P \to V$ type decays. We define form factors as q^2-dependent functions, one multiplying each Lorentz-invariant. It is in the definition of the form factors that the various models tend to differ. Two widely used and successful models by Grinstein, Isgur, Scora and Wise (ISGW)[59] and Wirbel, Stech and Bauer (WSB)[60] will be examined here in detail. Many of the other models are quite similar in spirit to these two, but differ in the phenomenologically inspired form of the form factors. Once the form factors are defined, one may then calculate individually and sum all decay channels that contribute to 3 body semileptonic decay (1 hadron, 2 leptons).

The matrix element for the hadronic current

$$B \to Dl\overline{\nu}_l \qquad \text{of the type} \quad P \to P \tag{53}$$

can be written:

$$< D|J_\mu|B > \equiv < D|f_+(q^2)(p_B + p_D) + f_-(q^2)(p_B - p_D)|B > \tag{54}$$

and, if the lepton masses are ignored, the second term disappears, leaving only one form factor, $f_+(q^2)$.

The ISGW model uses exponential form factors.

The WSB model uses single pole form factors.

For the decay

$$B \to D^* l\overline{\nu}_l \qquad P \to V \tag{55}$$

there are 4 form factors, but, in the approximation of neglecting the lepton masses, only 3 independent form factors remain, one for each of the 3 helicity states of the spin 1 D* meson.

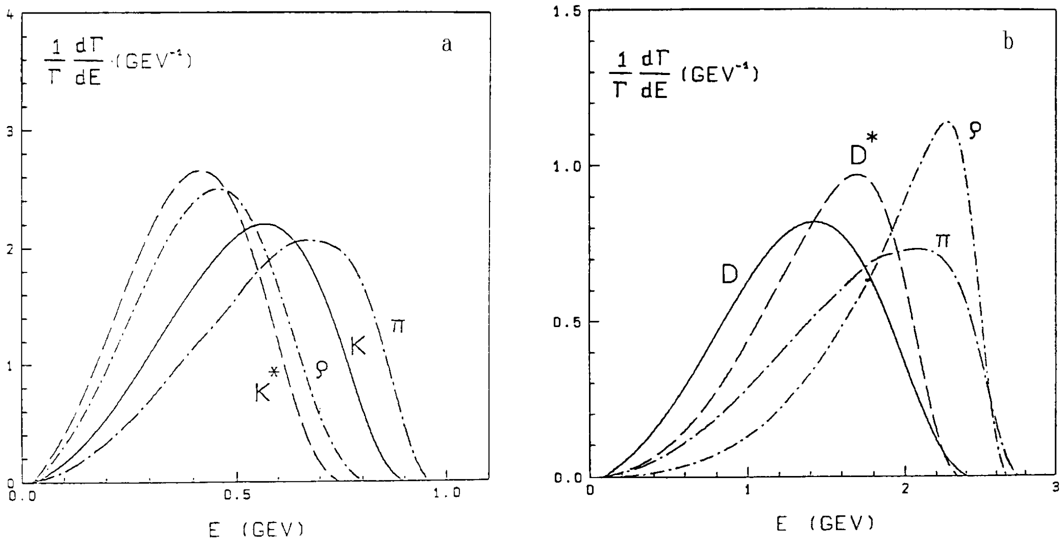

Figure 28: Predicted lepton spectra in the WSB Model.[60]
a) Normalized theoretical spectra for D decays to K, K^*, π and ρ mesons.
b) Normalized theoretical spectra for B decays to D, D^*, π and ρ mesons.

The dominant difference in various models is in the phenomenologically obtained form factors.

4.3 The Wirbel-Stech-Bauer Model

In the WSB model [60], the hadronic current J_μ is written in terms of monopole form factors:

$$f(q^2) \simeq \frac{h}{1 - q^2/M_P} \tag{56}$$

The meson wave functions are solved in a relativistic harmonic oscillator potential. The form factor h represents the overlap of the initial and final state mesons, since $f(q^2 = 0) = h$.

The WSB solutions for semileptonic B and D decays are shown in Figure 28. The theoretical spectrum for D decay to K and K^* mesons fits the DELCO [58] lepton data well, just as was the case for the ACCMM model.

4.4 The Isgur-Scora-Grinstein-Wise Model

In the model of Isgur, Scora, Grinstein and Wise (ISGW) [61, 59] the hadronic matrix element is expressed in terms of a set of Lorentz invariants times form factors. The form factors may then be calculated using a quark model 'mock-meson' [54, 59] method, by making a one-to-one correspondence between the form factors in the hadronic current and those obtained in the quark model solutions, normalizing at zero recoil of the D, (where q^2 is maximum). The meson wave functions are solutions to the Schrödinger equation in a Coulomb plus linear QCD-inspired potential. The final state mesons are summed over

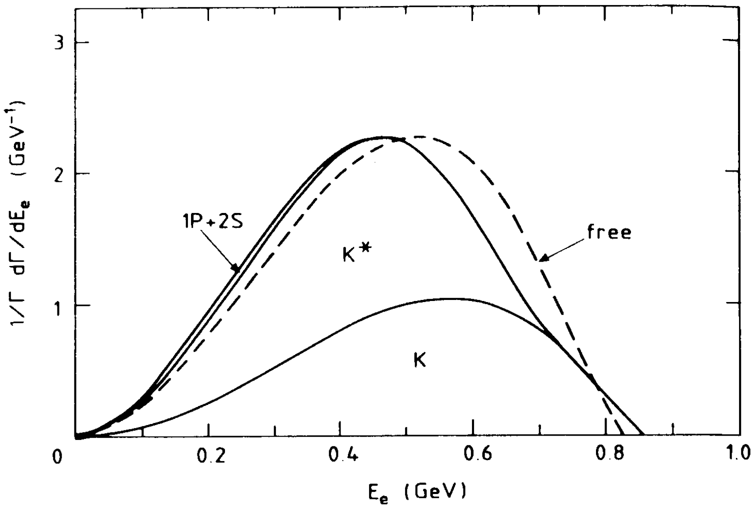

Figure 29: $\frac{1}{\Gamma}\frac{d\Gamma}{dE_e}$ for $D \to X_S e^+\nu_e$ for the ISGW model, showing K and K^* contributions, and the free quark prediction.[59]

1S, 2S and 1P wave functions. There are no normalizations, free parameters, or fudge constants in this model. It predicts:

$$\begin{aligned} \Gamma(D^0 \to X e^+\nu_e) &= \Gamma(D^+ \to X e^+\nu_e) \\ &= .19|V_{cs}|^2 \times 10^{12} s^{-1} \end{aligned} \tag{57}$$

which agrees with world average experimentally obtained results for lifetimes and semileptonic branching ratios quoted by the Particle Data Group [5] if $|V_{cs}| \simeq .97$. Conversely if we use this model to extract $|V_{cs}|$, we obtain a result in agreement with the ν and $\overline{\nu}$ experimental $|V_{cs}|$ results.

In the B system, the prediction is:

$$\begin{aligned} \Gamma(\overline{B}^0 \to X e^-\overline{\nu}_e) &= \Gamma(B^- \to X e^-\overline{\nu}_e) \\ &= .41|V_{cb}|^2 \times 10^{12} s^{-1} \end{aligned} \tag{58}$$

This model may therefore be used to predict $|V_{cb}|$, given the B^+ and B^0 lifetimes and semileptonic branching ratios.

The ISGW spectra for semileptonic D decays is shown in Figure 29. Note that by construction, the model includes only 1S, 2S and 1P contributions; higher order K^* final states are not included, but they are expected to be small. This model fits the DELCO $D \to X e^+\nu_e$ data [58] well, just as the ACCMM and WSB models did.

The ISGW spectra for B decays are shown in Figures 30 and 31, for $b \to c$ and $b \to u$ semileptonic decays, respectively. Note that in the $b \to c$ case, the spectrum is close that of the free quark model. The model predicts 11% p-wave D^{**} mesons in the $b \to c$ spectrum. In the $b \to u$ case, the ISGW spectrum is much softer than that predicted in the free quark model, and the normalizations differ drastically. It is conceded that the 1S, 1P, and 2S states do not saturate the rate in the $b \to u$ case, but the calculation does saturate the

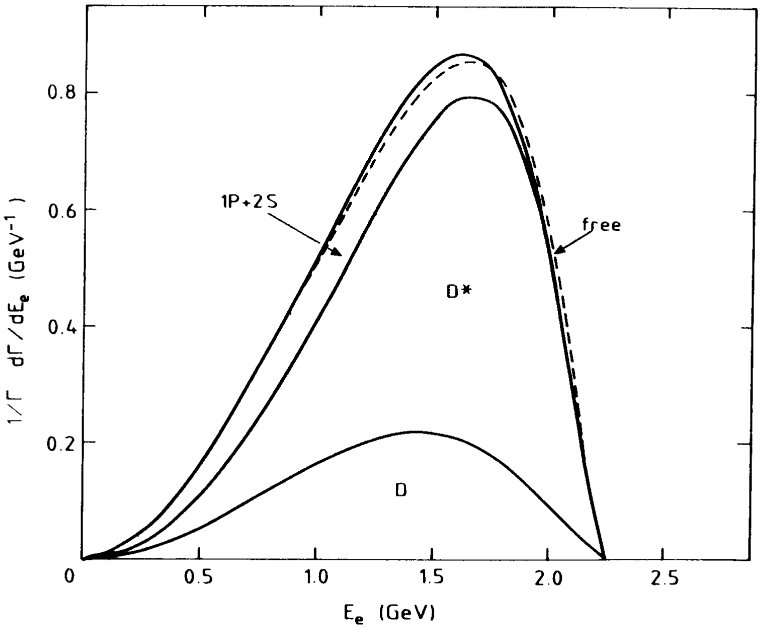

Figure 30: $\frac{1}{\Gamma}\frac{d\Gamma}{dE_e}$ for $B \to X_c e^- \overline{\nu}_e$ in the ISGW model. The free quark prediction is also shown.[59]

contributions in the region of the endpoint of the spectrum above the kinematic limit for $b \to c$ decay.

For $B \to X_c e^+ \nu_e$, the models predict:
$\Gamma_{ISGW} = .41 \times 10^{14} |V_{cb}|^2 s^{-1}$ whereas $\Gamma_{free} = .49 \times 10^{14} |V_{cb}|^2 s^{-1}$

For $B \to X_u e^+ \nu_e$:
$\Gamma_{ISGW} = .43 \times 10^{14} |V_{cb}|^2 s^{-1}$ and $\Gamma_{free} = 1.18 \times 10^{14} |V_{cb}|^2 s^{-1}$

4.5 Comparison of the Wirbel-Stech-Bauer and Isgur-Scora-Grinstein-Wise Models

A comparison of WSB and ISGW predictions is shown in Figure 32 [62]. These two models differ in many features, yet predict almost the same spectra and widths for $B \to D$ decays. The $B \to D$ lepton spectrum is also very similar to that of ACCMM model, which doesn't consider specific final D meson states. All three models differ drastically in their predictions for charmless B decays, and therefore any extraction of $|V_{ub}|/|V_{cb}|$ from data will depend strongly upon which specific model is applied.

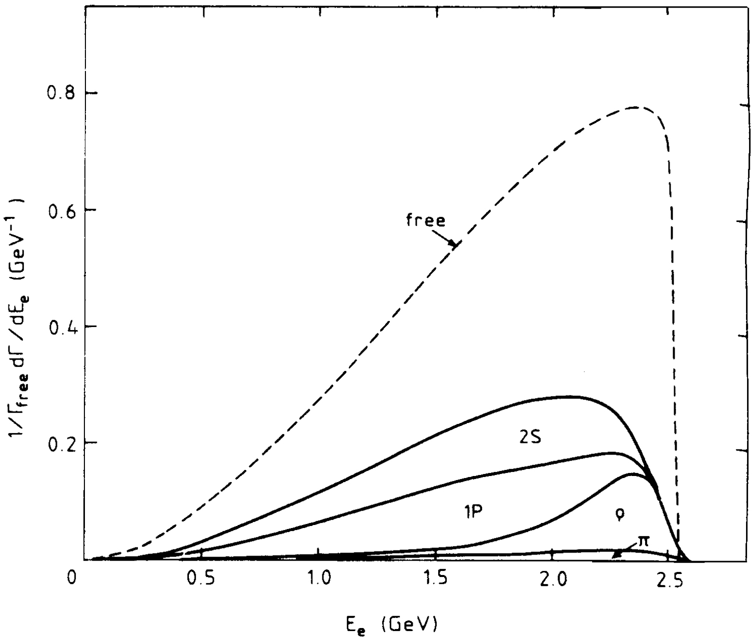

Figure 31: $\frac{1}{\Gamma_{free}}\frac{d\Gamma}{dE_e}$ for $B \to X_u e^- \overline{\nu}_e$, in the ISGW model, normalized to the free quark expectation, which is also shown. [59]

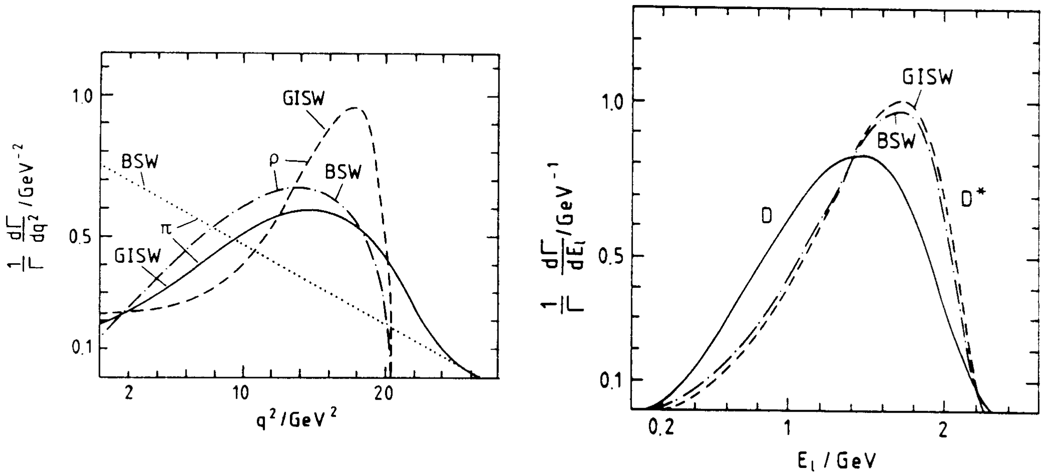

Figure 32: A comparison of the WSB and ISGW models. The $B \to D$ spectra are almost identical for both models, while the charmless B decay spectra differ considerably. a) $B \to \pi, \rho$, as a function of q^2. b) $B \to D, D^*$, as a function of the lepton's energy.[62]

4.6 Exclusive Semileptonic D Decays

The semileptonic decay models may be compared with experimental results in D decay in the channels $D \to K\ell^+\nu_\ell$, and $D \to K^*\ell^+\nu_\ell$. Recently the experiment E-653 at FNAL, a $\pi^- N$ fixed target emulsion experiment, measured the D semileptonic branching ratios to K^* with extremely high precision.[63]

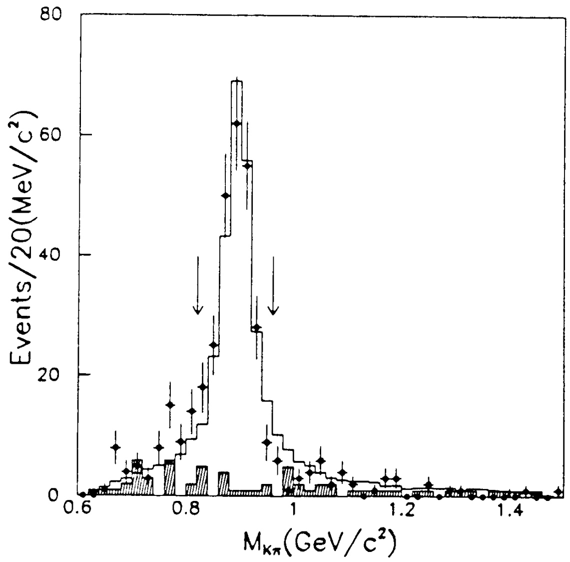

Figure 33: Mass distribution of E-653's $K\pi$ candidates in a three-prong secondary vertex which includes an identified muon candidate, consistent with the decay $D^+ \to \overline{K^*}^0 \mu^+ \nu_\mu$. The background is the shaded histogram, while the fit to the data is the white open histogram. The cuts used to determine the branching ratio are shown as arrows.[63]

The experiment takes advantage of silicon microstrip detectors to cleanly locate secondary vertices in heavy quark decays. The signal for $D^+ \to \overline{K^*}^0 \mu^+ \nu_\mu$ is shown in Figure 33.

The E-653 signal is excruciatingly clean, and may be compared with predictions of the semileptonic decay models, since in D system, $|V_{cs}|$ is well measured. Experimental results for $D \to K \ell \nu_\ell$ agree with both the ISGW and WSB models very well. In Table 6 experimental results in the $D \to K^*$ system are listed; they hint (strongly) at a discrepancy between the data and models.

As seen in Sections 4.1, 4.3 and 4.4, the shape of the spectra are fine and are compatible with DELCO inclusive lepton data. There does appear to be some problem in the normalization of models. Perhaps there are higher wave final state mesons which cannot be ignored, for example the K^{**} excited p-wave K mesons. The lattice QCD calculations tend to agree better with the experimental results. The form factors for the decay $D^+ \to \overline{K^*}^0 \mu^+ \nu_\mu$ were extracted by fitting angular distributions. The form factors agree well with the predictions of both the ISGW and WSB models.

4.7 Exclusive Semileptonic B Decays

The presence of an undetected ν makes it difficult to reconstruct semileptonic decays of B mesons. At $\Upsilon(4S)$ experiments, the classic semileptonic B recon-

	$\Gamma(D^+ \to K^{*0} l \nu_l)$ $(10^{10} s^{-1})$	$\Gamma(D^0 \to K^{*-} l \nu_l)$ $(10^{10} s^{-1})$	$\frac{\Gamma(D \to K^* l \nu)}{\Gamma(D \to K l \nu)}$
Experiment			
E653	$3.36 \pm .90$		$.43 \pm .09 \pm .09$
ARGUS	$4.7 \pm 0.7 \pm 0.9$	$5.2 \pm 0.9 \pm 1.4$	
WA82	$5.3 \pm 1.5 \pm 0.6$		
Mark-III	$5.0 \pm {}^{1.8}_{1.0} \pm 0.6$	$10.4 \pm {}^{4.5}_{2.4} \pm 1.6$	
CLEO		$4.5 \pm 1.4 \pm 1.1$	$.51 \pm .18 \pm .06$
TPS (E-691)	$4.1 \pm 0.4 \pm 0.8$		$.62 \pm .13$
Theory			
ISGW	9.6		1.08
WSB	9.5		1.14
Lattice QCD	5.2 ± 1.9		1.1 ± 0.3

Table 6: Comparison of experimental results and the model predictions of WSB and ISGW. (Table from Reference [63]).

struction technique involves looking for missing energy or mass:

$$M^2_{miss} = (E_B - E_D - E_l)^2 - (\vec{p}_B - \vec{p}_D - \vec{p}_l)^2 \tag{59}$$

$$E_B = E_{beam} \quad |\vec{p}_B| \simeq 0, \quad M_{miss} \simeq M_\nu = 0 \tag{60}$$

Since the B meson is produced almost at rest, the 'missing' mass recoiling against the $(D^*\ell)$ system is approximately the neutrino mass, or 0. The width of the M^2_{miss} distribution is dominated by the approximation which sets the B to rest, $|\vec{p}_B| = 0$.

$(D^{*+}l)$ pairs with $M^2_{miss} \approx 0$ originate from 4 sources:

I	$\overline{B}^0 \to D^{*+} l^- \overline{\nu}$	The $D^* l$ signal
II	$\overline{B}^0 \to D^{**+} l^- \overline{\nu}$ $D^{**+} \to D^{*+} \pi^0$ $B^- \to D^{**0} l^- \overline{\nu}$ $D^{**0} \to D^{*+} \pi^-$	The $D^{**} l$ signal
III	$B \to l^- X$ $B \to D^{*+} Y$	Background from uncorrelated D^*s and leptons.
IV	$c\overline{c} \to D^{*+} l^- X X$	Background from primary charm in the continuum

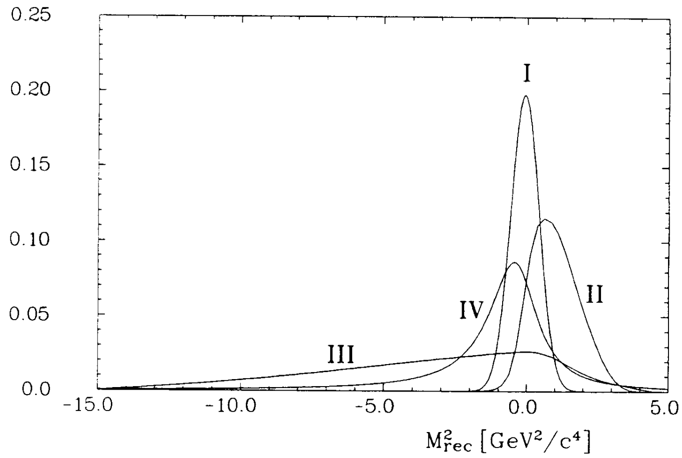

Figure 34: The M^2_{miss} distributions for signal and backgrounds, arbitrarily normalized.[64]

The M^2_{miss} distributions for each of the signals, I and II, and the backgrounds, III and IV, are shown in Figure 34.

The ARGUS e^+e^- at Υ(4S) experiment at DESY performed an analysis [64] reconstructing D^0's in the presence of an identified high momentum lepton with $p > 1$ GeV/c , and correct charge correlation with the D^*. The ARGUS D^0 mass distribution in events with a high momentum identified lepton is shown in Figure 35. The four components of the M^2_{miss} spectrum are then fit, with the resulting compositions shown in Figure 36. The components $\overline{B}^0 \to D^{*+}l^-\overline{\nu}$ (white area), and $\overline{B}^0 \to D^{**+}l^-\overline{\nu}$ and $B^- \to D^{**0}l^-\overline{\nu}$ (shaded area) dominate. There are very few events at $M^2_{miss} < -2$ GeV, indicating very little continuum background or background from uncorrelated (D^*l)'s.

The branching ratios over the full spectrum may be extracted using semileptonic decay models.

$$\mathrm{Br}(\overline{B}^0 \to D^{*+}l^-\overline{\nu}) = (5.2 \pm 0.5 \pm 0.6)\% \tag{61}$$

There is very little model dependence in this decay channel.

For the semileptonic B decays to p-wave D** mesons, the models do not predict identical results, and ARGUS extracted the model-dependent branching ratios.[64] The WSB model does not include p-wave mesons, so in this case we consider models by ISGW and Balk, Hussain, Körner, and Thompson (BHKT):[65]

$$\begin{aligned}\mathrm{Br}(\overline{B}^0 \to D^{**+}l^-\overline{\nu}) &= (2.7 \pm 0.5 \pm 0.5)\% \ \text{(ISGW)} &(62)\\ &= (2.3 \pm 0.6 \pm 0.4)\% \ \text{(BHKT)} &(63)\end{aligned}$$

In Tables 7 and 8 branching ratios for semileptonic $B \to D^*, D$ decays are tabulated. There is very little model dependence in extraction of branching

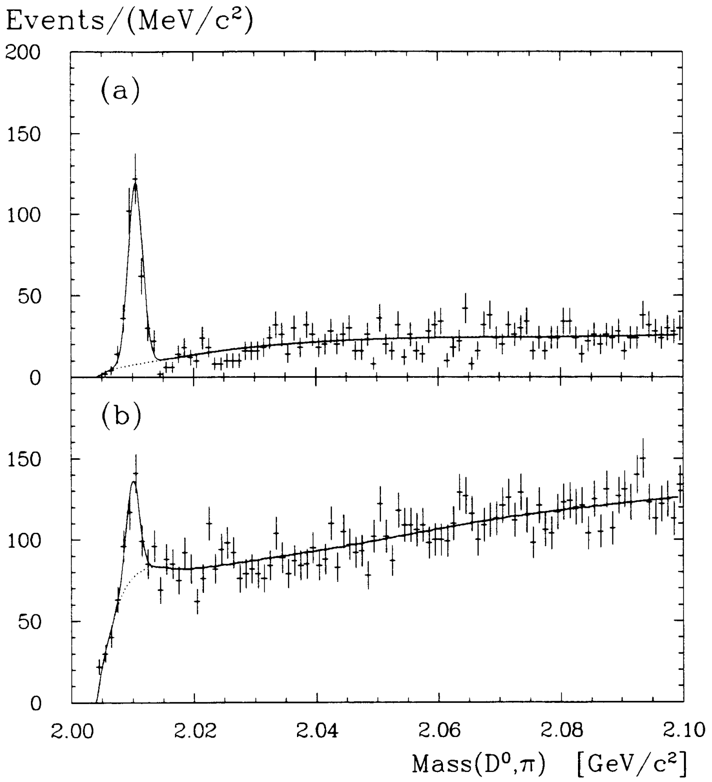

Figure 35: ARGUS's invariant mass distributions for $(D^0\pi^+)$ combinations with a) $D^0 \to K^-\pi^+$ and b) $D^0 \to K^-\pi^+\pi^-\pi^+$, in events which contain a high momentum identified lepton.[64]

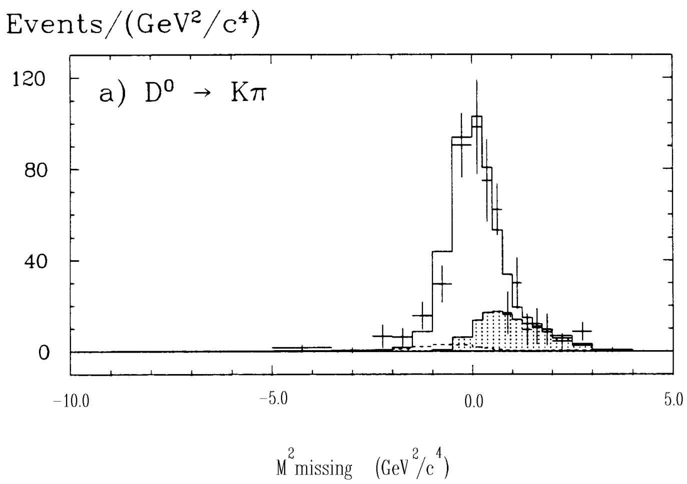

Figure 36: Fit to the ARGUS M^2_{miss} spectrum for the $D^0 \to K^-\pi^+$ sample.[64]

ratios. [2] In these tables, 'excl' refers to the experimental measurement of the exclusive semileptonic decay, whereas '(Dl) ' implies the Dl spectrum was fit

[2] I have not corrected the results to reflect the change in τ_b: $|V_{cb}| \propto \frac{1}{\sqrt{\tau_b}}$. In 6 months, τ_b has gone from 1.18 ps to 1.4 ps (and is still changing!)

Experiment	$\mathrm{Br}(\overline{B}^0 \to D^{*+} l \nu_l)$	$\mathrm{Br}(B^- \to D^{*0} l \nu_l)$	Reference
ARGUS excl	$5.2 \pm 0.5 \pm 0.6$	$5.8 \pm 1.4 \pm 1.3$	[64, 66]
CLEO excl	$4.6 \pm 0.5 \pm 0.7$		[67]
ARGUS (Dl)	$5.2 \pm 0.8 \pm 0.8$	$4.9 \pm 0.7 \pm 0.7$	[68]
CLEO (Dl)	$4.6 \pm 0.5 \pm 0.7$	$4.1 \pm 0.8 \pm {}^{0.8}_{0.9}$	[69]

Table 7: Semileptonic $B \to D^* l \nu$ branching ratios from ARGUS and CLEO.

Experiment	$\mathrm{Br}(\overline{B}^0 \to D^{+} l \nu_l)$	$\mathrm{Br}(B^- \to D^{0} l \nu_l)$	Reference
ARGUS (Dl)	$1.9 \pm 0.6 \pm 0.5$	$1.8 \pm 0.6 \pm 0.4$	[68]
CLEO (Dl)	$1.8 \pm 0.6 \pm 0.3$	$1.6 \pm 0.6 \pm 0.3$	[69]

Table 8: Semileptonic $B \to D l \nu$ branching ratios from ARGUS and CLEO.

Model	$\lvert V_{cb} \rvert$
ISGW	$.036 \pm .003$
KS	$.039 \pm .003$
WBS	$.040 \pm .003$

Table 9: Extraction of $|V_{cb}|$ from an average of ARGUS and CLEO semileptonic $B \to Dl$ and $B \to D^*l$ data compiled in [70].

and components due to Dl, D^*l and $D^{**}l$ were extracted through a fit.

In Table 9, the model dependences are taken into account in the extraction of $|V_{cb}|$ from the $B \to Dl$ and $B \to D^*l$ data compiled by Stone [70]. The model of Körner and Schuler (KS) [71] is very similar to that of WSB in that it uses monopole type form factors, and is included here for comparison's sake. Unfortunately, it is already evident that a limiting factor in the extraction of $|V_{cb}|$ is the model-dependence.

It is interesting to compare the relative amounts of D* and D measured with models' predictions, as listed in Table 10. The models and data agree quite well in the vector/pseudoscalar B→ D*/D components in semileptonic B decay, unlike the situation in D→ K*/K, discussed in Section 4.6.

4.8 Inclusive Semileptonic B Decays

The inclusive lepton spectrum in B decay may be used to measure inclusive semileptonic branching ratios and to test the models with better statistical pre-

Experiment	D^*/D
CLEO	$2.6 \pm {}^{1.1}_{0.6} \pm {}^{1.0}_{0.8}$
ARGUS	$2.9 \pm {}^{1.3}_{0.6} \pm {}^{0.5}_{0.3}$
Theory	
ISGW	2.4
WSB	3.3
KS	2.8

Table 10: Comparison of measured and modeled vector/pseudoscalar D components in semileptonic B decay.[69, 68]

cision. The inclusive lepton spectrum from CLEO [72] is shown in Figure 37, fit to three models, ACCMM, ISGW, and ISGW**, where ISGW** is ISGW, with the relative amount of D^{**}/D_{all} as a free parameter. (Recall that the ISGW model has *no* free parameters and predicts that the relative branching ratios of B mesons to D, D^*, and D^{**}, are 27%, 62%, and 11%, respectively.) The ACCMM model describes the CLEO data well. The ISGW model does not fit the data as well as the ACCMM model. Allowing the fraction of D^{**} to be fit as a free parameter gives a better fit, and the resulting D^{**} fraction is (32±5)%, which is in agreement with both CLEO and ARGUS's exclusive measurements of $B \to D^{**} l \nu$.

Table 11 summarizes the data on inclusive semileptonic B branching ratios for all four $\Upsilon(4S)$ experiments. Note that the models agree at about the 5% level, although Crystal Ball's measurements appear to be slightly higher than the other three experiments. The extracted values of $|V_{cb}|$ are limited by theoretical input via the models.

4.9 Charmless B Decays

The measurement of the KM matrix element V_{ub} is critical in testing the Standard Model. If the matrix element V_{ub} were exactly zero, (or if *any* KM matrix element were in fact zero) then an alternate mechanism outside of the Standard Model would be needed to explain the CP-violation observed in the kaon system. The KM matrix element V_{ub} may be obtained by measuring branching ratios in charmless B decay. At this time, the $b \to u$ transition has been observed only in semileptonic B decays, illustrated in Figure 38.

The CLEO group first observed evidence of the $b \to u$ transition in the inclusive lepton spectrum from B decays.[75] Because the final state u-type hadron can be very light (relative to a charmed hadron), there is more energy available for the lepton in charmless $b \to u$ decays. The strategy is to search for an excess of leptons above the kinematic limit for $b \to c$ decays; *i.e.* leptons

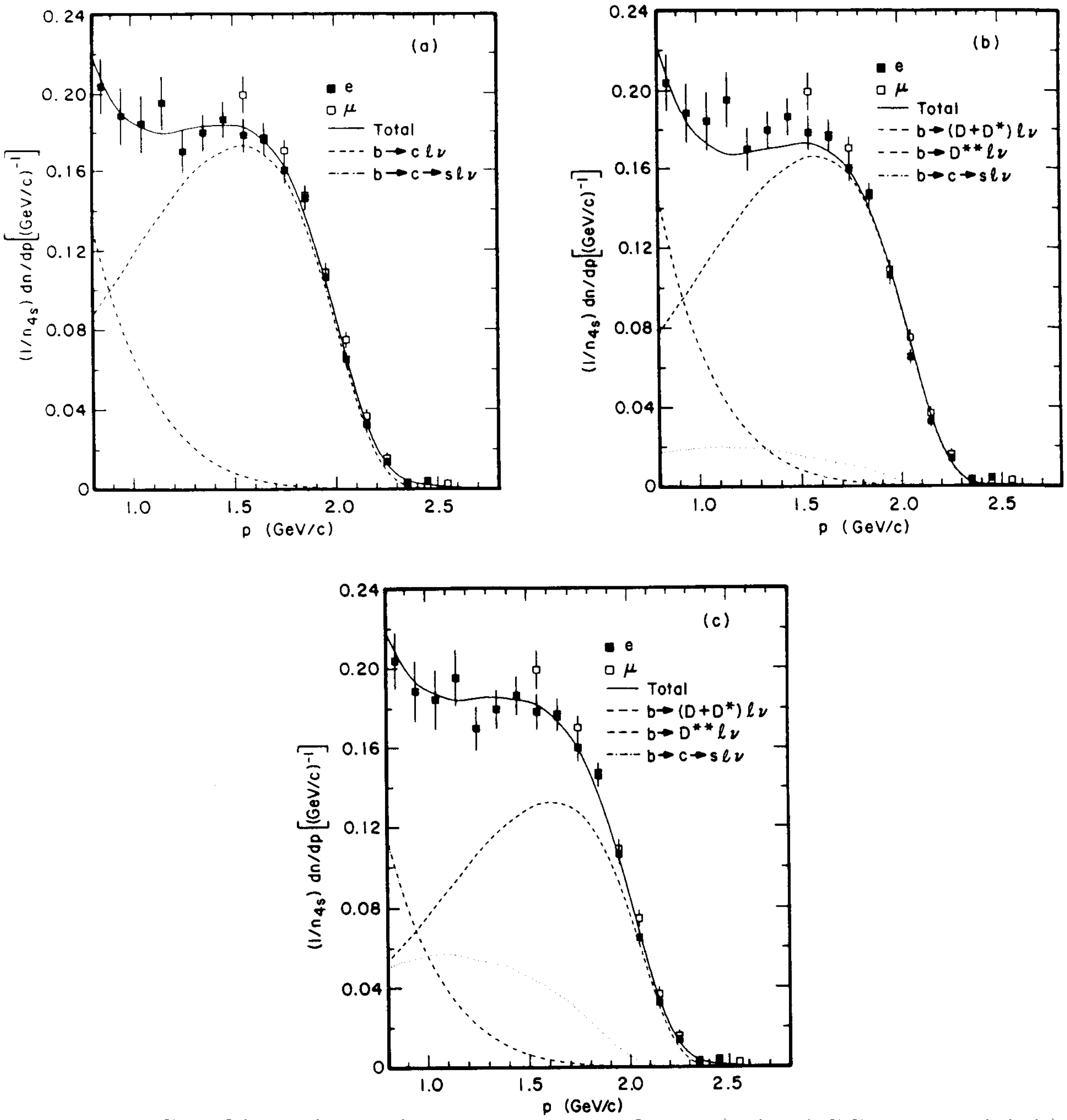

Figure 37: CLEO's inclusive lepton spectrum fit to a) the ACCMM model, b) the ISGW model, and c) the ISGW** model where the D^{**} fraction is allowed to vary.[72]

in the momentum region $2.3 < p_l < 2.6$ GeV/c.

Since $|V_{ub}| \ll |V_{cb}|$, the measurement is technically very difficult; backgrounds from fake leptons and the underlying continuum must be well understood and the detector resolution must also be well known. Additionally there must be no leptons with $p > 2.8$ GeV/c originating from B decay, as this is above the kinematic limit for both $b \to c$ and $b \to u$ decays; such fast leptons may only originate from fakes and underlying continuum. The continuum background may be greatly suppressed by using event-shape cuts which discriminate spherical $B\overline{B}$ event topologies from the jet-like continuum events. It is possible to measure any remaining continuum lepton background by running at a center-of-mass energy just below the $\Upsilon(4S)$ resonance.

While most of the models discussed agree relatively well for $b \to c$ decays,

Experiment	Model	Br($B \to lX$)	$\lvert V_{cb}\rvert$
CLEO	ACCMM	$10.5 \pm .2 \pm .4$	$.048 \pm .002 \pm .005$
CLEO	ISGW	$9.9 \pm .1 \pm .4$	$.044 \pm .002 \pm .004$
CLEO	ISGW**	$11.2 \pm .3 \pm .4$	$.042 \pm .002 \pm .004$
ARGUS	ACCMM	$10.2 \pm .6 \pm .2$	$.047 \pm .004$
ARGUS	ISGW	$9.9 \pm .4$	$.046 \pm .006$
ARGUS	KS	$10.1 \pm .6 \pm .2$	$.047 \pm .001*$
ARGUS	WSB	$8.4 \pm .7$	$.051 \pm .001*$
CUSB	ACCMM	$10.0 \pm .4 \pm .3$	$.044 \pm .004$
CUSB	ISGW	$10.0 \pm .4 \pm .3$	$.046 \pm .007$
XBALL	ACCMM	$12.0 \pm .5 \pm .7$	$.053 \pm .009$
XBALL	ISGW	$11.9 \pm .4 \pm .7$	$.051 \pm .005$
XBALL	WSB	$10.8 \pm .4 \pm .7$	$.055 \pm .005$
XBALL	KS	$10.1 \pm .5 \pm .5$	$.050 \pm .005$

Table 11: Inclusive semileptonic B branching ratios, and determination of $|V_{cb}|$.[72, 73, 74, 70] Entries with $*$ have only statistical error listed on $|V_{cb}|$.

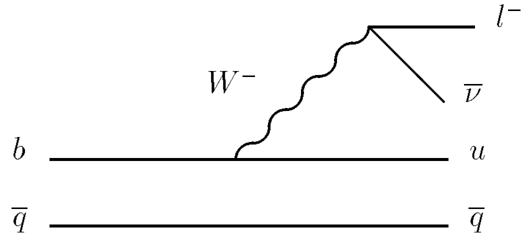

Figure 38: Feynman diagram for semileptonic $b \to u$ decay.

they differ appreciably for $b \to u$ decays, not only in shape, but particularly in absolute normalization. The problem is analogous to measuring the 'tip of the iceberg', and then extrapolating over the complete lepton momentum spectrum using the models, to obtain $|V_{ub}|$. The extrapolation is enormous and the models are very sensitive to which specific hadronic states contribute to the region near the lepton endpoint.

CLEO's lepton spectrum in the 2.0 to 3.0 GeV/c region in shown in Figure 39. An excess of events above the continuum background in the $2.4 < p_l < 2.6$ GeV/c region is the signal for $b \to u$ decays.[75]

The ARGUS experiment chooses to use a two methods of continuum background suppression.[76, 77] They examine the scalar sum of momentum transverse to the lepton's momentum, (large for spherical B events, small for con-

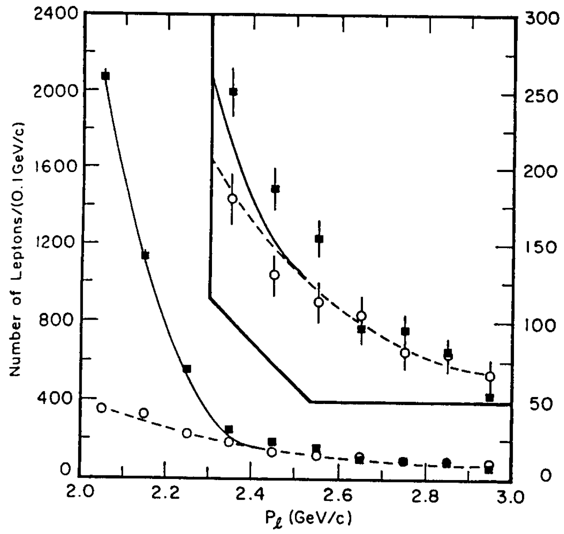

Figure 39: CLEO's inclusive lepton spectrum for data on the $\Upsilon(4S)$ resonance (solid squares) and continuum data just below the resonance (open circles). The continuum data have been scaled so as to represent the background under the $\Upsilon(4S)$ resonance. The dashed line is a fit to the continuum background, the solid line is the continuum background plus $b \to cl\nu$ signal. The magnified inset plot clearly shows an excess, which is evidence for $b \to ul\nu$.[75]

tinuum jet-like events) and require the missing momentum in an event to be consistent with expectations for a missing energetic neutrino in $b \to ul\nu$ decay. In a second check, they examine events with a second identified lepton in the $b \to cl\nu$ range, $1.2 < p_l < 2.3\,\mathrm{GeV/c}$, which effectively tags an event as a $B\overline{B}$ event, as opposed to a continuum background event. Clear excesses in both ARGUS analyses confirm CLEO's observation.

The extraction of $|V_{ub}|$ from the excess of leptons in the high momentum tail of the semileptonic B decay spectrum is non-trivial. Recall from Equation 51, that the $b \to c$ and $b \to u$ contributions, are:

$$\Gamma_{SL}(b \to c) \;=\; \frac{{G_F}^2 {m_b}^5}{192\pi^3}\,K_1|V_{cb}|^2 \quad \text{and} \quad \Gamma_{SL}(b \to u) \;=\; \frac{{G_F}^2 {m_b}^5}{192\pi^3}\,K_2|V_{ub}|^2 \tag{64}$$

with models agreeing very well on the value of K_1, but K_2, and the fraction of the $b \to u$ lepton spectrum which lies in the experimentally examined high momentum region, varies from model to model. The models vary in their normalizations of the absolute rates of $b \to u$ as well, as seen in Figure 32 and discussed in Section 4.5.

It is clear that due to this strong model dependence, extracting $|V_{ub}|/|V_{cb}|$ from the endpoint of the lepton spectrum may not be the best way to measure this quantity. Table 12 lists $|V_{ub}|/|V_{cb}|$ and the model dependences.

While model dependences prevent a precise measurement of $|V_{ub}|$, it is clear that it is non-zero, and we can expect that either CP-violation will be observed in the B system, or some gross discrepancy in the Standard Model will surface.

Model	$\lvert V_{ub}\rvert/\lvert V_{cb}\rvert$ CLEO $2.4 < p < 2.6$ GeV	ARGUS $2.3 < p < 2.6$ GeV
ISGW	$.19 \pm .03$	$.18 \pm .02$
ACCMM	$.12 \pm .02$	$.10 \pm .02$
KS	$.10 \pm .02$	$.09 \pm .01$
WSB	$.13 \pm .02$	$.12 \pm .02$

Table 12: Inclusive semileptonic B branching ratios, and determination of $|V_{ub}|/|V_{cb}|$.[70]

	CLEO	ARGUS
$\mathrm{Br}(B^- \to \rho^0 l^- \overline{\nu})$	$< (.16 - .27) \times 10^{-3}$	$(1.03 \pm .36 \pm 25 \times 10^{-3})$
$\mathrm{Br}(B^- \to V_0 l^- \overline{\nu})$	$< .2 - .3 \times 10^{-3}$	

Table 13: ARGUS and CLEO results on exclusive semileptonic charmless B decays.[77, 79]

4.9.1 Exclusive Charmless B Decays

ARGUS and CLEO have both searched for exclusive charmless B decays, in B $\to$ multiple π modes. Efficiencies for such charmless B decays are reasonably high, but background from continuum non-b decays is a problem. Neither group sees any evidence for hadronic charmless B decays, and 90% CL upper limits on charmless B hadronic branching ratios are obtained. The smallest upper limits are in the 10^{-5} range: [78]

$$\begin{aligned}
\mathrm{Br}(B \to \pi^+\pi^-) &< 4.8 \times 10^{-5}, \\
\mathrm{Br}(B \to \pi^+\rho^-) &< 2.9 \times 10^{-4}, \\
\mathrm{Br}(B \to \pi^+\rho^0) &< 1.5 \times 10^{-4}, \\
\mathrm{Br}(B \to \pi^+\pi^0) &< 2.4 \times 10^{-4}, \\
\mathrm{Br}(B \to p\overline{p}) &< 4.0 \times 10^{-5}
\end{aligned}$$

These limits are just approaching theoretical predictions [45] for $|V_{ub}|/|V_{cb}| \simeq .1$

ARGUS has successfully reconstructed semileptonic $b \to u$ decays in the $B^- \to \rho^0 l^- \overline{\nu}$ channel, and obtains a branching ratio that disagrees with CLEO's upper limit [79, 80]:

Additionally, both ARGUS [77] and CLEO [79] have searched for $\overline{B}^0 \to \rho^+ l^- \overline{\nu}$, $B^- \to \omega^0 l^- \overline{\nu}$, $\overline{B}^0 \to \pi^+ l^- \overline{\nu}$. CLEO sees nothing, and places a 90% CL limit on neutral vector meson V_0 decays, $b \to u$ decays, listed in

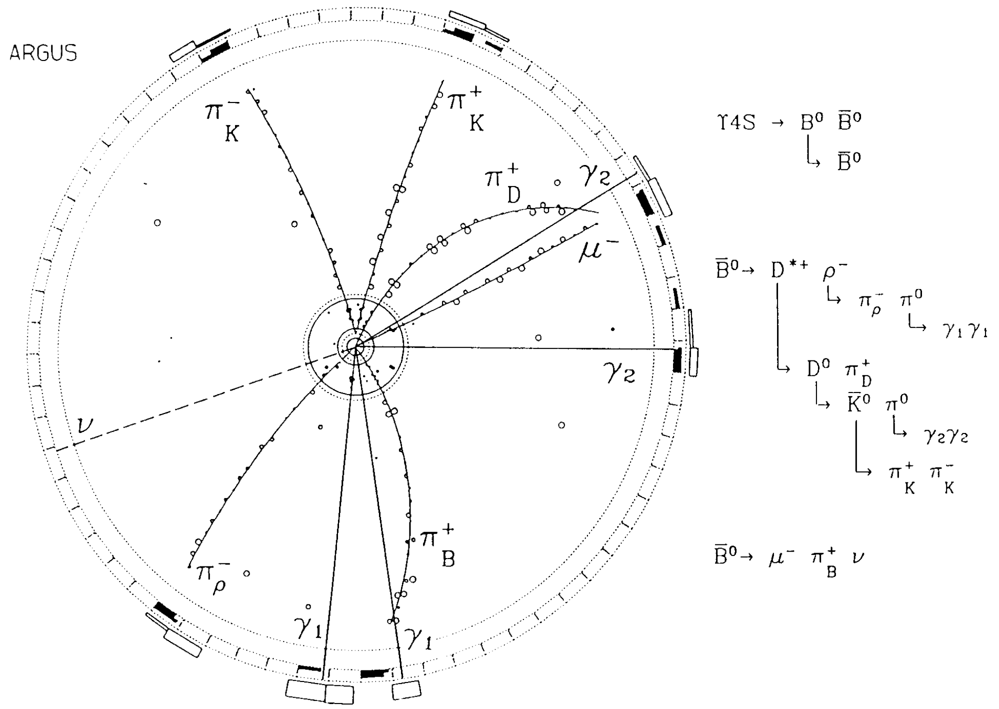

Figure 40: A completely reconstructed $\Upsilon(4S) \to B^0\overline{B}^0$ event in the B^0 mixes $\to \overline{B}^0$, with subsequent decays $\overline{B}^0 \to \pi^+\mu^-\overline{\nu}$ and $\overline{B}^0 \to D^{*+}\rho^-$.[77]

Table 13. (The range in the upper limit is due to the differences in models used to calculate it).

ARGUS has fully reconstructed 2 events with $b \to u$ semileptonic decays:

$\Upsilon(4S) \to B^0\overline{B}^0$, the B^0 mixes, $B^0 \to \overline{B}^0$, and then $\overline{B}^0 \to \pi^+\mu^-\overline{\nu}$ and $\overline{B}^0 \to D^{*+}\rho^-$. (This event is shown in Figure 40.)

$\Upsilon(4S) \to B^-B^+$, $B^+ \to \omega\mu^+\nu$ and $B^- \to D^{*0}\pi^+\pi^-\pi^-$.

While the experiments agree on inclusive leptonic measurement, the exclusive semileptonic decay rates conflict. Not only do the models differ significantly in their $b \to u$ predictions, but the two experiments disagree even when using the same models. More data and larger statistics could improve the situation.

5 Heavy Quark Effective Theory

or: The B meson as the Hydrogen atom of Particle Physics

In the previous two sections, we've seen that B decays provide a rich and varied source of information enabling us to probe weak decays in the Standard Model, although it is also apparent that the model dependences of the hadronic form factors often prove to be the impassable stumbling block hindering further progress in studying the weak interaction and extracting the KM

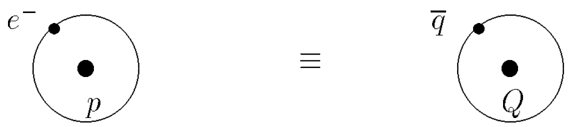

$m_p \sim 1000$ MeV $\qquad\qquad$ $m_b \sim 5000$ MeV

$m_e \sim .5$ MeV $\qquad\qquad$ $m_{\overline{q}} \leq 300$ MeV

$Q\overline{q}$ Heavy quark meson $\Longleftrightarrow$ H atom

$\Psi_{\overline{q}}$ independent of m_Q, $\qquad$ Ψ_Q free particle wave function

$$\Psi_{Q\overline{q}} = \Psi_Q \ \Psi_{\overline{q}}$$

Figure 41: The heavy meson system is strikingly similar to the H atom.

matrix parameters. Recall that the form-factors are phenomenologically postulated (although they are physics-inspired), and we have no basis upon which to judge which theories' form-factors are better, except through comparison of the models with data. It was initially realized by Voloshin and Shifman [81] and more recently elaborated and popularized by Isgur and Wise [82], that exploiting the symmetries in a system consisting of one very heavy quark (with $m_Q \gg \Lambda_{\rm QCD}$) with a very light one can remove much of the model dependences in the form factors in heavy quark decays. Such a heavy quark-light quark system is in many aspects analogous to the hydrogen atom system, as illustrated in Figure 41.

When $m_Q \gg \Lambda_{\rm QCD}$, the heavy quark acts as a source of static colour charge at origin, leaving light quark degrees of freedom independent of the heavy flavour. This is analogous to the hydrogen atom with its free heavy proton static electric field source stationary at the origin, orbited by an light bound electron, whose wavefunction is completely decoupled from that of the heavy proton. So, the flavour of the heavy quark is irrelevant, so long as it is heavy, $m_Q \to \infty$.

Additionally, since spin decouples like $1/m_Q$, as in atomic physics, there is an SU(2N) flavour-spin symmetry, with spin becoming irrelevant as $m_Q \to \infty$, so that all spin states of the heavy $Q\overline{q}$ system become degenerate:

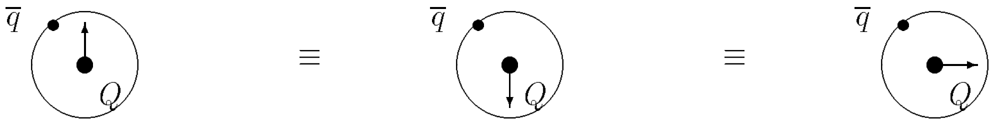

This implies factorization, which lets us divide the heavy quark decay problem into 2 parts: 1 exactly solvable, and 1 incalculable, but with a universal form factor, $\xi\,(v \cdot v')$, dependent only on the initial and final velocities, thanks to the heavy quark SU(N) symmetries of QCD. This heavy quark symmetry

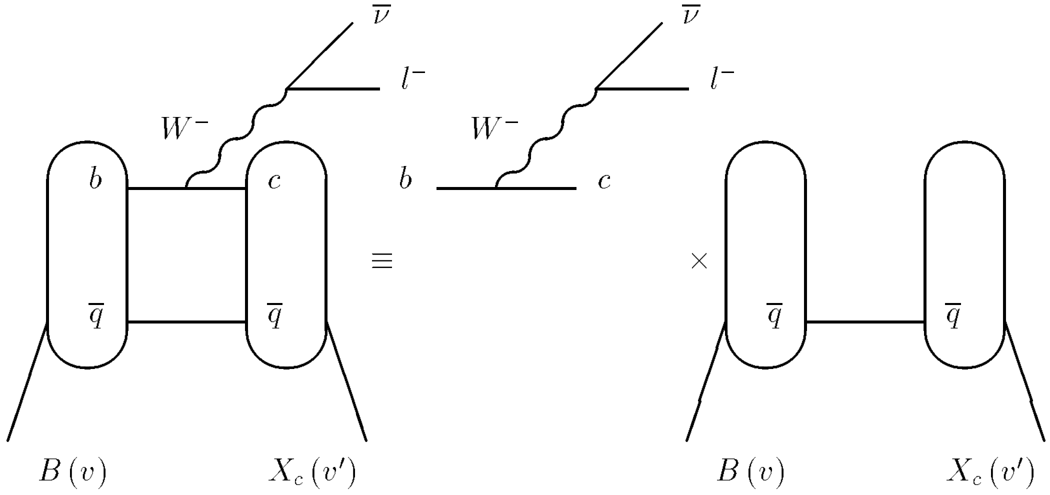

Observable $\quad=\quad$ Calculable $\quad\times\quad$ Universal $\xi\,(v \cdot v')$

Figure 42: The Heavy Quark Effective Theory applied to semileptonic decay. The leptonic and hadronic parts of the weak decay decouple, and the heavy quark symmetry allows us to consider all the form factors, whether for axial, vector, pseudoscalar, tensor or scalar currents, as related, dependent only upon the initial and final heavy quark velocities, v and v'.

is not some ad-hoc phenomenological quark model, but an exact solution of QCD as in the limit as $m_Q \to \infty$.

For example, consider the decay: $\overline{B^0} \to D^{*+}\, l^-\, \overline{\nu}$, in the $\overline{B^0}$ rest-frame:

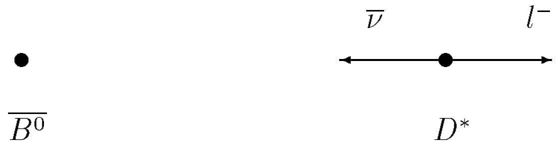

In the special case where the B decays to a D* at rest, the four-velocities of the B and D are parallel (with only time-like components), (since $v^\mu \equiv p^\mu_Q/m_Q$), so that

$$v_B \cdot v'_D = 1 \tag{65}$$

Such a system is now solvable in HQET, as we can choose to normalize the form factor at the 'velocity-transfer' $q^2 = {q_{max}}^2 = 1$.

$$\Rightarrow \xi\left(q^2 = {q_{max}}^2 = 1\right) = 1 \tag{66}$$

The functional form and values of ξ at $q^2 \neq 1$ are not predicted, but the value of the form factor at $q^2 = 1$ is known to be 1.

In real life, the situation is a little more complicated; $m_b \neq \infty$ and $\Lambda_{\rm QCD}/m_b \simeq .03$, and $\Lambda_{\rm QCD}/m_c \simeq .1$ *i.e.* the heavy quark is not infinitely heavy, and therefore, the symmetry is broken. Leading order corrections in

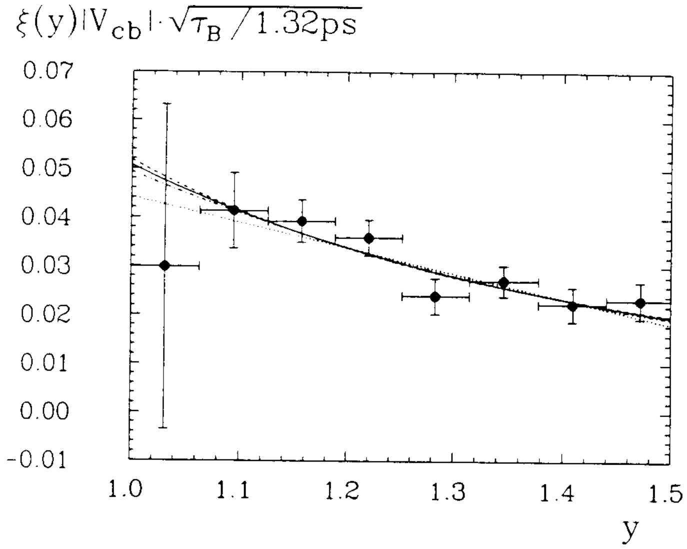

Figure 43: The measured $\frac{d}{dy}Br(\overline{B}^0 \to D^{*+}l^-\overline{\nu})$ distribution from ARGUS, fit to the functions listed in Table 14.[64]

$\Lambda_{\rm QCD}/m_c$ for the imperfect symmetry may be calculated [83], and fortuitously, at $q^2 = {q_{max}}^2$, the leading order correction $\Lambda_{\rm QCD}/m_Q$ term disappears.[84]

Since the strange quark mass is not very large compared to $\Lambda_{\rm QCD}$, we expect sizable corrections in the strange quark case; if the top quark lives long enough to form top hadrons, we expect HQET do be best in the top system.

Using HQET, all hadronic matrix elements may be written in terms of a single form factor, $\xi(v\cdot v')$, instead of many different form factors. Additionally the value of ξ at $q^2 = 1$ is 1, by the choice of where to normalize. This is potentially great news for the extraction of V_{cb} and V_{ub} in semileptonic decays!

5.1 HQET and Experimental Data

In a study of the decays $\overline{B}^0 \to D^{*+}l^-\overline{\nu}$ and $\overline{B} \to D^{**}l^-\overline{\nu}$, ARGUS [64] has used HQET and fit the q^2 spectrum to extract a value of $|V_{cb}|$. In the zero recoil case, where $q^2 = 1$, $\xi(1) = 1$, and the $\Lambda_{\rm QCD}/m_Q$ corrections vanish. ARGUS fits the y distribution, $y = v_B \cdot v_{D^*} = (m_B^2 + m_{D^*}^2 - q^2)/(2m_B m_{D^*})$.

The differential width may be written:

$$\frac{1}{\tau_B}\cdot\frac{d}{dy}\mathrm{Br}(\overline{B}^0 \to D^{*+}l^-\overline{\nu}) = |V_{cb}|^2\xi^2(y)f(y, m_B, m_{D^*}) \tag{67}$$

The measured $\frac{d}{dy}\mathrm{Br}(\overline{B}^0 \to D^{*+}l^-\overline{\nu})$ distribution is shown in Figure 43, fit to the four analytical expressions of the Isgur-Wise function listed in Table 14.

The problem is to find the functional form of ξ. Various parametrizations [85] of ξ and extracted values of $|V_{cb}|$ are shown in Table 14. Without further information on the functional form of ξ, the theoretical uncertainty in the determination of $|V_{cb}|$ using HQET is comparable to that obtained with the quark model form factor decay models.[60, 59, 71, 65] Unfortunately, the data

$\xi(y)$	ρ	$\lvert V_{cb}\rvert \times 10^{-3}$
$1-\rho^2(y-1)$	$1.08 \pm .11 \pm .03$	$45 \pm 5 \pm 3$
$\frac{2}{y+1}\exp\left(-(2\rho^2-1)(\frac{y+1}{y-1})\right)$	$1.52 \pm .21 \pm .10$	$53 \pm 8 \pm 3$
$\left(\frac{2}{y+1}\right)^{2\rho^2}$	$1.45 \pm .19 \pm .09$	$51 \pm 8 \pm 3$
$\exp\left(-\rho^2(y-1)\right)$	$1.37 \pm .19 \pm .08$	$50 \pm 8 \pm 2$

Table 14: ARGUS's $|V_{cb}|$ and the charge radius ρ from various parametrizations [85] of the Isgur-Wise function $\xi(y)$ for fitting the q^2 distribution.[64]

at lowest y value, the zero recoil case, have the strongest sensitivity to ξ but also have the poorest statistical precision.

6 Penguin Decays

In the Standard Model, flavour changing neutral currents are forbidden at tree level. Penguin decays are predicted by the Standard Model, they are effective flavour changing neutral currents, but at the one loop level. The Standard Model one-loop radiative and gluonic penguin decays are shown in Figure 25. They are extremely interesting because of their sensitivity to yet unmeasured quantities in the Standard Model, such as $|V_{ts}|$ and m_{top}.[86] The B system is a particularly interesting place to look for penguin decays, as $|V_{cb}| \simeq .045$, is already quite small, which effectively enhances the rarer B penguin decays. Additionally, the amplitude for a B penguin decay increases as the top quark mass increases, and $|V_{tb}|$ is expected to be very close to 1. These effects together combine to give an enhancement of B penguin decays relative to the analogous K penguin decays by a factor of about 10^5.

Large QCD corrections modify the $b \to s\gamma$ penguin amplitude, increasing it by an order of magnitude, but unfortunately, diminishing the sensitivity to m_{top}.[87] Penguins are also quite exciting because the loop in the penguin diagram is sensitive to any new particles at higher mass scales. SUSY particles, Higgs particles, quarks of a fourth generation family, or anything new.

No penguin decays have been observed yet, but limits at ARGUS and CLEO are presently just at threshold of theoretical predictions of $\sim 10^{-5}$ for dominant modes.[88, 89] Table 15 summarizes the lowest limits from just a few of the penguin decay modes examined by ARGUS and CLEO.

The fact that experiment is just at the threshold of the theoretical penguin decay branching ratios, ensures us excitement in that either penguins will very soon be discovered, or something new in the Standard Model will be uncovered.

Mode	Limit ($\times 10^{-5}$)
$\overline{B}^0 \to K^{*0}\gamma$	9.
$B^- \to K^{*-}\gamma$	37.
$\overline{B}^0 \to K^-\pi^+$	9.
$B^- \to \overline{K}^0\pi^-$	5.
$\overline{B}^0 \to \overline{K}^0\rho^0$	32.
$B^- \to K^-\rho^0$	7.
$\overline{B}^0 \to K^{*-}\pi^+$	44.
$B^- \to \overline{K^*}^0\pi^-$	13.

Table 15: CLEO and ARGUS limits on penguin decay branching ratios.[88, 89]

7 Production and Decay of Heavy Quarks at the Z^0 Resonance

Heavy quark physics at LEP has recently become extremely interesting. Definitive tests of the Standard Model couplings of specific quark species to the Z^0 can be performed using tagged charm or beauty quarks. (The lighter quarks are less simple to tag cleanly.) Additionally, at LEP, a mixture of B^0, B^+, B^0_S, possibly even B^+_C, excited states of all these mesons, plus heavy B baryons and all their excited states are produced in Z^{0}decay. At the $\Upsilon(4S)$ experiments, very little data has been taken above the $\Upsilon(4S)$ resonance, and hence detailed studies of B^0 and B^+ at rest have been the central thrust of the research programs of those experiments. At LEP, the fact that all B hadrons have a large Lorentz boost makes interesting prospects for measuring all B hadron lifetimes, averaged and individually.

7.1 The Width $Z \to b\,\overline{b}$ and the Semileptonic B Branching Ratio

The couplings of the quarks to the Z^0 boson were outlined in Section 1.1 and the relevant Feynman diagram and couplings are in Figure 1. For light quarks, the width $\Gamma_{Z^0 \to q\overline{q}}$ has an uncertainty dominated by the unknown top quark mass, through radiative top loop corrections of the type shown in Figure 44, leading to an uncertainty $\Delta\Gamma_{Z\to q\overline{q}} \simeq 10$ MeV. While all quarks contribute to the radiative loops corrections, the contributions from the lighter quarks with known masses can be calculated. The amplitude associated with the radiative loop diagram increases as the loop quark mass increases, and hence the top quark, with large but unknown mass, has the largest such radiative loop correction.

In the case of the b quark, the isospin partner of the t quark, the extra

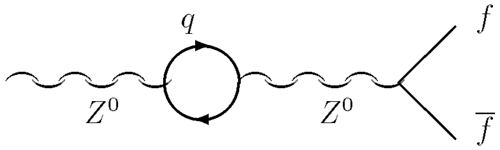

Figure 44: The unknown top quark mass contributes to uncertainties in Z^0 decay widths to fermion pairs.

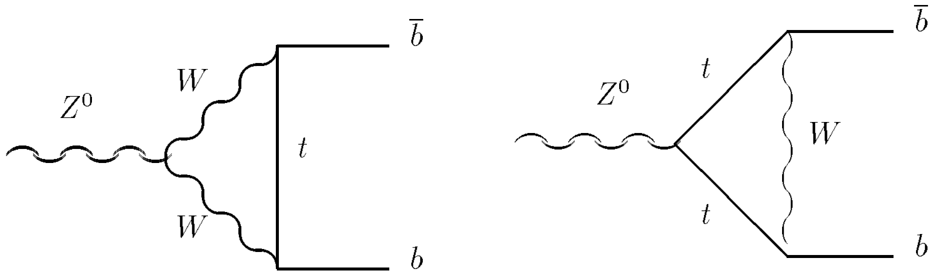

Figure 45: Extra W-t vertex diagrams cancel most of the m_{top} dependence in $\Gamma_{b\overline{b}}$.

$W - t$ vertex diagrams, shown in Figure 45, fortuitously cancel most of the m_{top} dependence in $\Gamma_{b\overline{b}}$. These cancellations are only significant in the case of the b quark, as $|V_{tb}| \simeq 1$, whereas the other quarks have very tiny KM matrix elements for vertices involving the top quark.[90] The b quark is unique in that $\Gamma_{b\overline{b}}$ alone has very little m_{top} dependence, thanks to the cancellations of vertex and radiative top loop corrections.

$\Gamma_{b\overline{b}}$ is measured by normalizing the b-tagged events to the measured luminosity. Alternatively, $\frac{\Gamma_{b\overline{b}}}{\Gamma_{\mathrm{had}}}$ is sensitive to m_{top}, and is measured when b-tagged events are normalized to all Z hadronic decays. The dependence of the Z width to b and d quarks, as a function of m_{top} is shown in Figure 46.

7.1.1 Measuring $\Gamma_{b\overline{b}}$ and Br$(b \to lX)$ at LEP

The first measurements of $\Gamma_{b\overline{b}}$ at LEP tagged b-hadrons via the distinct signature for semileptonic b-quark decay, discussed in Section 2.3.1. The leptons from semileptonic B decay tend to have high energy relative to the beam energy, and large momentum in the B rest frame, which may result in high p_{T} with respect to boosted B direction, thereby making them distinct from leptons and background resulting from non-b processes.

One of the simpler techniques has been to count $Z \to b\ \overline{b}$ pairs using a lepton tag, then correct for inefficiencies and acceptances. It is therefore easy to measure $\Gamma_{b\overline{b}} \cdot \mathrm{Br}\,(b \to lX)$. Individually measuring $\Gamma_{b\overline{b}}$ and $\mathrm{Br}(b \to lX)$ requires additional information:

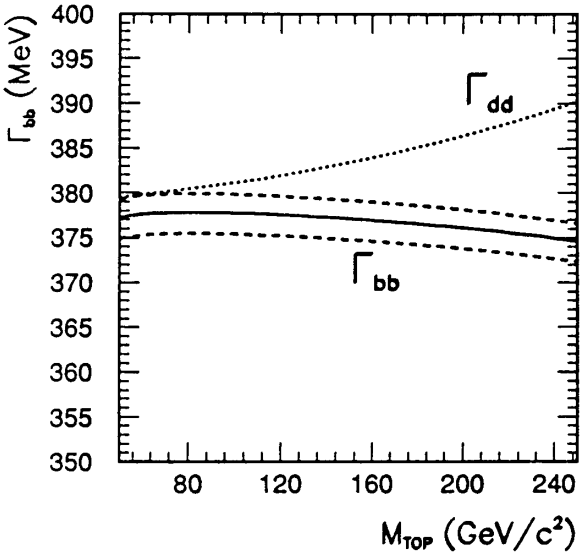

Figure 46: Dependence of the Z width to b and d quarks as a function of $m_{\rm top}$. The dashed lines represent the uncertainty associated with $\alpha_{\rm S}$ and $m_{\rm Higgs}$.

- Assume the world average $\mathrm{Br}(b \to lX)$ to obtain $\Gamma_{b\bar{b}}$, or
- Assume the Standard Model prediction for $\Gamma_{b\bar{b}}$ to measure $\mathrm{Br}(b \to lX)$

It is important to note that we don't necessarily expect the same $\mathrm{Br}(b \to lX)$ at LEP as was measured at the $\Upsilon(4S)$ experiments. The mixture of B hadrons at LEP differs, due to the presence of B^0_S, B-baryons, and other B-hadrons not produced at the $\Upsilon(4S)$ experiments, although they are expected to agree with the results from the PEP and PETRA experiments.

L3 was the first LEP experiment to use both single and di-lepton events to disentangle $\mathrm{Br}(b \to lX)$ and $\Gamma_{b\bar{b}}$. Measurement of both the single lepton b-tagged event fraction and the double lepton b-tagged event fractions enable separation of $\mathrm{Br}(b \to lX)$ and $\Gamma_{b\bar{b}}$:

$$\frac{N_l}{N_{had}} \propto \frac{\Gamma_{b\bar{b}}}{\Gamma_{had}} 2\mathrm{Br}(b \to l)(1 - \mathrm{Br}(b \to l)) \qquad \frac{N_{ll}}{N_{had}} \propto \frac{\Gamma_{b\bar{b}}}{\Gamma_{had}} \mathrm{Br}(b \to l)^2 \tag{68}$$

where N_l is the number of singly-tagged b candidate events, and N_{ll} is the number of doubly-tagged b candidate events.

L3 obtains a result, independent of $\Gamma_{b\bar{b}}$: $\mathrm{Br}\,(b \to lX) = .118 \pm .005 \pm .006$. [91] This result agrees well with PEP and PETRA world average [5] results. The statistical error is dominated by number of dilepton events. L3 then averages this measurement with PEP and PETRA measurements, and extracts:

$$\Gamma_{b\bar{b}} = 385 \pm 23\,\mathrm{MeV} \tag{69}$$

in excellent agreement with the Standard Model prediction of 378 ± 3 MeV.

LEP results for $\mathrm{Br}(b \to lX)$ and $\Gamma_{b\bar{b}}/\Gamma_{\rm had}$ are listed in Table 16. The $\Gamma_{b\bar{b}}$ measurements are a combination of all such measurements done by each

Experiment	$\mathrm{Br}(b \to lX)$	$\Gamma_{b\bar{b}}/\Gamma_{\mathrm{had}}$
ALEPH	$.110 \pm .004 \pm .004$	$.211 \pm .007 \pm .008$
DELPHI (SM)	$.100 \pm .006$	
DELPHI		$.219 \pm .014 \pm .019$
L3	$.118 \pm .005 \pm .006$	$.221 \pm .004 \pm .006 \pm .011$
L3 (SM)	$.119 \pm .001 \pm .006$	
OPAL e (SM)	$.110 \pm .004 \pm .009$	
OPAL μ (SM)	$.104 \pm .003 \pm .006$	
OPAL		$.226 \pm .008 \pm .018(e+\mu)$
LEP average	$.112 \pm .006$	$.217 \pm .007$

Table 16: Summary of LEP $\mathrm{Br}(b \to lX)$ results. (SM) indicates that the Standard Model width was used to extract $\mathrm{Br}(b \to lX)$.[91, 94, 92]

experiment.[92] The ALEPH results in Table 16 are from a combined fit to determine $\Gamma_{b\bar{b}}/\Gamma_{\mathrm{had}}$, $\Gamma_{c\bar{c}}/\Gamma_{\mathrm{had}}$, $\mathrm{Br}(b \to lX)$, $\mathrm{Br}(c \to lX)$, $\langle x_E \rangle_b$, $\langle x_E \rangle_c$, and χ simultaneously, with very few assumptions.[93]

These results in Table 16 are completely systematics limited, and the largest contributions are due to the modeling of the semileptonic decay, which contributes $\simeq .003$ in $\mathrm{Br}(b \to lX)$.

7.1.2 $\Gamma_{b\bar{b}}$ Using Vertex, Lifetime, and Event Shape Tags

Although tagging b quarks with high p, high p_{T} leptons, has proven to be successful, we are presently at the level at which systematic uncertainties in semileptonic b decay modeling will prevent any significant improvement in the measurement of $\Gamma_{b\bar{b}}$.

Mark-II [95] pioneered the technique of taking advantage of the long lifetime of the b quark to separate $b\bar{b}$ decays of the Z^0 from Z^0 decays to lighter quarks. Because of the long lifetime of the B hadrons, and relatively large B hadron mass, many of the tracks of B decay products do not point back to the primary interaction point, while most of the tracks from lighter quark events do. Therefore $b\bar{b}$ decays of the Z^0 can be selected by requiring several tracks to intersect the b thrust axis in front of the interaction point. Such a lifetime or vertex tag has recently been used at LEP. Because the B branching ratio to hadrons is much larger than to leptons, the efficiency of this technique is greatly improved over B-tagging using leptons. A drawback of this technique is the detector response, beam spot, and B lifetime and B decay multiplicity must be well understood. Additionally, charmed hadrons have a lifetimes not so different than B-hadrons, and are a non-trivial background to b-tagging using lifetime techniques.

Other global event attributes may be used to separate $b\bar{b}$ events from Z^0

Experiment	Technique	$\Gamma_{b\bar{b}}/\Gamma_{\rm had}$
ALEPH	neural network double-tag	$.2283 \pm .0054 \pm .0044$
ALEPH	lifetime double-tag	$.2183 \pm .0022 \pm .0035$
DELPHI	boosted sphericity product tag	$.219 \pm .014 \pm .019$
DELPHI	neural network tag	$.232 \pm .005 \pm .017$
L3	neural network tag	$.222 \pm .003 \pm .007$
OPAL	lifetime double tag	$.223 \pm .010 \pm .008$
OPAL	mixed vertex-lepton tag	$.215 \pm .006 \pm .007 \pm .007$
LEP average	all b tags combined	$.220 \pm .003$

Table 17: Summary of LEP measurements of $\Gamma_{b\bar{b}}$ using lifetime, vertex and event shape tags. LEP average is for all $\Gamma_{b\bar{b}}$ tags listed here and in Table 16.[92]

decays to the lighter quarks. Because of the relatively large B-hadron mass, the boosted sphericity product has been used to tag B's successfully [96], and artificial neural networks [97]. Table 17 summarizes LEP measurements on $\Gamma_{b\bar{b}}$ using such vertex, lifetime, and event shape B-tags.

7.2 Semileptonic $B \to \tau X \overline{\nu}_\tau$ Decays at LEP

In the Standard Model, $\frac{\Gamma(B\to\tau X)}{\Gamma(B\to e X)} = .266$, a prediction obtained from phase space considerations and lepton universality.

ALEPH is the only experiment to have measured the semileptonic branching ratio of B hadrons to τ leptons.[98] Their strategy was to take advantage of the fact that there are two undetected neutrinos in the final state for hadronic tau decay, so large missing energy in otherwise well-contained events is a key signature. The decay chain, depicted in Figure 47 is:

$$B \to \tau^- \overline{\nu}_\tau X \quad \tau^- \to \nu_\tau Y \tag{70}$$

where X and Y are one or more hadrons.

ALEPH's $B \to \tau X \overline{\nu}_\tau$ strategy:

- Select well-contained events
- Reject events with an identified e^- or μ^-, since $b \to c\, e^- \overline{\nu}_e$ has considerable missing energy, and would otherwise have a similar signature.
- Require the probability that all tracks in event come from primary vertex to be less than 0.5% (make use silicon microvertex detector tracker for precise vertex information).
- Divide event into 2 hemispheres along the thrust axis, and look at $E_{\rm miss}$, the missing energy.

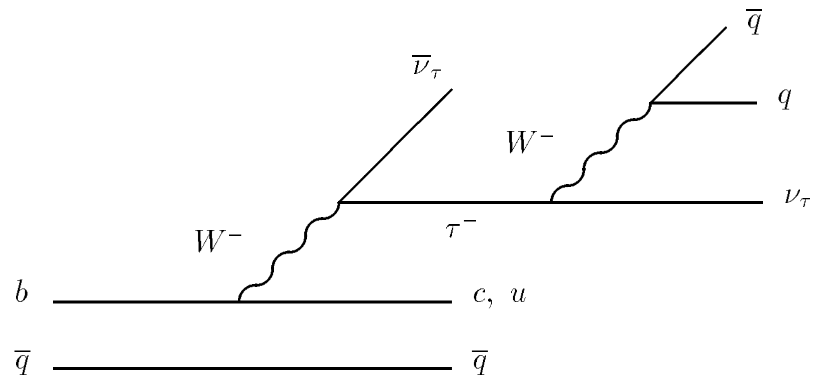

Figure 47: Feynman diagram for semileptonic B-hadron to τ lepton decay.

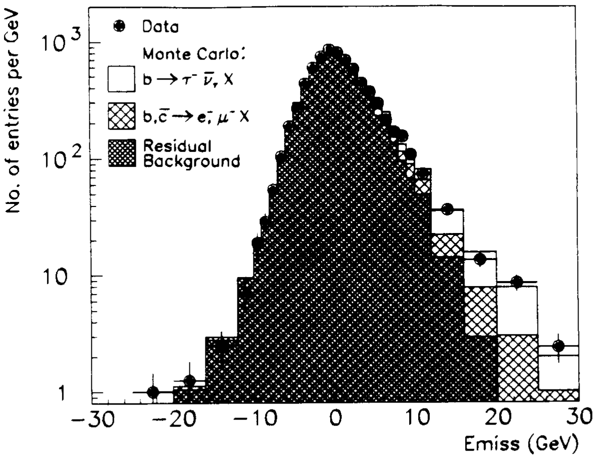

Figure 48: The ALEPH missing energy spectrum after selection cuts for $B \to \tau X \overline{\nu}_\tau$ have been performed. Contributions to the spectrum from $b \to \tau \nu_\tau X$ decays, $b, c \to e^-(\mu^-)X$ decays and background are depicted.[98]

- Correct the Monte Carlo simulation so tails in the missing energy spectrum agree with those observed in the data.

The result is [98]: $\mathrm{Br}(B \to \tau \overline{\nu}_\tau X\ ) = (4.08 \pm .76 \pm .62)\%$. This is in agreement with the Standard Model prediction, and excludes some exotic two Higgs doublet models.

8 $B^0 - \overline{B}^0$ Mixing

Oscillations between a neutral meson and its antiparticle are predicted in the Standard Model. $K^0 - \overline{K^0}$ mixing was predicted and observed over three decades ago.[99, 100] In 1987, the ARGUS experiment measured a surprisingly large $B_d^0 - \overline{B_d^0}$ mixing.[101] The simplest interpretation within the Standard

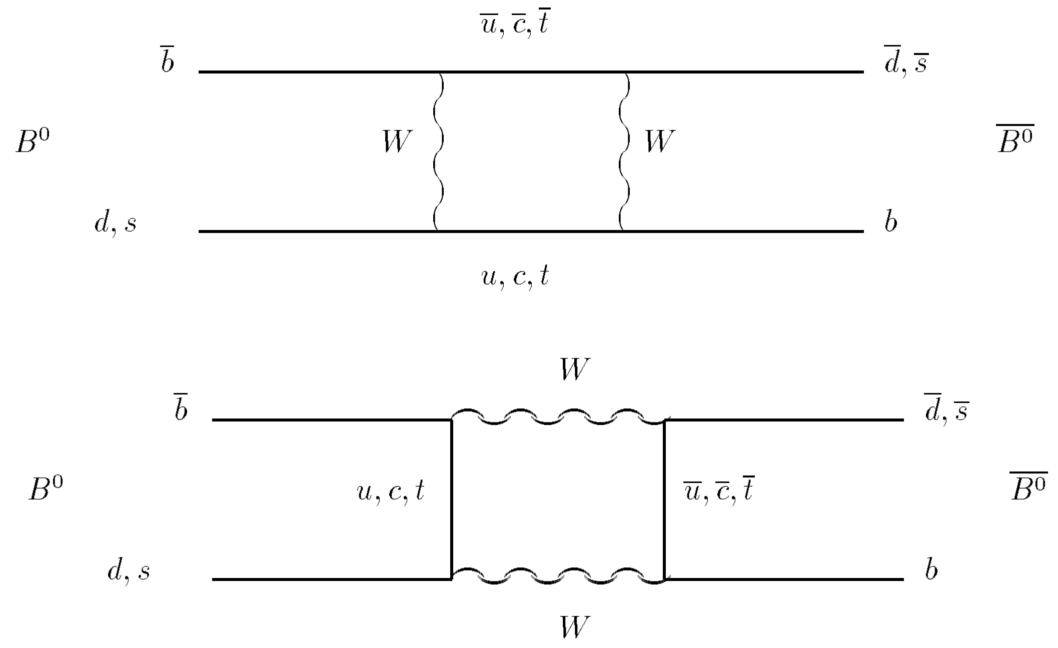

Figure 49: Box diagrams for $B^0 - \overline{B^0}$ mixing.

Model was that the top quark mass was extremely heavy, $m_{\rm top} > 50\,{\rm GeV}$, which was thought to be very high, at that time.

Mixing is expected in all neutral mesons, to some level, and proceeds via the second order weak interaction box diagrams [102] illustrated in Figure 49.

Mixing is quantified by the parameter x:

$$x \equiv \frac{\Delta M}{\Gamma} = \frac{\text{lifetime}}{\text{oscillation time}} \tag{71}$$

In discussing the LEP and $\Upsilon(4S)$ experiments, different notations are used in measuring the mixing: (at LEP, B^0 is B^0_d and B^0_S)

$$\Upsilon(4S)\text{ experiments}: \quad r \equiv (N_{B^0B^0} + N_{\overline{B}^0\overline{B}^0})/N_{\overline{B}^0B^0} = \frac{x^2}{2+x^2} \tag{72}$$

$$Z^0\text{ experiments}: \quad \chi \equiv (N_{B^0B^0} + N_{\overline{B}^0\overline{B}^0})/N_{b\bar{b}} = \frac{x^2}{2+2x^2} \tag{73}$$

8.1 Experimental Procedure for Measuring Mixing

All experiments which have measured $B^0 - \overline{B^0}$ mixing have relied on the fact that $b-\overline{b}$ quarks are pair-produced. In semileptonic B decay, the sign of lepton determines the b or $\overline{b}$ flavour:

no mixing	$\overline{B^0} \to l^-\overline{\nu}\ X$	$B^0 \to l^+\overline{\nu}\ X$
mixing	$\overline{B^0} \to l^-\overline{\nu}\ X$	$B^0 \to \overline{B^0} \to l^-\overline{\nu}\ X$

	ARGUS	CLEO
r (B^0 l)	$.231 \pm .118 \pm .034$	
r (l l)	$.198 \pm .052 \pm .067$	$.19 \pm .06 \pm .06$

Table 18: ARGUS and CLEO results on $B_d^0 - \overline{B}_d^0$ mixing.

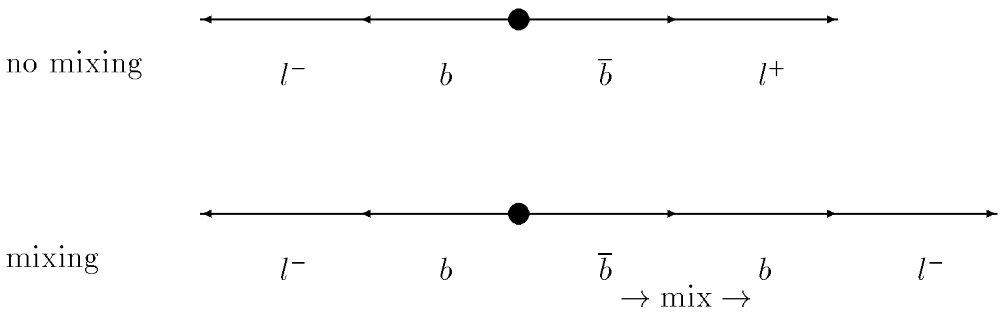

The 'Classic Procedure' is to use the signs of both leptons in a $B\overline{B}$ pair which both decay semileptonically to tag the b or $\overline{b}$, carefully taking into account standard lepton backgrounds from cascade decays, fakes, charm, as discussed in Section 2.3, and illustrated in Figure 13.

8.1.1 Mixing at $\Upsilon(4S)$

In order to measure $B_d^0 - \overline{B}_d^0$ oscillations at $\Upsilon(4S)$ energies, two popular techniques have been used:

- Look for events with a B^0 and a lepton, where the B^0 is reconstructed in the clean $\overline{B}^0 \rightarrow D^{*+}l^-\overline{\nu}$ channel. Check for mixed, unmixed sign correlations.
  $\Rightarrow$ This technique has low backgrounds, low statistics.

- Look for events with two high momentum leptons. Count like sign and unlike sign dilepton pairs.
  $\Rightarrow$ This technique has higher backgrounds, higher statistics.

The measured mixing results using these techniques at ARGUS [103] and CLEO [104] are listed in Table 18.

8.1.2 Mixing at Higher Energies

At the energies of PEP, PETRA and LEP, B_d^0 and B_s^0 are both produced. When a B hadron is tagged via a lepton tag, a combination of B_d^0 and B_s^0 mixings is measured:

$$\chi = f_d\chi_d \ + \ f_s\chi_s \tag{74}$$

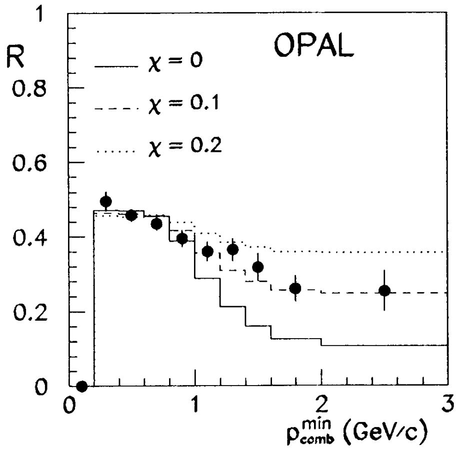

Figure 50: The OPAL distributions for R, the fraction of large angle dilepton events which are like-sign, versus $p^{\rm min}_{\rm comb}$, for all combined $\mu\mu$, $e\mu$, and ee dilepton events. Monte Carlo predictions for $\chi = 0$, $\chi = .1$, and $\chi = .2$ are shown as solid and dashed histograms.[105]

where f_q is the fraction of b quarks that hadronize with quark q to form the meson $\overline{B}^0_q$. From measurements of $s\overline{s}$ popping in hadronization, we expect these unknown parameters to be: $f_d \sim .40 \sim f_u$ and $f_s \sim .12$.

The OPAL B-mixing analysis tags b quarks via their semileptonic decay to high p, high $p_{\rm T}$ leptons.[105] Since there are relatively few events with two leptons, mixing measurements using this technique tend to be statistics limited. It is undesirable to cut hard into the lepton momentum spectrum, further diminishing precious statistics. Instead, the full lepton p and $p_{\rm T}$ spectrum for opposite-hemisphere di-lepton events is fit, in terms of the lepton discrimination variable $p^{\rm min}_{\rm comb}$, which provides good separation of the $b \to l$ signal from the non-prompt backgrounds:

$$p_{\rm comb} \equiv \sqrt{\left(\frac{p}{10}\right)^2 + {p_T}^2} \tag{75}$$

$p^{\rm min}_{\rm comb}$ is the minimum $p_{\rm comb}$ of the two leptons. The dominant source of like-sign lepton background is:

$$b_1 \to l^- \qquad \overline{b}_2 \to \overline{c} \to l^- \tag{76}$$

i.e. one b decays semileptonically, the second b decays to charm, which then decays semileptonically.

OPAL defines ratio $R = \frac{\rm like-sign\ dilepton\ events}{\rm all\ dilepton\ events}$ and fits the $p^{\rm min}_{\rm comb}$ spectrum, as shown in Figure 50. Note that at high p and high $p_{\rm T}$, where $p^{\rm min}_{\rm comb}$ is large and the B purity is high, and the sensitivity to mixing is greatest, as expected.

The OPAL result, obtained from fitting R distributions as in Figure 50 is:

$$\chi = .125 \pm {}^{.017}_{.016} \pm .015 \tag{77}$$

Experiment	$\chi = f_d\chi_d + f_x\chi_s$
OPAL	$.125 \pm {}^{.017}_{.016} \pm .015$
DELPHI	$.121 \pm .042 \pm .007$
ALEPH	$.137 \pm .015 \pm .007$
L3	$.121 \pm .017 \pm .006$

Table 19: B mixing results from the LEP experiments.

B-mixing measurements from dilepton measurements at the LEP experiments are summarized in Table 19.[105, 106, 107, 108] These measurements assume that the semileptonic branching ratios for B_d^0 and B_s^0 are the same.

ALEPH has additionally measured $B_0 - \overline{B}^0$ mixing using a 'jet-charge' method[109], in which the charge of one b quark is tagged by a high-energy, high p_{T} lepton, and the other b is derived from a momentum weighted sum of particle charges in its jet, which yields the result: $\chi = .113 \pm .018 \pm .027$.

8.1.3 Interpretation of Mixing Results

The ARGUS and CLEO experiments run below the $B_s^0\,\overline{B_s^0}$ production threshold and hence measure only χ_d, the mixing in the B_d^0 system, while the higher energy experiments measure a combination of B_d^0 and B_s^0 mixing.

Mixing may be predicted from the Standard Model via the box diagram transitions depicted in Figure 49, if the quark masses and KM matrix elements are known. Consequently, we measure mixing and then may use it to constrain the unknown top quark mass and KM parameters involving the top quark.

$$x = \mathrm{MIXING} \;=\; \frac{\Delta M}{\Gamma} = \tau_b \frac{{G_F}^2 m_B}{6\pi^2} B_B {f_B}^2 \mid V_{tb}\; {V_{td}}^* \mid {m_t}^2 f\left(\frac{{m_t}^2}{{m_W}^2}\right)\eta_{QCD} \tag{78}$$

where B_B is the 'bag model' vacuum insertion parameter, $B_B \simeq 1.0$; f_B is the B pseudoscalar meson decay constant, $f_B \simeq 100 - 300\,\mathrm{MeV}$ range, but has yet to be measured; $\eta_{QCD} \simeq .8 - .85$, and is a result of perturbative QCD corrections to the box diagram; and $f({m_t}^2/{m_W}^2)$ is a known function. We again run into the problem that theory deals with quarks, while experiment deals with hadrons, hence the QCD corrections, bag model parameter and the decay constant introduce uncertainties. The KM matrix element V_{td} is obtained from χ_d at ARGUS and CLEO. Uncertainties in B_B, f_B and m_{top} dominate, resulting in $0.003 < |V_{td}| < 0.018$. V_{ts} may then be obtained from χ_s at LEP, using the χ_d from lower energy experiments. Uncertainties in χ_d, f_d and f_s dominate, and unfortunately, as $\chi_s \to .5$, it becomes insensitive to

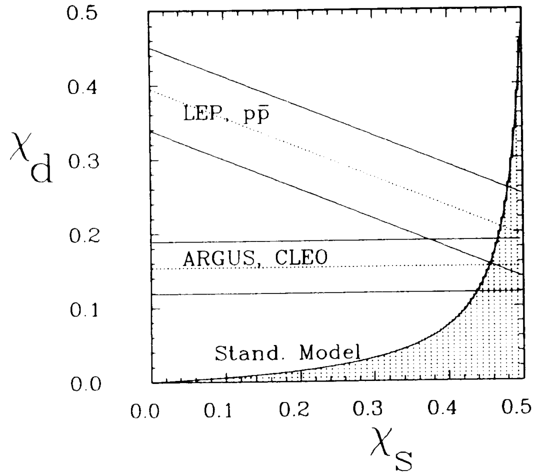

Figure 51: Constraints on mixing parameters χ_d and χ_s The hatched region allowed in the Standard Model with a three-generation unitary KM matrix.[15]

$\Delta M/\Gamma \sim |V_{ts}|^2$, as may be deduced from Equation 79.

$$\chi = \frac{\left(\frac{\Delta M}{\Gamma}\right)^2}{2\ +\ 2\ \left(\frac{\Delta M}{\Gamma}\right)^2} \tag{79}$$

The combined results for χ_d and χ_s are shown in Figure 51. The hatched region in the plot is derived from the Standard Model, constraining the three-generation KM matrix to be unitary, which results in $|V_{td}|^2/|V_{ts}|^2 < .21$. [110]

From the measurements of χ_d and χ_s and the limits on unitarity of the KM matrix, a stronger limit on χ_s is obtained: $\chi_s > .44$, which implies that the mixing in the B_s system is consistent with full mixing, which may then be used to deduce that $f_s = .12 \pm .06$, consistent with expectations.

9 Heavy Quark Decay Asymmetry

In the Standard Model, interference between axial and vector currents in the decay $e^+e^- \to Z^0 \to q\overline{q}$ produces an asymmetry $\mathrm{A_{FB}^q}$ in the angular distribution of quarks.

$$\mathrm{A_{FB}^q} = \frac{\sigma_F^q - \sigma_B^q}{\sigma_F^q + \sigma_B^q} \tag{80}$$

σ_F^q and σ_B^q are the cross sections for positive quarks to be found in the forward and backward hemispheres, respectively.

$$\sigma_F^q \equiv \int_0^1 \frac{d\sigma^q}{d\cos\theta} d\cos\theta \tag{81}$$

where θ is the polar angle between the incoming electron and the outgoing quark. ‘Forward’ events are those with $\cos\theta > 0$, ‘backward’ are those with $\cos\theta < 0$.

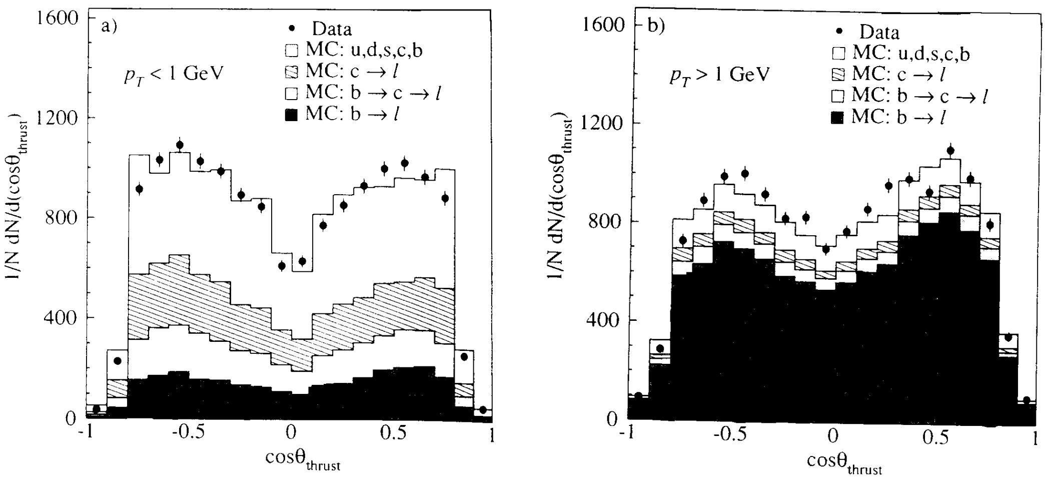

Figure 52: Measured angular distribution of the thrust axis for events with:
a) A low p_T ($< 1\,\mathrm{GeV}$) lepton,
b) A high p_T ($> 1\,\mathrm{GeV}$) lepton,
with contributions from various lepton sources indicated. (from L3)[112]

The forward-backward asymmetry is sensitive to the axial and vector couplings in the Standard Model, and may be used to measure $\sin^2\theta_W$ and check Standard Model for consistency. (Refer to Section 1.1 and Figure 1 for the axial and vector couplings and notation.) In the improved Born approximation framework[111], the asymmetry at the Z^{0}peak is given by:

$$\mathrm{A_{FB}^{q}} = \frac{3}{4}\left(\frac{2c_V{}^q\, c_A{}^q}{(c_V{}^q)^2+(c_A{}^q)^2}\right)\left(\frac{2c_V{}^e\, c_A{}^e}{(c_V{}^e)^2+(c_A{}^e)^2}\right) \tag{82}$$

so that the cross-section has the form:

$$\frac{d\sigma^q}{d\cos\theta} \propto 1 + \frac{8}{3}\cos\theta\ \mathrm{A_{FB}^{q}} + \cos^2\theta \tag{83}$$

Z^0 decays into heavy quarks, such as charm and beauty, may be tagged via a lepton in semileptonic decays, and the sign of the quark charge may be inferred from the sign of the lepton.

The L3 experiment was the first to simultaneously measure the forward-backward asymmetry for charm and beauty quarks[112]. Their strategy was to use all leptons, the full p and p_T spectrum, and then extract simultaneously $\mathrm{A_{FB}^{b}}$ and $\mathrm{A_{FB}^{c}}$:

- The b quark has characteristically hard fragmentation; the large b mass insures that events with high p_T and p leptons are predominantly $b\overline{b}$ events.

- The c quark has lower mass and softer fragmentation, but leptons in $c\overline{c}$ events still have higher p and p_T than those produced in the decay of the lighter quarks and fake leptons.

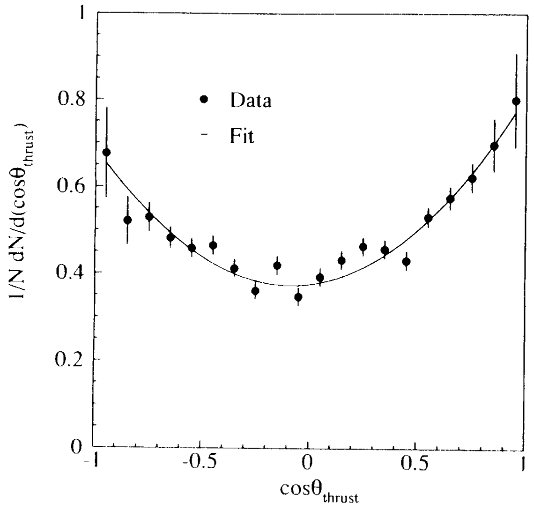

Figure 53: Acceptance corrected angular distribution of the thrust axis, the data are points, the solid curve the result of the fit, from L3[112].

In events with an identified lepton, the angular distribution of the thrust axis, which is an approximation to the originally produced quark's direction, is illustrated in Figure 52. The high p_{T} sample is dominated by events with primary b quarks, while the low p_{T} sample has a sizable c quark contribution.

Initially, the standard technique was to identify high p_{T} leptons with $p_{\mathrm{T}} > 1$ GeV. The thrust axis, signed by charge of lepton, is used to estimate the original quark direction. The angular distribution of $-Q\cos\theta_{\mathrm{thrust}}$ is then fit for the asymmetry, as shown in Figure 53. The resulting observed asymmetry[112] is $A_{FB}^{obs} = 0.062 \pm 0.013$. This method does not make use of a wealth of information in p and p_{T} spectra; using the full spectrum of leptons, and simultaneously fitting for components from b and c, increases the sensitivity of the measurement and extracts both $\mathrm{A_{FB}^{b}}$ and $\mathrm{A_{FB}^{c}}$, and their correlations. The L3 analysis [112] performs such a combined fit on the lepton distributions, shown in Figure 52, and obtains: $\mathrm{A_{FB}^{b}} = .086 \pm .015 \pm .007$ and $\mathrm{A_{FB}^{c}} = .083 \pm .038 \pm .027$

In the Standard Model, $\mathrm{A_{FB}^{q}}$ is energy dependent. In Figure 54, $\mathrm{A_{FB}^{b}}$ is compared to Standard Model predictions for $\sin^2\overline{\theta}_W = .2336$. The measurements agree with expectations.

Mixing decreases the observed asymmetry; the wrong sign of lepton after B-mixing is observed. The correction for mixing is:

$$(\mathrm{A_{FB}^{q}})_{\substack{\mathrm{mixing} \\ \mathrm{corrected}}} = \frac{1}{1 - 2\chi}(\mathrm{A_{FB}^{q}})_{\mathrm{measured}} \tag{84}$$

The forward-backward asymmetry in $e^+e^- \to b\bar{b}$ has been measured by all four LEP experiments [113, 112]; the most recent results are listed in Table 20, the averages are from a compilation [114] and takes common systematics into account.

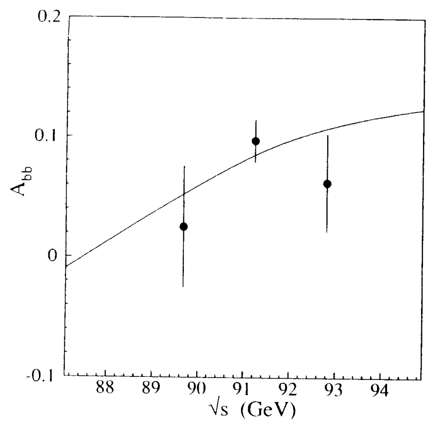

Figure 54: Energy dependence of A_{FB}^{b} compared to the Standard Model expectation for $\sin^2\overline{\theta}_W = .2336$, from L3[112].

Experiment	A_{FB}^{b}
ALEPH	$.061 \pm .013 \pm .003$
DELPHI	$.094 \pm .019 \pm .012$
L3	$.066 \pm .011 \pm .004$
OPAL	$.074 \pm .014 \pm .007$
LEP average	$.069 \pm .007 \pm .004$
LEP average, mixing corrected	$.093 \pm .010 \pm .006$

Table 20: Summary of LEP results on A_{FB}^{b}.[114]

Both ALEPH and L3 have measured A_{FB}^{c} from a combined b and c fit to the inclusive lepton spectrum. Additionally, A_{FB}^{c} can be measured by tagging charm using high momentum D^*'s via the clean chain: $D^{*+} \to D^0\pi^+$. The statistics in the D^* tag are limited, and improvement is foreseen with more data.

LEP results on A_{FB}^{c} are listed in Table 21 , where l denotes the charm asymmetry measurement from an inclusive lepton fit, and D^* denotes the charm asymmetry measurement is from a primary D^* tag.

9.0.4 Interpreting the Asymmetry Results

The top quark, partner of the beautiful quark, has not yet been observed directly. Currently we know $m_{\rm top} > 108$ GeV/c^2, from the Fermilab TeVatron collider.[115] The LEP experiments are sensitive to $m_{\rm top}$, but only indirectly, through radiative corrections involving top quark loops. Many Standard Model electroweak measurements have calculable contributions from the

Experiment	A_{FB}^{c}
ALEPH l	$.064 \pm .039 \pm .030$
L3 l	$.083 \pm .038 \pm .027$
ALEPH D^*	$.045 \pm .076 \pm .004$
DELPHI D^*	$.107 \pm .075 \pm .013$
OPAL D^*	$.064 \pm .049 \pm .024$
LEP average	$.072 \pm .027$

Table 21: Summary of LEP results on A_{FB}^{c}, where l denotes a measurement from inclusive lepton fit, and D^* from a primary D^* tag. The average assumes no correlations.[114]

LEP average A_{FB}^{b}

For $m_H = 300$ GeV,
$\Rightarrow\ m_{\rm top} = 176 \pm ^{49}_{68}$ GeV
$\Rightarrow\ \sin^2\theta_W = .2321 \pm .0020$

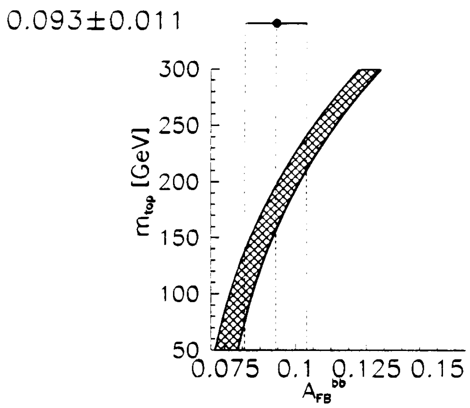

Figure 55: Forward-backward b quark asymmetry, as a function of top quark mass, with LEP average, mixing corrected measurement shown.[114]

top quark, including the forward-backward asymmetries. We may therefore examine the LEP average $A_{FB}^{b} = .093 \pm .011$ to place constraints on the top quark mass, as shown in Figure 55. From these asymmetry results alone, one can deduce that $m_{\rm top} = 176 \pm ^{49}_{68}$ GeV, for $m_H = 300$ GeV, in the context of the 3 generation Standard Model with no new physics. Furthermore, once top is discovered and its mass measured, we could be sensitive to the Higgs boson mass.

10 Specific Beautiful Hadrons

The average lifetime of B-hadrons has been determined at LEP to better than 3% precision, as was seen in Table 3. A pressing issue is now whether the lifetimes of individual B hadrons are all consistent with the average. This would be the case if spectator diagrams dominate in B decay, but recall that this was (to great surprise) not the case in the charm system. As discussed in Section 3.2, it is expected that non-spectator amplitudes are greatly reduced in the B system, partially due to reduced final state interactions, and also because the annihilation and exchange diagrams in the B system are drastically reduced due to the fact that $|V_{ub}|$ is extremely small, in addition to possible helicity suppression. Nevertheless, the non-spectator contributions to B decay, while small, are expected to be non-zero, thus leading to the prediction of the same lifetime hierarchy in the B system as was observed in the charm system:

$$\tau(B^+) \ > \tau(B_S) \ \geq \ \tau(B^0) \ > \ \tau(\Lambda_b) \tag{85}$$

In the B system however, we expect *at most* 10% variation [116] in the exclusive B lifetimes, due to the small amplitudes associated with the non-spectator decays, in sharp contrast with the factor of 5 variation in exclusive lifetimes observed in the charm system, from Λ_c^+ to D^+.

In order to identify an exclusive B hadron, either the B hadron must be completely reconstructed, or some unambiguous flavour tag is necessary. It is interesting to study how often a b quark hadronizes to produce a Λ_b, Ξ_b, B^+, B^0, B_s, B_c, or other B hadron. There is also potential for extracting more information on KM matrix elements and the non-perturbative QCD of weak B decays by studying specific individual B species, and measuring their lifetimes.

Since semileptonic decays are typically low multiplicity, they present a good starting place to try to separate individual B species, via B decays to a charmed hadron plus a lepton and an anti-neutrino. The first semi-exclusive B decays reconstructed at PEP [117] and then at LEP, were of this type.

10.1 The Lightest Beautiful Mesons, B^0 and B^+

B^0 and B^+ mesons may be reconstructed via semileptonic decays of the type

$$\overline{B} \ \rightarrow \ D \ l^- \overline{\nu} \ X \tag{86}$$

where D can be D^{*+}, D^0, or D^+, as in Figure 56. The subsequent decays:

$$\begin{array}{ll} D^{*+} \rightarrow D^0 \pi^+ & D^0 \rightarrow K^- \pi^+ \\ D^{*+} \rightarrow K^- \pi^+ \pi^+ & D^0 \rightarrow K^- \pi^+ \pi^+ \pi^- \end{array} \tag{87}$$

are the cleanest and most accessible experimentally. The strategy in reconstructing semileptonic $\overline{B}^0$ and B^- decays is to look for a D and l of the correct charge correlation, which are kinematically consistent with coming from a common B meson.

It is possible to estimate the ratio of B^+ to B^0 lifetimes from the ratio of their semileptonic branching fractions:

$$\frac{\tau(B^-)}{\tau(B^0)} = \frac{\mathrm{Br}(B^- \ \rightarrow \ D^{*0} \ l^- \overline{\nu})}{\mathrm{Br}(\overline{B}^0 \ \rightarrow \ D^{*+} \ l^- \overline{\nu})} \tag{88}$$

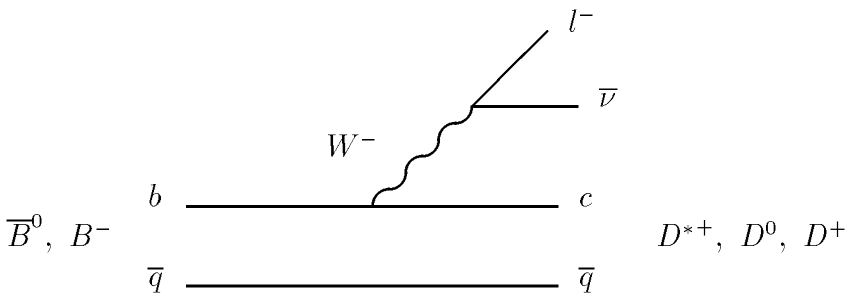

Figure 56: Feynman diagram for $\overline{B}^0$ and B^- semileptonic decays.

and likewise for D^0 and D^+ lifetimes.

ARGUS [68] and CLEO [69] have performed such indirect measurements of the ratio of B^0 to B^+ lifetimes, based on the ratios of exclusive semileptonic B branching ratios:

$$\text{Results: } \frac{\tau(B^-)}{\tau(B^0)} \;=\; \begin{array}{ll} .89 \pm .19 \pm .13 & \text{(CLEO)} \\ .95 \pm .15 \pm .19 & \text{(ARGUS)} \end{array}$$

where it is assumed that the $\Upsilon(4S)$ decays equally to neutral and charged B's.

10.1.1 B^0 and B^+ Lifetime Measurements at LEP

At LEP, it is possible to measure directly the lifetimes of the B mesons via their semileptonic decays. The strategy is to partially reconstruct B's in the channels:

$$\overline{B}^0 \;\to\; D^{*+}\, l^-\overline{\nu} \qquad B^- \;\to\; D^0\, l^-\overline{\nu}, \qquad \overline{B}^0 \;\to\; D^+\, l^-\overline{\nu} \tag{89}$$

and try to separate feed-down from the D^* channels to the D channels. If there were no p-wave D^{**}'s, all true $(D^{*+}\ l^-)$'s and $(D^+\ l^-)$'s would originate from $\overline{B}^0$'s.

All D^{*0}'s decay to D^0's, whereas D^{*+}'s feed into both D^0's and D^+'s:

$$D^{*0} \to D^0\pi^0,\ D^0\gamma, \qquad\qquad D^{*+} \to D^0\pi^+,\ D^+\pi^0 \tag{90}$$

We see that all D^{*+}, D^+ are from $\overline{B}^0$'s only, if we ignore the D^{**}'s for the moment. The neutral D^0's however are fed through both D^{*0} and D^{*+} decay channels. If we now additionally consider that up to $\frac{1}{3}$ [72, 64] of semileptonic B decay is through the p-wave D^{**} meson, we can still separate out the original B^+ and B^0 mesons, but with an additional error due to the uncertainty in the semileptonic B branching ratio to D^{**}'s, and the uncertainties in the $D^{**} \to D$ branching ratios, which in unmeasured channels, may be estimated from isospin symmetry arguments and theoretical input.

At LEP, DELPHI [118] has reconstructed D^{*+}, D^0, and D^+ mesons in same hemisphere as an identified lepton. The signals obtained are shown in

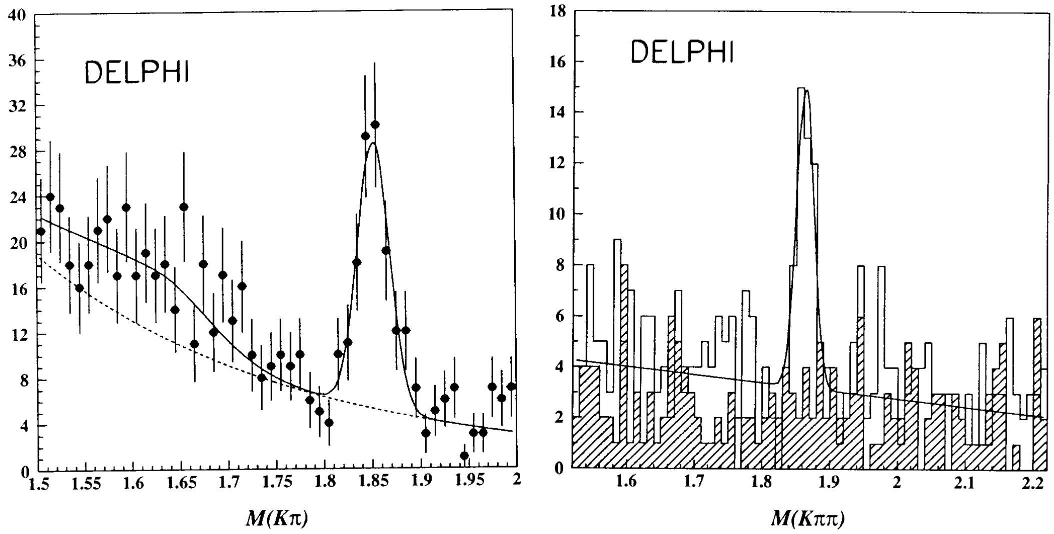

Figure 57: D^0 and D^+ meson signals used in the DELPHI [118] B^+ and B^0 lifetime analysis. Mass distributions are for events with an identified lepton which is in the same hemisphere as the D meson candidate.
a) The $K^-\pi^+$ mass distribution. The points are data, with correct sign D^0 l^- correlation, fit to a curve of background, plus $D^0 \to K^-\pi^+$ signal, plus the D^0 'satellite' peak resulting from $D^0 \to K^-\pi^+\pi^0$ decays.
b) The $K^-\pi^+\pi^+$ mass distribution. The solid line histogram is data, with correct charge correlation, D^+ $l-$, the curve is a fit to the signal plus background, and the hatched histogram is data with the wrong sign D^- l^- correlation.

Figures 57 and 58. The lifetimes of the D^0l^-, D^+l^- and $D^{*+}l^-$ samples are shown in Figure 59. As a cross check of the procedure, the lifetimes of the D^0 and D^+ mesons were derived from DELPHI's B meson sample by measuring the decay length from B decay vertex to D decay vertex. The proper times for the D^0 and D^+ lifetimes are shown in Figure 60, and the values obtained agree with world average values.

The other LEP experiments have performed similar analyses [119, 120], and the results on B^0 and B^+ lifetime measurements are summarized in Table 22. The ratio of the B^+ to B^0 lifetimes, which has reduced errors due to cancellation in common systematic errors, are listed in Table 23.

The individual B^0 and B^+ lifetimes are consistent with each other and with the average inclusive B hadron lifetime. The LEP results agree with the CLEO and ARGUS ratio of lifetimes derived from ratio of semileptonic branching fractions. These results agree with the reasoning that the naïve spectator model would be more applicable in the B system than it was in the D system, resulting in the B lifetimes differing by less than 10%.

10.1.2 Fixed Target B^0 and B^+ Lifetime Measurements

The Fermilab Hybrid Emulsion Spectrometer experiment E-653, has also measured charged and neutral B-hadron lifetimes, produced in a fixed target π^-

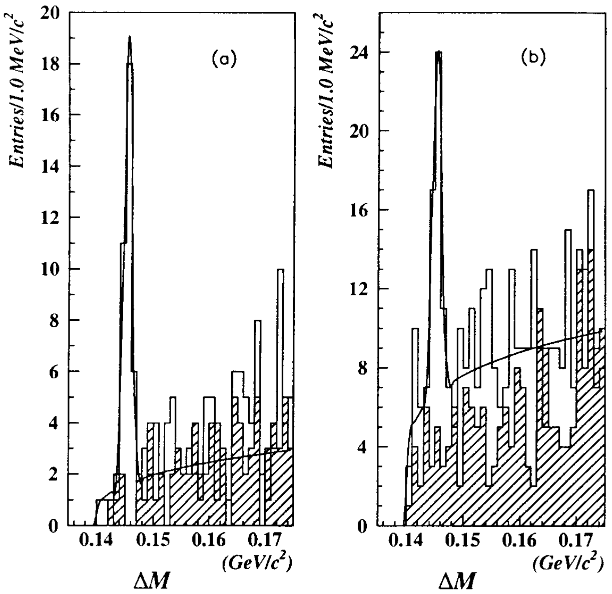

Figure 58: D^{*+} meson signals in the DELPHI [118] B^+ and B^0 lifetime analysis. Mass distributions are for events with an identified lepton in the same hemisphere as the D^* meson candidate. The solid histogram represents data, with correct sign D^{*+} - l^- correlation. The hatched histogram is data with the wrong sign $D^{*+} - l^+$ correlation,
a) The $\Delta M(D^{*+} - D^0)$ mass distribution for the $D^0 \to K^-\pi^+$ channel.
b) The $\Delta M(D^{*+} - D^0)$ mass distribution for the $D^0 \to K^-\pi^+\pi^+\pi^-$ channel.

Experiment	B^0 $\tau(10^{-12}s)$	B^+ $\tau(10^{-12}s)$
OPAL	$1.51 \pm {}^{.24}_{.23} \pm {}^{.11}_{.13}$	$1.52 \pm {}^{.29}_{.27} \pm {}^{.11}_{.12}$
DELPHI	$1.17 \pm {}^{.29}_{.23} \pm .15 \pm .05$	$1.30 \pm {}^{.33}_{.29} \pm .15 \pm .05$
ALEPH	$1.52 \pm {}^{.20}_{.18} \pm {}^{.07}_{.13}$	$1.47 \pm {}^{.22}_{.19} \pm {}^{.15}_{.14}$

Table 22: Summary of LEP B^0 and B^+ lifetime measurements.[119, 120, 118]

beam.[121] Their $b\bar{b}$ analysis triggers on the high momentum, high p_{T} muons expected in semileptonic B decay. The primary event vertex is located in the emulsion with very high efficiency. They then search for upstream multiple vertices, at least one of which must be too heavy for charm (invariant mass $> 2\,\mathrm{GeV}$). Muons from kaon and pion decay are easily identified and eliminated. Of the 359 events with a μ from an upstream vertex, 9 events are from beauty, having at least 3 identified vertices consistent with $b\bar{b}$ decay and charm cascade decay. 175 events are consistent with charm, and provide an excellent cross-check sample, in which the D^+ and D^0 lifetimes are measured and found to be consistent with world average values. They measure an average B hadron

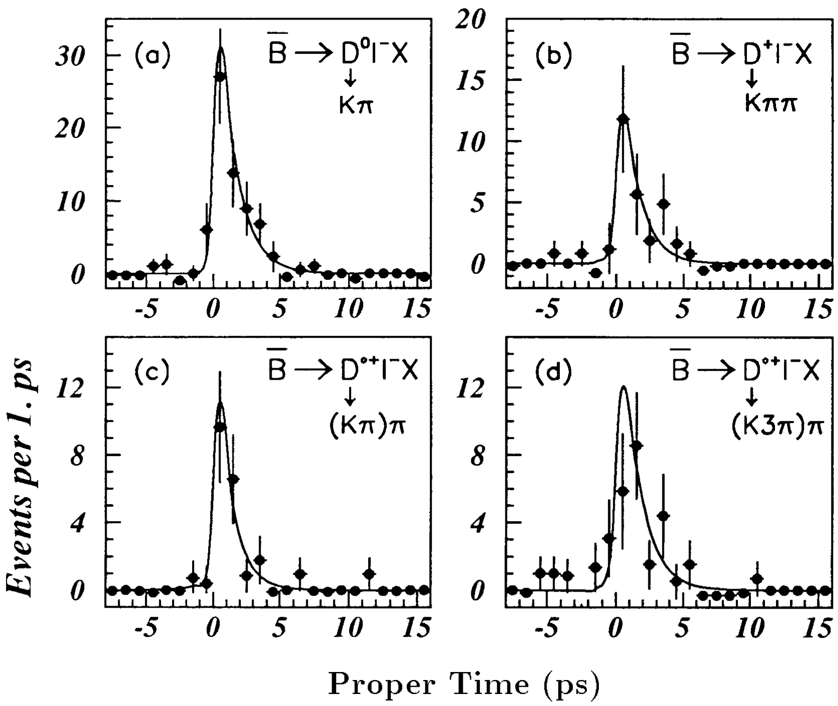

Figure 59: Measured B meson proper time distributions in DELPHI's four Dl samples.
a) $\overline{B} \to D^0 l^- X$, followed by $D^0 \to K^- \pi^+$.
b) $\overline{B} \to D^+ l^- X$, followed by $D^+ \to K^- \pi^+ \pi^+$.
c) $\overline{B} \to D^{*+} l^- X$, followed by $D^{*+} \to D^0 \pi^+$, $D^0 \to K^- \pi^+$.
d) $\overline{B} \to D^{*+} l^- X$, followed by $D^{*+} \to D^0 \pi^+$, $D^0 \to K^- \pi^+ \pi^+ \pi^-$.

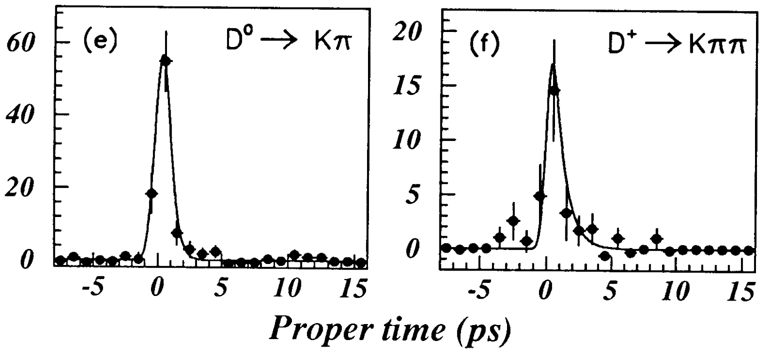

Figure 60: D meson proper time distributions in the DELPHI analysis.
a) $D^0 \to K^- \pi^+$. b) $D^+ \to K^- \pi^+ \pi^+$.

lifetime:

$$\tau_b = 1.86 \pm {}^{1.13}_{.61} \pm {}^{.52}_{.02} \mathrm{ps} \tag{91}$$

which is in agreement with the world average.

Experiment	Ratio $\tau(B^+)/\tau(B^0)$
OPAL	$1.01 \pm ^{.32}_{.24} \pm ^{.06}_{.07}$
DELPHI	$1.11 \pm ^{.51}_{.39} \pm .05 \pm .10$
ALEPH	$0.96 \pm ^{.19}_{.15} \pm ^{.18}_{.12}$

Table 23: The ratio of B^+ to B^0 lifetimes from LEP.[119, 120, 118]

Since E-653 do not explicitly identify and reconstruct B-hadrons, they divide the event sample into charged B-vertex and neutral B-vertex events, and measure the lifetime of each sample:

$$\tau^0 = .81 \pm ^{.34}_{.22} \pm ^{.09}_{.02} \quad \text{ps} \quad 12 \text{ Candidates} \tag{92}$$

$$\tau^\pm = 3.84 \pm ^{2.73}_{1.36} \pm ^{1.39}_{0.15} \quad \text{ps} \quad 6 \text{ Candidates} \tag{93}$$

It is expected that the charged B sample is dominated by B_u^+, but may have a few B_c^+ and Ξ_B^+ as well. The neutral sample is expected to be a mix of B_d^0, B_S^0 and Λ_b events.

While the statistics are low, the result appears to conflict with the ARGUS, CLEO and LEP measurements that B^0 and B^+ have approximately the same lifetime. This might be a consequence of low statistics with a statistical fluctuation, or could be a hint at new physics. The data are currently being re-scanned with lower selection thresholds, and the B sample should increase in the near future. Additionally, E-791 at Fermilab will soon release their first results on fixed-target B hadrons detected in the Tagged Photon Spectrometer in a π^- beam, and several other fixed target B experiments are presently awaiting approval to run at Fermilab.

10.2 The Strange Beautiful Meson, B_S

It is clearly of interest to isolate a sample of B_S^0 mesons to gain insight into the hadronization of b quarks, to study its decay properties, and to measure $B_S^0 - \overline{B}_S^0$ mixing separately from $B_d^0 - \overline{B}_d^0$ mixing. Additionally, the lifetime of the B_S is expected to be close to that of the B^0 and B^- mesons, since non-spectator amplitudes in the B system are anticipated to be small, and testing this hypothesis is essential to understand the B system.

At LEP, searches for ${B_S}^0$ $(\bar{b}s)$ via semi-leptonic decay

$$\overline{B_S}^0 \rightarrow {D_S}^+ \, l^- \overline{\nu} \, X \tag{94}$$

with subsequent decays

$${D_S}^+ \rightarrow \phi\pi^+ \quad \text{or} \quad {D_S}^+ \rightarrow K^{*0} K^+ \tag{95}$$

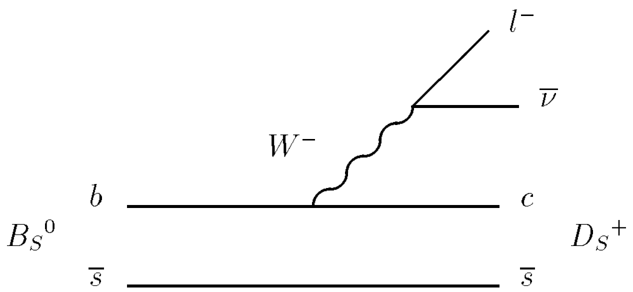

Figure 61: Feynman diagram for semileptonic B_S^0 decay.

have been performed. The relevant Feynman diagram is depicted in Figure 61.

There is a correlation between the charge of the D_S and l in B_S decays, whereas random D_S's and l's will be uncorrelated. There are very few background processes which will produce a D_S with an opposite sign high p_T lepton in the same event. Such backgrounds are produced in:

- Cascade decays of B^0 or B^+ mesons such that two charm daughters are produced in one B decay, *i.e.* $B \to \overline{D} D_S X$, with the $\overline{D}$ subsequently decaying semileptonically.
- a misidentified lepton with a genuine D_S.
- Decays of B^0 or B^+ mesons $B \to D^- l^+ \nu X$, where the $D^- \to K^{*0}\pi^-$ and may be mistaken for $D_S \to K^{*0} K^-$ (often referred to as a D^+ "reflection").

ALEPH has reconstructed the D_S [122], shown in Figure 62, in the $\phi\pi$ and K^*K channels. The D_S candidates are paired with a high p identified lepton, and the invariant mass is required to be $> 3\,\mathrm{GeV}$. To further reduce combinatorial background in the K^*K channel only, the D_S vertex was required to be at least .08 cm transverse to the beam direction with respect to the average fill-by-fill beam spot. The invariant $\phi\pi$ mass for right and wrong-sign $D_S l$ combinations is shown in Figure 63. The B_S^0 production cross-section times branching ratio determined by ALEPH is:

$$f\left(\overline{b} \to B_S{}^0\right) \cdot \mathrm{Br}\left(B_S{}^0 \to D_S{}^- l^+ \nu X\right) = \left(.040 \pm .011 \pm {}^{.010}_{.012}\right) \tag{96}$$

All LEP results on production cross-section times branching ratio are shown in Table 24.

Preliminary measurements of the B_S lifetime from the LEP experiments are listed in Table 25. Details on the ALEPH analysis are given in [124] at this conference.

It may be concluded that the B_S^0 exists, and its lifetime is consistent with the expectations, close to or slightly less than the average B-hadron lifetime.

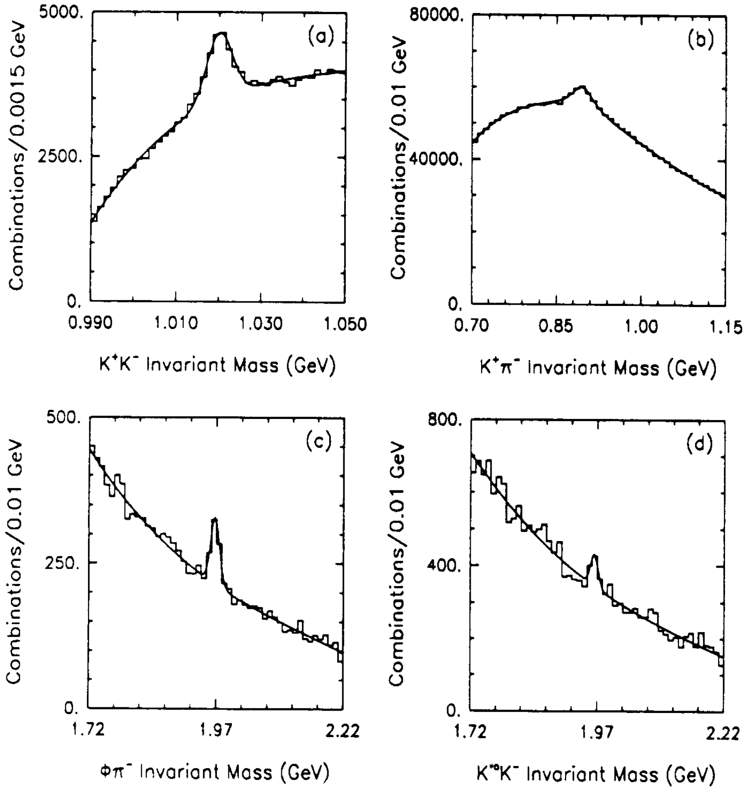

Figure 62: From the ALEPH [122] B_S analysis, D_S^+ reconstruction:
a) The K^+K^- invariant mass distribution, with clear ϕ resonance.
b) The $K^+\pi^-$ invariant mass distribution, with clear K^* resonance.
c) Invariant mass distribution of $D_S^+ \to \phi\pi$ combinations with $p > 8\,\mathrm{GeV}$.
d) Invariant mass distribution of $D_S^+ \to \overline{K^*}^0 K^+$ combinations with $p > 8\,\mathrm{GeV}$.

Experiment	$\#\ B_S$ Events	$f\left(\bar{b} \to {B_S}^0\right) \cdot \mathrm{Br}\left({B_S}^0 \to {D_S}^- l^+ \nu X\right)$
ALEPH	$26.8 \pm 7 \pm {}^{0}_{3.8}$	$(19.2 \pm 4.8 \pm 4.0) \times 10^{-3}$
DELPHI	17.5 ± 2.8	$(14.8 \pm 6.6 \pm 2.7) \times 10^{-3}$
OPAL	$18.3 \pm 5.2 \pm 0.9$	$(13.9 \pm 3.9 \pm 3.4) \times 10^{-3}$
Average		$(16.1 \pm 3.0 \pm 2.9) \times 10^{-3}$

Table 24: LEP results for B_S production.[123]

10.3 Beautiful Baryons

A search for B baryons and measurement of their lifetime has been undertaken at the LEP experiments. The Λ_b $(b\,(ud)_0)$, consisting of a b quark, with a (ud)

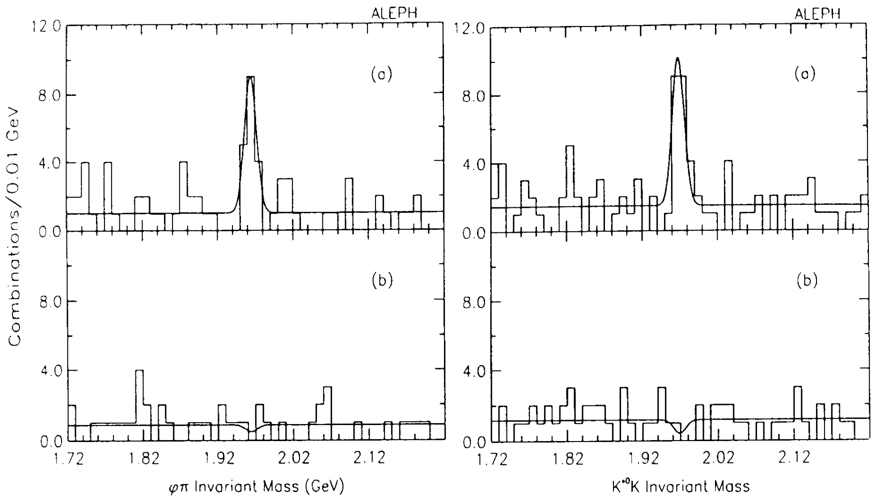

Right sign combination

Wrong sign combination

Figure 63: From ALEPH [122], B_S analysis, $D_S l$ combinations:
a) Right-sign $D_S^+ l^-$ combinations in the $D_S^+ \to \phi\pi^+$ channel.
b) Wrong-sign $D_S^+ l^+$ combinations in the $D_S^+ \to \phi\pi^+$ channel.
c) Right-sign $D_S^+ l^-$ combinations in the $D_S^+ \to \overline{K^*}^0 K^+$ channel.
d) Wrong-sign $D_S^+ l^+$ combinations in the $D_S^+ \to \overline{K^*}^0 K^+$ channel.

Experiment	$B_S^0\ \tau(10^{-12}s)$
DELPHI	$1.0 \pm .3$
ALEPH	$1.02 \pm {}^{.46}_{.31} \pm .10$
OPAL	$1.13 \pm {}^{.37}_{.26} \pm .17$

Table 25: B_S lifetime results.[123, 92]

di-quark in a spin 0 configuration, may decay semi-leptonically, as in Figure 64:

$$\Lambda_b{}^0 \ \rightarrow\ \Lambda_c{}^+\ l^- \overline{\nu}\ X \tag{97}$$

with the subsequent decay

$$\Lambda_c{}^+ \rightarrow pK^-\pi^+ \qquad \text{or} \qquad \Lambda_c{}^+ \rightarrow \Lambda\ X \tag{98}$$

In the case where a Λ, rather than a Λ_c is detected, the analysis will also be sensitive to the Ξ_b, via its semileptonic decay $\Xi_b{}^0 \ \rightarrow\ \Xi_c{}^+\ l^-\overline{\nu}\ X$ with subsequent decay $\Xi_c{}^+ \rightarrow \Lambda\ X$, and possibly the Ω_b as well. As in the B_S^0 analysis, the basic idea is to examine right and wrong sign charge correlations between the l and either the Λ or Λ_c particle.

The ALEPH analysis, described in [124] in these proceedings, examines right and wrong sign charge correlation between lepton and charmed hadron.

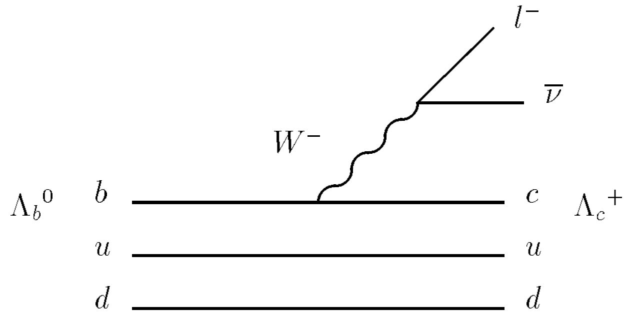

Figure 64: Feynman diagram for semileptonic B baryon decay.

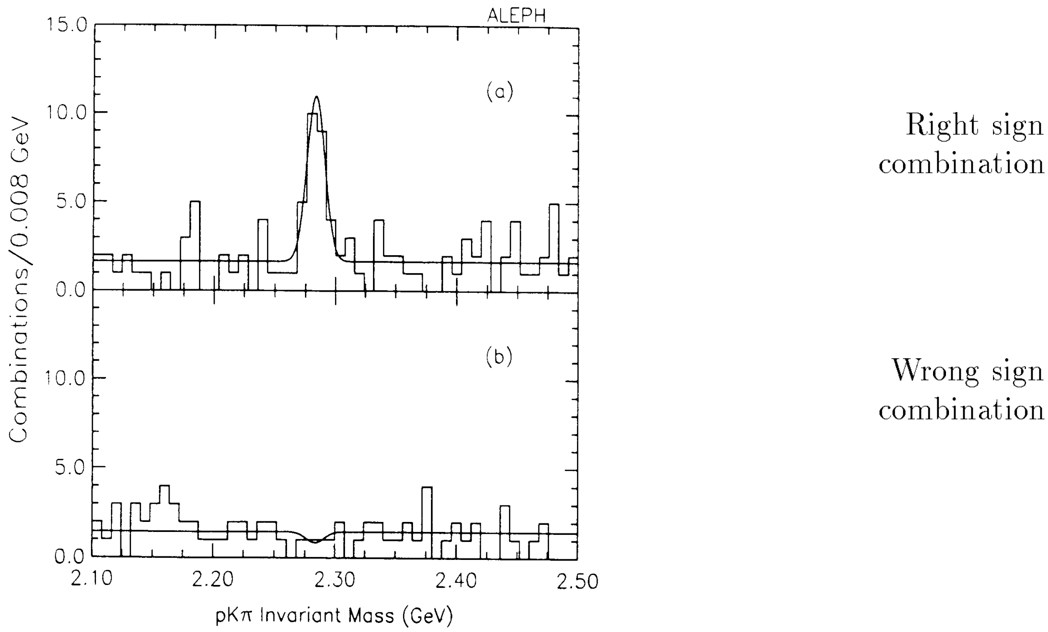

Figure 65: From ALEPH [122], Λ_b analysis, $\Lambda_c l$ combinations:
a) Right-sign $\Lambda_c^+ l^-$ combinations in the $\Lambda_c^+ \to pK^-\pi^+$ channel.
b) Wrong-sign $\Lambda_c^+ l^+$ combinations in the $\Lambda_c^+ \to pK^-\pi^+$ channel.

The ALEPH correlations between a Λ_c and lepton are shown in Figure 65. The b baryon lifetime was determined at ALEPH from the larger statistics Λl sample, using the impact parameter of the lepton to determine the lifetime. Details of the ALEPH analysis are in [124]., The result of the lifetime fit is shown in Figure 66. OPAL's results are also detailed in these proceedings. [125] A summary of the LEP b baryon lifetimes is in Table 26.

In summary, B baryons exist, and their lifetime is consistent with trend observed in the charm baryons, *i.e.* the baryons have the shortest lifetime of the measured B hadrons, but are still within theoretical expectations that spectator diagrams dominate, as their lifetimes are quite close to the average B hadron lifetime.

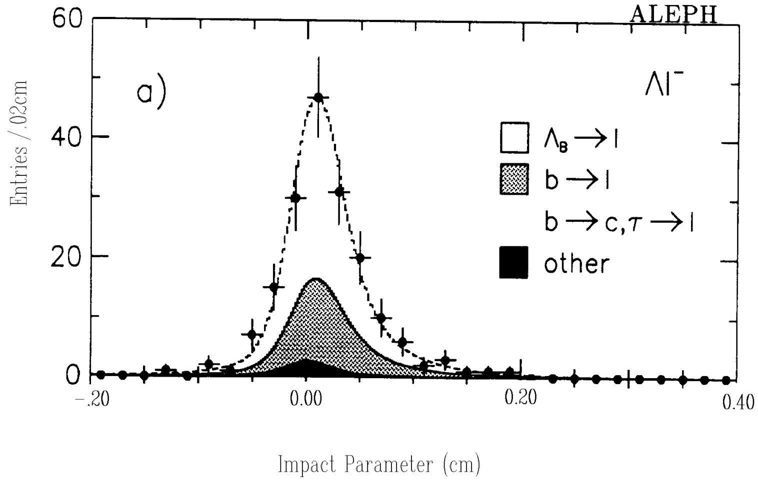

Figure 66: From the ALEPH [126] B baryon analysis, the lepton impact parameter distribution for the Λ-lepton sample.

Experiment	Λ_b $\tau(10^{-12}s)$	Technique
DELPHI	$1.04 \pm ^{.48}_{.38} \pm .09$	Decay Length
ALEPH	$1.12 \pm ^{.32}_{.24} \pm .16$	Impact Parameter
OPAL	$1.01 \pm ^{.20}_{.18} \pm .08$	Decay Length

Table 26: Summary of b baryon lifetimes measured at LEP. Both OPAL and DELPHI use the decay length of a reconstructed vertex, while ALEPH uses the impact parameter of the lepton.[127, 126, 125]

11 Summary and Outlook

11.1 Summary and Highlights

The Standard Model still stands strong, and we are rapidly gaining information on KM couplings. In the context of the Standard Model, the top mass is presently restricted, from both B-mixing results, and LEP electroweak measurements. When the top is discovered, perhaps we will be able to deduce restrictions on the Higgs mass next.

In weak decay physics, simple modifications to spectator picture do a pretty good job of describing the beauty and charm systems. Semileptonic decays of heavy flavours are becoming well-understood, and theoretical modeling is improving quickly.

Combining LEP and ARGUS/CLEO measurements on B-mixing indicates that mixing is near maximal in the B_S system; this is good news for the next generation of B-factories. Rare $b \to u$ decays have been observed and measured.

Measurements of exclusive B lifetimes show much promise at LEP.

11.2 Outlook

Within coming year, we expect more precise exclusive B lifetimes from LEP: τ_{Λ_b}, τ_{B_s}, τ_{B^0}, τ_{B^+}. All four LEP experiments will have installed silicon micro-vertex detectors for the 1993 run. The extensive B studies that will be performed will supply us with much better KM matrix element measurements, particularly for the less well-measured matrix elements involving the b quark. Many hadronic decay modes of B will be seen and measured precisely at CLEO, as the CESR luminosity has been steadily increasing. Hadronic B-hadron decays will be a hot topic at LEP as well, in the coming year. We will therefore be able to do detailed studies of weak decays in the beauty sector, just as was done in charm sector.

Additionally, rare B decays, such as penguins are expected to soon be discovered at CLEO.

And hopefully, a new heavy flavour, top, will be discovered at the Fermilab TeVatron collider very soon, giving us yet a new system to test all we've learned and deduced about the charm and beauty quarks, and apply it to the top quark. Interestingly enough, the top quark is expected to have such a short lifetime, that it will probably decay before hadronizing, thus simplifying some of our hadronic modeling problems that have been difficult to deal with in the charm and beauty systems.

A high luminosity B-factory will be built in the next 3 years. All knowledge and experience gained from heavy quark studies at present machines will be needed at a B-factory to do high statistics studies in B's to probe CP-violation.

Acknowledgements

I would like to thank the organizers of the Lake Louise Winter Institute for hosting such a pleasant meeting in a truly spectacular 'Canadian Rockies' mountain setting. Thanks go to Tom Mattison for his critical reading of this manuscript.

References

[1] See lectures presented by D.Gingrich, P.Jenni, and K.Ragan, at this Institute for summaries and prospects for exciting heavy quark physics at ep, pp, and $p\overline{p}$ colliders.

[2] S.L.Glashow, Nucl. Phys. **22,** 579 (1961),
S.Weinberg, Phys. Rev. Lett. **19,** 1264 (1967),
A.Salam and J.C.Ward, Phys. Lett. **13,** 168 (1964).

[3] See for example "Gauge Theories of the Strong, Weak, and Electromagnetic Interactions", C.Quigg, Benjamin/Cummings Publishing Company,

1983, or "Gauge Theories in Particle Physics", Aitchison and Hey, Adam Hilger Publishing Ltd., 1982.

[4] M.Kobayashi and T.Maskawa, Prog. Theor. Phys. **49,** 652 (1973).

[5] K.Hikasa *et al.* , Particle Data Book, Phys. Rev. **D45,** 1 (1992).

[6] L.Wolfenstein, Phys. Rev. Lett. **51,** 1945 (1984).

[7] See any particle physics textbook, or for example, A.Ali, p. 1, in "B Decays", ed. S.Stone, World Scientific Publishing Co., 1992.

[8] N.Cabibbo, Phys. Rev. Lett. **10,** 531 (1963).

[9] S.L.Glashow, J.Iliopoulos and L. Maiani, Phys. Rev. **D2,** 1285 (1970).

[10] M.K.Gaillard, B.W.Lee and J.L.Rosner, Rev. Mod. Phys. **47,** 277 (1975).

[11] J.J.Aubert *et al.* (MIT-Brookhaven Collaboration), Phys. Rev. Lett. **33,** 1404 (1974),
J.Augustin *et al.* (SLAC-Berkeley Collaboration), Phys. Rev. Lett. **33,** 1406 (1974).

[12] S.W.Herb *et al.* , Phys. Rev. Lett. **39,** 252 (1977),
W.R.Innes *et al.* , Phys. Rev. Lett. **39,** 1240 (1977).

[13] D.Besson *et al.* (CLEO Collaboration), Phys. Rev. Lett. **54,** 381 (1985).

[14] D.Akerib *et al.* (CLEO Collaboration), Phys. Rev. Lett. **67,** 1692 (1991).

[15] H.Schröder, Rep. Prog. Phys. **52,** 765 (1989).

[16] V.Barger, W.Long and S.Pakvasa, J. Phys. G **5,** L147 (1985).

[17] E.Fernandez *et al.* (MAC Collaboration), Phys. Rev. Lett. **51,** 1022 (1983).

[18] N.S.Lockyer *et al.* (MarkII Collaboration), Phys. Rev. Lett. **51,** 1316 (1983).

[19] V.Lüth, in "High Energy Electron-Positron Physics", Eds. A.Ali and P.Söding, 358, (1989).

[20] W.Atwood and J.Jaros in "B Decays", p. 261, ed. S.Stone, World Scientific Publishing Co., 1992.

[21] P.Frabetti *et al.* (E-687 Collaboration), Phys. Lett. **B263,** 584 (1991).

[22] P.Frabetti *et al.* (E-687 Collaboration), Phys. Lett. **B251,** 639 (1990).

[23] N.Ushida *et al.* (E-531 Collaboration), Phys. Rev. Lett. **56,** 1767 (1986),
N.Ushida *et al.* (E-531 Collaboration), Phys. Rev. Lett. **56,** 1771 (1986).

[24] M.Adamovich *et al.* (Photon Emulsion Collaboration), Euro. Phys. Lett. **4,** 887 (1987.

[25] M.Aguilar-Benetez *et al.* (LEBC Collaboration), Phys. Lett. **B193,** 140 (1987).

[26] K.Abe *et al.* (SLAC Hybrid Facility Photon Collaboration), Phys. Rev. **D33,** 1 (1986).

[27] S. Barlag *et al.* (ACCMOR Collaboration), Z. Phys. **C37,** 17 (1987),
S. Barlag *et al.* (ACCMOR Collaboration), Z. Phys. **C46,** 563 (1990),
S. Barlag *et al.* (ACCMOR Collaboration), Phys. Lett. **B218,** 374 (1989).

[28] M.P.Alvarez *et al.* (NA-14 Collaboration), Z. Phys. **C47,** 539 (1990).

[29] J.R.Raab *et al.* (E-691 Collaboration), Phys. Rev. **D37,** 2391 (1988),
J.C.Anjos *et al.* (E-691 Collaboration), Phys. Rev. Lett. **60,** 1379 (1988).

[30] S.E.Csorna *et al.* (CLEO Collaboration), Phys. Lett. **B191,** 318 (1987).

[31] H.Albrecht *et al.* (ARGUS Collaboration), Phys. Lett. **B210,** 267 (1988).

[32] D.Averill *et al.* (HRS Collaboration), Phys. Rev. **D39,** 123 (1989).

[33] M.Aguilar-Benetez *et al.* (LEBC Collaboration), Z. Phys. **C40,** 321 (1988).

[34] S.R.Amendolia *et al.* (NA-1 Collaboration), Z. Phys. **C36,** 513 (1987).

[35] H.Becker *et al.* (NA-11/NA-32 Collaboration), Phys. Lett. **B184,** 277 (1987).

[36] W.Braunschweig *et al.* (TASSO Collaboration), Z. Phys. **C35,** 317 (1987).

[37] R.Baltrusaitis *et al.* (MarkIII Collaboration), Phys. Rev. Lett. **54,** 1976 (1985).

[38] R.Ong, Ph.D. Thesis, SLAC Report 320, (1987),
R.Ong *et al.* (Mark-II Collaboration), Phys. Rev. Lett. **60,** 2587 (1989).

[39] P.Acton *et al.* (OPAL Collaboration), Phys. Lett. **B274,** 513 (1992).

[40] J.Hagemann *et al.* (JADE Collaboration), Z. Phys. **C48,** 401 (1990),
W.Braunschweig *et al.* (TASSO Collaboration), Z. Phys. **C44,** 1 (1989),
D.Klem *et al.* (DELCO Collaboration), Phys. Rev. **D37,** 41 (1988),
W.Ash *et al.* (MAC Collaboration), Phys. Rev. Lett. **58,** 640 (1987),
J.M.Brom *et al.* (MAC Collaboration), Phys. Lett. **B195,** 301 (1987).

[41] D.Buskulic *et al.* (ALEPH Collaboration), Phys. Lett. **B295,** 174 (1992),
P.Abreu *et al.* (DELPHI Collaboration), Z. Phys. **C53,** 567 (1992),
B.Adeva *et al.* (L3 Collaboration), Phys. Lett. **B270,** 111 (1991).

[42] R.P.Feynman, in "Symmetries in Elementary Particle Physics", Erice 1964, ed. A.Zichichi, Academic Press, 1965.

[43] A.N.Kamal, Q.P.Xu, and A.Czarnecki, preprint Alberta-Thy 3-93, 1993.

[44] R.Rückl, Habilitationsschrift, University of Munich (1983).

[45] M.Bauer, B.Stech and M.Wirbel, Z. Phys. **C34,** 103 (1987).

[46] M.Bauer and B.Stech, Phys. Lett. **B152,** 380 (1985).

[47] A.J.Buras, J.M.Gérard and R.Rückl, Nucl. Phys. B**268,** 16 (1986).

[48] M.Wirbel, Prog. in Part. and Nucl. Phys. **21,** 33 (1988).

[49] H.Albrecht *et al.* (ARGUS Collaboration), Z. Phys. **C48,** 543 (1990).

[50] D.Bortoletto *et al.* (CLEO Collaboration), Phys. Rev. **D45,** 21 (1992).

[51] W.Bernreuther, O.Nachtmann, and B.Stech, Z. Phys. **C4,** 257 (1980).

[52] A.N.Kamal, J. Mod. Phys. **A7,** 3503 (1992),
A.N.Kamal, N.Sinha and R.Sinha, Phys. Rev. **D39,** 3503 (1989),
L.L.Chau and H.Y.Cheng, Phys. Rev. **D36,** 137 (1987).

[53] S.Aoki *et al.* (WA75 Collaboration), CERN-PPE 92-157, (1992).

[54] S.Godfrey and N.Isgur, Phys. Rev. **D32,** 189 (1985).

[55] H.Albrecht *et al.* (ARGUS Collaboration), Z. Phys. **C54,** 1 (1992).

[56] J.Adler *et al.* (MarkIII Collaboration), Phys. Rev. Lett. **60,** 1375 (1988).

[57] G.Altarelli, N.Cabibbo, G.Corbo, L.Maiani and G.Martinelli, Nucl. Phys. B**208,** 365 (1982).

[58] W.Bacino *et al.* (DELCO Collaboration), Phys. Rev. Lett. **43,** 1073 (1979).

[59] N.Isgur, D.Scora, B.Grinstein, and M.B.Wise, Phys. Rev. **D39,** 799 (1989).

[60] M.Wirbel, B.Stech and M.Bauer, Z. Phys. **C29,** 637 (1985).

[61] B.Grinstein, M.B.Wise and N.Isgur, Phys. Rev. Lett. **56,** 298 (1986).

[62] M.Wirbel, Nucl. Phys. B, Proc. Suppl. **13,** 255 (1990).

[63] K.Kodama *et al.* (E-653 Collaboration), Phys. Lett. **B286,** 187 (1992).

[64] H.Albrecht *et al.* (ARGUS Collaboration), DESY-92-146, (1992).

[65] S.Balk, F.Hussain, J.G.Körner, and G.Thompson, MZ-TH-92-22 (1992).

[66] H.Albrecht *et al.* (ARGUS Collaboration), Phys. Lett. **B275,** 195 (1992).

[67] D.Bortoletto *et al.* (CLEO Collaboration), Phys. Rev. Lett. **63,** 1667 (1989).

[68] H.Albrecht *et al.* (ARGUS Collaboration), DESY-92-029, (1992).

[69] R.Fulton *et al.* (CLEO Collaboration), Phys. Rev. **D43,** 651 (1991).

[70] S.Stone in “B Decays”, p. 210, ed. S.Stone, World Scientific Publishing Co., 1992.

[71] J.G.Körner, and G.A.Schuler, Z. Phys. **C38,** 511 (1988);
ibid, (erratum) **C41**, 690, (1989).

[72] S.Henderson *et al.* (CLEO Collaboration), Phys. Rev. **D45,** 2212 (1992).

[73] H.Albrecht *et al.* (ARGUS Collaboration), Phys. Lett. **B249,** 359 (1990).

[74] K.Wachs *et al.* (Crystal Ball Collaboration), Z. Phys. **C42,** 33 (1989),
C.Yanagisawa *et al.* (CUSB Collaboration), Phys. Rev. Lett. **66,** 2436 (1991).

[75] R.Fulton *et al.* (CLEO Collaboration), Phys. Rev. Lett. **64,** 16 (1990).

[76] H.Albrecht *et al.* (ARGUS Collaboration), Phys. Lett. **B234,** 409 (1990).

[77] H.Albrecht *et al.* (ARGUS Collaboration), Phys. Lett. **B255,** 297 (1991).

[78] D.Bortoletto *et al.* (CLEO Collaboration), Phys. Rev. Lett. **62,** 2436 (1989),
H.Albrecht *et al.* (ARGUS Collaboration), Phys. Lett. **B241,** 278 (1990),
S.Playfer *et al.* (CLEO Collaboration), DPF talk, Fermilab, November 1992.

[79] A.Bean *et al.* (CLEO Collaboration), CLNS-92-1174, (1992).

[80] P.Drell and R.Patterson, CLNS-92-1177, presented at XXVI International Conference on High Energy Physics, Dallas, Texas, USA, August, 1992.

[81] M.B.Voloshin and M.A.Shifman Sov. J. Nucl. Phys. **45,** 292 (1987),
M.B.Voloshin and M.A.Shifman Sov. J. Nucl. Phys. **47,** 511 (1988).

[82] N.Isgur and M.B.Wise, Phys. Lett. **B232,** 113 (1989),
N.Isgur and M.B.Wise, Phys. Lett. **B237,** 527 (1990).

[83] M.E.Luke, Phys. Lett. **B252,** 447 (1990).

[84] C.G.Boyd and D.E.Brahm, Phys. Lett. **B257,** 393 (1991).

[85] M.Neubert, Phys. Lett. **B264,** 455 (1991),
M.Neubert, Phys. Rev. **D46,** 3914 (1992).

[86] B.A.Campbell and P.J.O’Donnell, Phys. Rev. **D25,** 1989 (1982).

[87] M.A.Shifman, A.I.Vainshtein and V.I.Zakharov, Phys. Rev. **D18,** 2583 (1978),
B.Grinstein, R.Springer and M.B.Wise, Phys. Lett. **B202,** 138 (1988).

[88] P.Avery *et al.* (CLEO Collaboration), Phys. Lett. **B223,** 470 (1989).

[89] H.Albrecht *et al.* (ARGUS Collaboration), Phys. Lett. **B254,** 288 (1991).

[90] B.W.Lynn and R.G.Stuart, Phys. Lett. **B252,** 676 (1990).

[91] R.Clare, presented at XXVI International Conference on High Energy Physics, Dallas, Texas, USA, August, 1992.

[92] R.Tenchini, talk at Rencontres de Moriond, February 1993.

[93] ALEPH Collaboration, "Heavy Flavour Physics with Leptons", Contributed paper to XXVI International Conference on High Energy Physics, Dallas, Texas, USA, August, 1992.

[94] D.Decamp *et al.* (ALEPH Collaboration), Phys. Lett. **B244,** 551 (1990), B.Adeva *et al.* (L3 Collaboration), Phys. Lett. **B261,** 177 (1990), M.Z.Akrawy *et al.* (OPAL Collaboration), Phys. Lett. **B263,** 311 (1991), P.Acton *et al.* (OPAL Collaboration), Z. Phys. **C55,** 191 (1992), P.Abreu *et al.* (DELPHI Collaboration), Z. Phys. **C56,** 47 (1992).

[95] R.Jacobsen *et al.* (Mark-II Collaboration), Phys. Rev. Lett. **67,** 3347 (1991).

[96] P.Abreu *et al.* (DELPHI Collaboration), Phys. Lett. **B281,** 383 (1992).

[97] P.Abreu *et al.* (DELPHI Collaboration), Phys. Lett. **B295,** 383 (1992).

[98] D.Buskulic *et al.* (ALEPH Collaboration), Phys. Lett. **B298,** 479 (1993).

[99] M.Gell-Mann and A.Pais, Phys. Rev. **97,** 1387 (1955).

[100] E.E.Landé *et al.* , Phys. Rev. **103,** 1901 (1956).

[101] H.Albrecht *et al.* (ARGUS Collaboration), Phys. Lett. **B186,** 247 (1987).

[102] M.K.Gaillard and B.W.Lee, Phys. Rev. **D10,** 897 (1974).

[103] H.Albrecht *et al.* (ARGUS Collaboration), Z. Phys. **C55,** 357 (1992).

[104] M.Artuso *et al.* (CLEO Collaboration), Phys. Rev. Lett. **62,** 2233 (1989).

[105] P.Acton *et al.* (OPAL Collaboration), Phys. Lett. **B276,** 379 (1992).

[106] D.Decamp *et al.* (ALEPH Collaboration), Phys. Lett. **B258,** 236 (1991).

[107] B.Adeva *et al.* (L3 Collaboration), Phys. Lett. **B288,** 395 (1992).

[108] P.Abreu *et al.* (DELPHI Collaboration), Phys. Lett. **B301,** 145 (1993).

[109] D.Buskulic *et al.* (ALEPH Collaboration), Phys. Lett. **B284,** 177 (1992).

[110] H.Schröder, in "B Decays", ed. S.Stone, p.292, World Scientific Publishing Co., 1992.

[111] M.Böhm and W.Hollik, "Z Physics at LEP-I" - Volume 1, ed. G.Altarelli, p.203, CERN 89-08 (1989).

[112] B.Adriani *et al.* (L3 Collaboration), Phys. Lett. **B292,** 454 (1992).

[113] D.Buskulic *et al.* (ALEPH Collaboration), Phys. Lett. **B263,** 325 (1991), M.Z.Akrawy *et al.* (OPAL Collaboration), CERN-PPE-92-139, 1992, P.Abreu *et al.* (DELPHI Collaboration), Phys. Lett. **B276,** 543 (1992).

[114] T.Wyatt, presented at XXVI International Conference on High Energy Physics, Dallas, Texas, USA, August, 1992.

[115] K.Ragan, presented at this conference, Lake Louise Winter Institute on Collider Physics, February, 1993.

[116] J.H.Kühn and P.M.Zerwas, "Physics at LEP-I" - Volume 1, ed. G.Altarelli, p.267, CERN 89-08 (1989).

[117] S.Wagner *et al.* (Mark-II Collaboration), Phys. Rev. Lett. **64,** 1095 (1990).

[118] P.Abreu *et al.* (DELPHI Collaboration), Z. Phys. **C57,** 181 (1993).

[119] D.Buskulic *et al.* (ALEPH Collaboration), CERN-PPE-93-42, 1993.

[120] P.Acton *et al.* (OPAL Collaboration), CERN-PPE-93-33, (1993).

[121] K.Kodama *et al.* (E-653 Collaboration), DPNU-92-37, (1992), K.Kodama *et al.* (E-653 Collaboration), Phys. Lett. **B274,** 246 (1992).

[122] D.Buskulic *et al.* (ALEPH Collaboration), Phys. Lett. **B294,** 195 (1992).

[123] V.Sharma, presented at XXVI International Conference on High Energy Physics, Dallas, Texas, USA, August, 1992.

[124] T.S.Mattison, presented at this conference, Lake Louise Winter Institute on Collider Physics, February, 1993.

[125] R.J.Hemingway, presented at this conference, Lake Louise Winter Institute on Collider Physics, February, 1993.

[126] D.Buskulic *et al.* (ALEPH Collaboration), CERN-PPE-92-138, (1992).

[127] P.Abreu *et al.* (DELPHI Collaboration), Phys. Lett. **B289,** 199 (1992).